

ATR-FTIR EVALUATION OF STRUCTURAL AND FUNCTIONAL
CHANGES ON MURINE MACROPHAGE CELLS UPON ACTIVATION AND
SUPPRESSION BY IMMUNO-THERAPEUTIC
OLIGODEOXYNUCLEOTIDES

A THESIS SUBMITTED TO
THE GRADUATE SCHOOL OF NATURAL AND ANPPLIED SCIENCES
OF
MIDDLE EAST TECHNICAL UNIVERSITY

BY
EMRULLA SPAHIU

IN PARTIAL FULFILLMENT OF THE REQUIREMENTS
FOR
THE DEGREE OF MASTER OF SCIENCE
IN
BIOLOGY

JANUARY 2015

Approval of the thesis:

**ATR-FTIR EVALUATION OF STRUCTURAL AND FUNCTIONAL
CHANGES ON MURINE MACROPHAGE CELLS UPON ACTIVATION
AND SUPPRESSION BY IMMUNOTHERAPEUTIC
OLIGODEOXYNUCLEOTIDES**

submitted by **EMRULLA SPAHIU** in partial fulfilment of the requirements for
the degree of **Master of Science in Biology Department, Middle East Technical
University** by,

Prof.Dr. M.Gülbin Dural Unver
Dean, Graduate School of Natural and Applied Sciences

Prof.Dr. Orhan Adali
Head of Department, Biology

Prof.Dr.Feride Severcan
Supervisor, Biology Department, METU

Assoc. Prof. Dr. Mayda Gürsel
Co-Supervisor, Biology Department, METU

Examining Committee Members:

Prof.Dr.Ayşegül Çetin Gözen
Biology Department, METU

Prof.Dr.Feride Severcan
Biology Department, METU

Assoc.Prof.Dr. Mayda Gürsel
Biology Department, METU

Prof.Dr.Ihsan Gürsel
Molecular Biology Dept., Bilkent

Assoc.Prof.Dr.Cağdaş Son
Biology Department, METU

Date: 19.01.2015

I hereby declare that all information in this document has been obtained and presented in accordance with academic rules and ethical conduct. I also declare that, as required by these rules and conduct, I have fully cited and referenced all material and results that are not original to this work.

Name, Last name: Emrulla Spahiu

Signature:

ABSTRACT

ATR-FTIR EVALUATION OF STRUCTURAL AND FUNCTIONAL CHANGES ON MURINE MACROPHAGE CELLS UPON ACTIVATION AND SUPPRESSION BY IMMUNOTHERAPEUTIC OLIGODEOXYNUCLEOTIDES

Spahiu, Emrulla

M.S., Department of Biology

Supervisor: Prof.Dr. Feride Severcan

Co-Supervisor: Assist.Prof.Dr.Mayda Gursel

January 2015, 89 pages

In the present study, ATR-FTIR was used to examine the structural and functional changes on murine macrophage cells upon activation and suppression by immunotherapeutic ODNs. Macrophage cells play a key role in innate and adaptive immunity. Their possession of high flexibility helps them to successfully respond to environmental signals. In this context, they can impressively alter their physiology in relation to their function and these changes have large molecular signals in the infrared spectral region that can be traced with FTIR spectroscopy. LPS and CpG ODN are used as well-known stimulants of macrophages to produce the powerful pro-inflammatory agents such as cytokines, chemokines and highly specific Ig's. CpG ODN is potentially used in many immunotherapeutic therapies,

but is found to cause allergy, toxic shock and death. The need for a suppressive agent led to the innovation of suppressive ODN, whose mechanism is not elucidated. In the present study, murine macrophage-like RAW 264.7 cells are treated with PBS medium, CpG ODN, LPS, suppressive ODN_{A151}, and K3 Flip-ODN in four different time scales, to monitor the changes on the course of time. Homogenous $2 \cdot 10^6/\mu\text{L}$ cell samples were prepared and FTIR spectra were recorded in triplicates. In total n=5 was performed. The spectra recorded underwent smoothing, baseline correction and normalization steps, and quantitative analysis was performed. One way-ANOVA with Dunnet's test for multiple comparisons and Kruskal–Wallis with Dunn's test for multiple comparisons was used for the analysis of normally and non-normally distributed data, respectively. All results were expressed as mean \pm SEM. The results clearly indicate that CpG-induced macrophage cells show prominent features in their IR spectra for their activation. The time period till 2h of stimulation seems to be the period of extensive RNA synthesis, and as it ceases, DNA synthesis starts from the 6th hour of stimulation upon both CpG ODN and LPS stimulation, except LPS at 6 hours, due to the property of LPS being an anti-proliferative agent. It is also found that stimulation of macrophage cells with CpG ODN and LPS decreases protein content. This is explained by the production of numerous oxidants, causing oxidative stress and in intention of protecting the cell; proteasomes start the degradation of oxidized proteins. The membrane fluidity increases during activation with CpG ODN and LPS, as a result of decreased unsaturated lipid content, increased lipid peroxidation and decreased cholesterol content. It was also noted that these changes may have altered the signal transduction processes, ion permeability and many other primary functions of cell membranes could be altered.

Keywords: Macrophage, CpG ODN, A151 ODN, FTIR spectroscopy

ÖZ

BASKILAYAN VE UYARAN İKİ TIP İMMÜNÖTERAPÖTİK OLİGODEOKSİNÜKLEOTİDLERİN İMMUNOLOJİK HÜCRELERDE YOL AÇTIĞI YAPISAL VE FONKSİYONEL DEĞİŞİMLERİN ATR-FTIR METODU İLE DEĞERLENDİRMESİ

Spahiu, Emrulla

Yüksek Lisans, Biyoloji Bölümü

Tez Yöneticisi: Prof.Dr. Feride Severcan

Ortak Tez Yöneticisi: Assist.Prof. Dr. Mayda Gursel

Ocak 2015, 89 sayfa

Bu çalışmada, ATR-FTIR metodu ile baskılayan ve uyaran iki tip immünoterapötik oligodeoksinükleotitlerin, makrofaj hücrelerinde yol açtıkları yapısal ve fonksiyonel değişimlerin değerlendirilmesi yapılmıştır. Makrofaj hücreleri, bağışıklık sisteminde anahtar rol oynamaktadır. Sahip oldukları yüksek fleksibilite ile çevresel sinyallere kolayca alışabilen hücrelerdir. Bu anlamda mükemmel bir şekilde fizyolojik değişikliklere mağruz kalabilme özelliğine sahiptirler. IR spektrumunda geniş çapta moleküler sinyaller verdiği için, ATR-FTIR başarılı bir şekilde kullanılabilir. LPS ve CpG ODN bağışıklık sistemini hızlıca arttırabilirler ve çok etkili pro-enflamatuar sitokin, kemokin ve spesifik Ig ajanları üretirler. CpG ODN immünoterapötik bir ilaç aktivitesi gösterebildiği açıklanmıştır. Ancak son zamanlarda çıkan klinik çalışmalarda, CpG'nin bazı ciddi

sorunları beraberinde getirdiği gözlenmiştir, ki bunlardan bazıları alerji, toksik şok hatta organizmanın ölümüne kadar götürmektedir. CpG ODN ile sürdürülen makrofajlardaki bu aktivasyonun yan etkilerini durdurma ihtiyacı, baskılayıcı ODN'lerin bulunmasına yol açmıştır, ki bunlardan birisi de A151 ODN'dir. A151 ODN'in çalışma mekanizması bilinmemektedir. Bu çalışmada, fare makrofaj RAW 264.7 hücreleri, PBS, CpG ODN, LPS, baskılayıcı ODN_{A151}, ve ters K3-ODN tretmanları ile dört değişik zaman dilimlerinde aşılanmıştır. Homojen $2 \cdot 10^6/\mu\text{L}$ konsantrasyonlu hücre örnekleri hazırlanıp üç replikada n=5 olmak üzere FTIR spektraları elde edilmiştir. Smoothing, baseline correction ve normalization adımlarından sonra spektralar kuantitatif incelemelere hazır olmuştur. Normal dağılımlı sonuçlar One-Way ANOVA ve Dunnet's test for multiple comparisons ile analizi yapılmıştır, normal dağılımı olmayan örnekler ise Kruskal–Wallis with Dunn's test for multiple comparisons ile incelenmiştir. Tüm sonuçlar ortalama \pm SEM olarak sunulmuştur. Sonuçlar, uyarıcı CpG ODN'nin IR spektrumunda yüksek değişimlere yol açtığı gözlenmiştir. İki saate kadar ki zaman dilimlerinde, CpG ODN ve LPS, RNA sentezinin bariz bir şekilde arttığı gözlenmiştir. 6 saatten sonra ki zaman dilimlerinde, DNA sentezi/değişikliği başladığı bulunmuştur. LPS, anti-proleferatif bir ajan olduğu için, 6 saatten sonra, DNA sentezi yapmamıştır. Stimulasyon ajanlarının kullanıldığı örneklerde, protein seviyelerinin düştüğü bulunmuştur, ki bu aktivasyona bağlı oksidantların oksidatif stres uygulamaları ile bağdaşmıştır. Bu etkileri düşürmek için, hücre içi proteozomların proteinleri degrade ettikleri bulunmuştur. Aktivasyona bağlı, membran akışkanlığında artış gözlenmiştir, ki bu doymamış yağların düşüşü ile, artan lipid peroksidasyonu ile ve düşen kolesterol miktarları ile doğru orantıda olduğu belirlenmiştir. Son olarak, bu değişimlerin sinyalizasyon mekanizmalarında, iyon geçirgenliğinde ve birçok membranlara bağlı hücre fonksiyonlarında değişimlere meydan açabileceğine sonuç bağlanmıştır.

Anahatar Kelimeler: Makrofaj, CpG ODN, A151 ODN, FTIR spektroskopisi

Dedicated to my lovely parents,
Without whose inspiration, drive and support,
I could not be as I am today:
To Zarife & Ibrahim Spahiu

ACKNOWLEDGMENTS

I would primarily like to express my thankfulness to my supervisor Prof. Dr. Feride Severcan and Assoc.Prof.Dr.Mayda Gursel for their supervision and motivation during my thesis study.

I would kindly express my thanks to Nihal Şimşek Özek, Sherif Abbas, Fatma Kucuk, Seher Gok, Ceren Aksoy, Dilek Yonar, Bilgi Gungor, Soner Yildiz, Esin Alpdundar and Richardas Rachkauskas for their valuable help both during the experimental stage and writing this thesis.

TABLE OF CONTENTS

ABSTRACT..	v
ÖZ.....	vii
ACKNOWLEDGEMENTS.....	x
TABLE OF CONTENTS.....	xi
LIST OF FIGURES.....	xvi
LIST OF TABLES.....	xiv
LIST OF ABBREVIATIONS	xxi

CHPATERS

1. INTRODUCTION.....	1
1.1. Immunity.....	1
1.2. Macrophages.....	3
1.2.1. Development and differentiation of macrophages.....	3
1.2.2. Functions of macrophages.....	4
1.3. Toll-like receptors (TLRs).....	6
1.4. Common activators and suppressors of macrophages.....	7
1.4.1. Lipopolysaccharide (LPS).....	7
1.4.2. CpG motif containing DNA.....	9
1.4.3. Synthetic CpG oligodeoxynucleotide.....	11
1.4.4. Suppressive oligodeoxynucleotide.....	14
1.5. Macromolecular changes at various stages following the activation of macrophages.....	15

1.6. Electromagnetic (EM) radiation.....	16
1.6.1. Electromagnetic spectrum.....	18
1.7. Spectroscopy.....	19
1.7.1. IR spectroscopy.....	22
1.7.2. Basic principles of Fourier Transformation Infra-Red (FTIR) spectroscopy.....	26
1.7.3. Attenuated Total Reflectance (ATR)-FTIR.....	27
1.7.4. Advantages of ATR-FTIR.....	29
1.7.5. Applications of FTIR spectroscopy.....	30
1.8. Aim of the study.....	31
2. MATERIALS AND METHODS	32
2.1. Materials.....	33
2.2 Growth, Stimulation and Preparation of cells.....	33
2.3. FTIR.....	35
2.3.1. Optimization studies.....	36
2.3.2. Data analysis procedures.....	39
2.3.2.1. Data processing.....	40
2.3.2.2. Chemometric analysis.....	42
2.4. Statistical analysis.....	42
3. RESULTS.....	43
3.1. General ftir spectra and band assignment of medium treated control macrophage group.....	43
3.2. General differences between resting, activated and suppressed macrophages.....	47
3.3. Lipid profile of murine macrophage cells.....	51

3.3.1. Saturated lipids.....	51
3.3.2. Unsaturated lipids.....	53
3.3.3. Cholesterol ester and triglycerides.....	54
3.3.4. Fatty acids.....	56
3.4. Protein profile.....	58
3.5. Nucleic acids.....	61
3.5.1. DNA.....	64
3.5.2. RNA.....	66
3.6. Examination of specific issues.....	66
3.6.1. Membrane fluidity.....	66
3.6.2. Lipid/protein.....	67
3.7. Cluster analysis.....	68
3.8. Principal component analysis (PCA).....	71
4. DISCUSSION.....	75
5. CONCLUSIONS.....	81
REFERENCES.....	83

LIST OF TABLES

TABLES

Table 1: Molecular transitions in different EM regions with their corresponding spectroscopic methods used. [Modified from (Harvey, 2009)]	21
Table 2: Band assignment of main absorption peaks in the ATR-FTIR spectra of murine macrophage RAW 264.7 cells.....	45
Table 3: Numerical analysis of fatty acid content, by the use of differences in 1400cm^{-1} IR band area of Medium, CpG ODN, A151 ODN, LPS and K3f ODN treated macrophage cell spectra, in different time points (10min, 30min, 2h and 6h). The statistically significant data are specified with $p<0.05^*$, $p<0.01^{**}$, and $p<0.001^{***}$ in comparison to medium treated group. The results are specified as mean \pm SEM.....	52
Table 4: Numerical analysis of saturated lipid content by the use of differences in 1500cm^{-1} IR band area of Medium, CpG ODN, A151 ODN, LPS and K3f ODN treated macrophage cell spectra, in different time points (10min, 30min, 2h and 6h). The statistically significant data are specified with $p<0.05^*$, $p<0.01^{**}$, and $p<0.001^{***}$ in comparison to medium treated group. The results are specified as mean \pm SEM.....	53
Table 5: Numerical analysis of cholesteryl ester and triglyceride content, by the use of differences in 1741cm^{-1} and 1170cm^{-1} IR band area of Medium, CpG ODN, A151 ODN, LPS and K3f ODN treated macrophage cell spectra, in different time points (10min, 30min, 2h and 6h). The statistically significant data are specified with $p<0.05^*$, $p<0.01^{**}$, and $p<0.001^{***}$ in comparison to medium treated group. The results are specified as mean \pm SEM.....	55

Table 6: Numerical analysis of fatty acid content, by the use of differences in 1400cm⁻¹ IR band area of Medium, CpG ODN, A151 ODN, LPS and K3f ODN treated macrophage cell spectra, in different time points (10min, 30min, 2h and 6h). The statistically significant data are specified with p<0.05*, p<0.01**, and p<0.001*** in comparison to medium treated group. The results are specified as mean ± SEM.....57

Table 7: Numerical analysis of protein content, by the use of differences in 1640 cm⁻¹ and 1543 cm⁻¹ IR band area of Medium, cpG ODN, A151 ODN, LPS and K3f ODN treated macrophage cell spectra, in different time points (10min, 30min, 2h and 6h). The statistically significant data are specified with p<0.05*, p<0.01**, and p<0.001*** in comparison to medium treated group. The results are specified as mean ± SEM.59

Table 8: Numerical analysis of DNA content, by the use of differences in 1236cm⁻¹, 1261cm⁻¹, 1080cm⁻¹ and 1100cm⁻¹ IR band areas of Medium, cpG ODN, A151 ODN, LPS and K3f ODN treated macrophage cell spectra, in different time points (10min, 30min, 2h and 6h). The statistically significant data are specified with p<0.05*, p<0.01**, and p<0.001*** in comparison to medium treated group. The results are specified as mean ± SEM. 62

Table 9: Numerical analysis of RNA content, by the use of differences in 915cm⁻¹ IR band areas of Medium, cpG ODN, A151 ODN, LPS and K3f ODN treated macrophage cell spectra, in different time points (10min, 30min, 2h and 6h). The statistically significant data are specified with p<0.05*, p<0.01**, and p<0.001*** in comparison to medium treated group. The results are specified as mean ± SEM.64

LIST OF FIGURES

FIGURES

Figure 1: The innate and adaptive immune system-cell repertoires (Dranoff, 2004)	2
Figure 2: The developmental journey of macrophage cells. The myeloid progenitor cell from bone marrow enters the blood, where it circulates before passing into tissues and become a tissue-specific macrophage cell such as a Kupffer cell (in liver tissue) or an Osteoclast cell (in bone tissue). (Amanda, 2009).....	4
Figure 3: The representative structure of bacterial LPS (Sigma-Aldrich, 2015)	8
Figure 4: Proteins employed in LPS reception: CD14, TLR4, and MD-2	8
Figure 5: The signal transduction cascade facilitated by the interaction of ligands with TLR's (O'Neill, 2013)	10
Figure 6: The structure of three main classes of cpg ODN's (invivogen, 2013).	18
Figure 7: Prospective therapeutic uses of cpg odns (Klinman, 2004).....	13
Figure 8: The illustration of the two components of electromagnetic radiation: electric field in red and magnetic field in blue. Amplitude is shown by A and wavelength by λ (Harvey, 2009)	17
Figure 9: The spectrum of light. The IR window with its components: NIR, MIR and FIR (Halifax Regional School Board, n.d.).....	18

Figure 10: Jablonksy energy diagram. It shows the excitation of molecules from ground to their excited states. Excitation occurs only if the energy of the striking photon, is equal to the change in the energy between the ground and excited states. (Harvey, 2009)	20
Figure 11: Energy-level diagram showing the vibrational transitions. A credible electronic transition is illustrated with a long arrow from the ground state to the first excited state and the short arrow showing a vibrational excitation in the vibrational levels of the ground state (Freifelder, 1982)	22
Figure 12: Dipole moment changes of a molecule. Bonds that are symmetrically stretched are IR-inactive since there is no change in the dipole moment of the molecule. The changing dipole in the antisymmetrically stretched bonds of the molecule makes it IR-active.	23
Figure 13: The illustration of common vibrational modes of molecules.	24
Figure 14: The schematic illustration of an ATR-FTIR instrument (Thomas, 2009).....	27
Figure 15: The corresponding bond types resulting from functional group vibrations over the spectrum (Jackson, 1996)	30
Figure 16: The effect of spectral resolution on the signal-to-noise ratio of ATR-FTIR spectra.....	37
Figure 17: The effect of subtraction method on the signal-to-noise ratio of ATR-FTIR spectra.....	37
Figure 18: Subtraction procedure. PBS recorded as a sample is subtracted from the sample spectra manually.....	38
Figure 19: The effect of cell concentration on the signal-to-noise ratio of ATR-FTIR spectra.....	38
Figure 20: The overview of data analysis procedures	39
Figure 21: A representative FTIR spectrum of murine macrophage cells with band assignments in $4000-400\text{cm}^{-1}$	44

Figure 22: The representative infrared spectra of control and treated (cpg, LPS, A151 and K3F) groups of murine macrophage RAW 264.7 cells in the 3000-2830 cm^{-1} region..... 48

Figure 23: The representative infrared spectra of control and treated (cpg, LPS, A151 and K3F) groups of murine macrophage RAW 264.7 cells in the 1800- 900 cm^{-1} region..... 49

Figure 24: ATR-FTIR difference spectra (treated-control). General view of the changes introduced on murine macrophage cells in 4000-650 cm^{-1} region..... 50

Figure 25: Histogram illustration of the saturated lipid content analysis by the use of differences in 1500 cm^{-1} IR band area ratio of Medium, cpg ODN, A151 ODN, LPS and K3f ODN treated macrophage cells, in different time points (10min, 30min, 2h and 6h)..... 52

Figure 26: Histogram illustration of the unsaturated lipid content analysis by the use of differences in 3014 cm^{-1} IR band area ratio of Medium, cpg ODN, A151 ODN, LPS and K3f ODN treated macrophage cells, in different time points (10min, 30min, 2h and 6h)..... 54

Figure 27: Histogram illustration of the cholesteryl ester and triglyceride content analysis by the use of differences in 1741 cm^{-1} and 1170 cm^{-1} IR band area ratio of Medium, cpg ODN, A151 ODN, LPS and K3f ODN treated macrophage cells, in different time points (10min, 30min, 2h and 6h)..... 56

Figure 28: Histogram illustration of the fatty acid content analysis by the use of differences in 1440 cm^{-1} IR band area ratio of Medium, cpg ODN, A151 ODN, LPS and K3f ODN treated macrophage cells, in different time points (10min, 30min, 2h and 6h)..... 57

Figure 29: Histogram illustration of the protein content analysis by the use of differences in 1640 cm^{-1} and 1543 cm^{-1} IR band area ratio of Medium, cpg ODN, A151 ODN, LPS and K3f ODN treated macrophage cells, in different time points (10min, 30min, 2h and 6h)..... 59

Figure 30: Histogram illustration of Amide I bandwidth analysis for conformational change on proteins..... 60

Figure 31: Histogram illustration of Amide I frequency analysis as indicator of conformational changes of proteins 60

Figure 32: Histogram illustration of the DNA content analysis by the use of differences in 1236 cm^{-1} , 1261 cm^{-1} , 1080 cm^{-1} and 1100 cm^{-1} IR band area ratio of Medium, cpg ODN, A151 ODN, LPS and K3f ODN treated macrophage cells, in different time points (10min, 30min, 2h and 6h)..... 63

Figure 33: Histogram illustration of the DNA-Z form content analysis by the use of differences in 925 cm^{-1} IR band area ratio of Medium, cpg ODN, A151 ODN, LPS and K3f ODN treated macrophage cells, in different time points (10min, 30min, 2h and 6h)..... 63

Figure 34: Histogram illustration of the RNA form content analysis by the use of differences in 915 cm^{-1} IR band area of Medium, cpg ODN, A151 ODN, LPS and K3f ODN treated macrophage cells, in different time points (10min, 30min, 2h and 6h)..... 65

Figure 35: Histogram illustration of the RNA to protein ratio form content analysis by the use of differences in 915 cm^{-1} IR band area to total protein ratio of Medium, cpg ODN, A151 ODN, LPS and K3f ODN treated macrophage cells, in different time points (10min, 30min, 2h and 6h).65

Figure 36: Histogram illustration of the membrane fluidity analysis by the use of differences in 2923 cm^{-1} and 2850 cm^{-1} IR bandwidth of Medium, cpg ODN, A151 ODN, LPS and K3f ODN treated macrophage cells, in different time points (10min, 30min, 2h and 6h).....66

Figure 37: Histogram illustration of the lipid to protein ratio form content analysis by the use of differences in total lipid bands' area to total protein bands' area ratio of Medium, cpg ODN, A151 ODN, LPS and K3f ODN treated macrophage cells, in different time points (10min, 30min, 2h and 6h)..... 67

Figure 38: Separation of murine macrophage samples by using Cluster Analysis, implemented on ATR-FTIR spectra smoothed in $4000-650\text{cm}^{-1}$ region with nine-point Savitsky-Golay. (A) Stimulated samples: Medium treated, K3 ODN and LPS. (B) Suppressed samples: Medium treated, K3f ODN and A151 ODN. All samples are separated successfully in different time points (10min, 30min, 2h and 6h).....69

Figure 39: Separation of murine macrophage samples by using Cluster Analysis, accomplished on all treatments' ATR-FTIR spectra smoothed in $4000-650\text{cm}^{-1}$ region with nine-point Savitsky-Golay”.....70

Figure 40: Separation of macrophage cell samples by using PCA analysis on the second derivative, vector normalized ATR-FTIR spectra in $4000-650\text{cm}^{-1}$ region with nine-point Savitsky-Golay smoothing. Five treatments: K3 CpG ODN, LPS, K3f ODN, and A151 ODN; are divided effectively on different time points (10min, 30min, 2h and 6h).”.....71

Figure 41: Separation of macrophage cell samples by using PCA analysis on the second derivative, vector normalized ATR-FTIR spectra in $4000-650\text{cm}^{-1}$ region with nine-point Savitsky-Golay smoothing. Five treatments: K3 CpG ODN, LPS, K3f ODN, and A151 ODN; are divided effectively on different time points (10min, 30min, 2h and 6h). *Medium treated group is denoted as “Unt”.....73

LIST OF ABBREVIATIONS

ODN	Oligodeoxynucleotide
FTIR	Fourier Transform Infra-Red
ATR	Attenuated total reflectance
TLR	Toll-like Receptor
PAMP	Pathogen Associated Molecular Pattern
EtOH	Ethanol
LPS	Lipopolysaccharide
DNA	Deoxyribonucleic Acid
IL-2	Inter Leukin-2
r.p.m.	Revolutions per minute
MyD88	Myeloid Differentiation primary-response gene 88

CHAPTER 1

Introduction

This thesis presents an ATR-FTIR biophysical study on the structural and functional evaluation of the changes on murine macrophage cells upon activation and suppression by immunotherapeutic oligodeoxynucleotides. Preceding the experimental part, this chapter gives detailed background information on the topics that the study is focused on. It starts by introducing the immunity system, macrophages as an important part of it, their activation and suppression, properties of light, spectroscopy as the study of light's interaction with matter, and ends with brief information on ATR-FTIR spectroscopy and its applications.

1.1. Immunity

Host defence against the pathogens is produced by the immunity system which constitutes of two components, both of which rely on the recognition of invading pathogens as non-self. These two components are innate and adaptive immunity (Takeda & Akira, 2005).

The "army" of adaptive immunity consists of B and T lymphocytes, by which an antigen-specific combat against the invading pathogens is mounted by the production of high-affinity antibodies to the antigens and cytotoxic T cells, respectively. Moreover, by producing the so-called memory T cells, these reactions provide a long-term and highly-specific protection to the organism

against the invading pathogen (Klinman, 2004). However, one drawback of this system is that the attack is accomplished in a period of 4-7 days after the pathogen has entered the body, which is an enough time-course for the pathogen to overwhelm the organism (Janeway, 2001). If we consider the fact that one bacterium alone, with a copying time of one hour in a complete driven infection, can give rise to 20 million copies in one day (Alberts B, 2002). Thus, the importance of innate immunity lies exactly here; with being the first line of defence, during the critical phases, it starts to combat the pathogens at the very first moments of their penetration to the body. The “army” of innate immunity consists of dendritic cells, macrophages, natural killer cells, mast cells and granulocytes (see Figure 1). These cells are able to recognize some common structures on pathogens, termed as Pathogen Associated Molecular Patterns (PAMPs) which are expressed by many pathogens (Medzhitov, 1998). These structures are ligands for the Toll-Like Receptors (TLRs) present on/in specific innate immune cells. In the presence of pathogen, by the accomplishment of PAMP-TLR interaction, innate immunity is activated and as a consequence of this, the production of pro-inflammatory cytokines, chemokines and poly-reactive IgM’s takes place. These reactions result in the prevention of proliferation of the infectious organisms *in vivo* (Klinman, 2004).

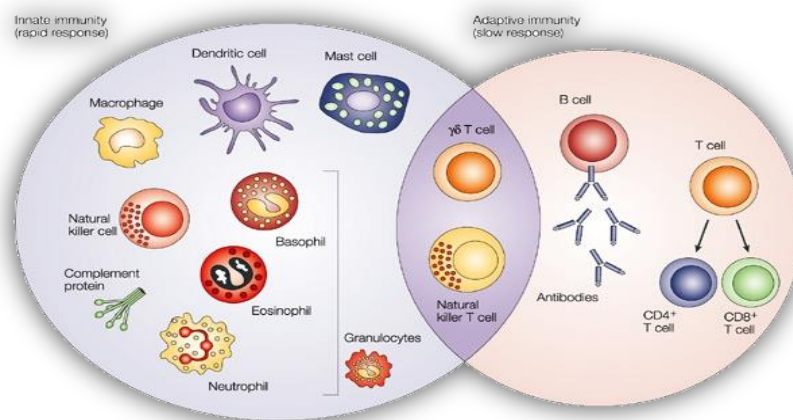


Figure 1: The innate and adaptive immune system-cell repertoires (Dranoff, 2004)

1.2. Macrophages

Once considered as having only the function of clearing the apoptotic cells and debris, macrophages are now gaining importance due to the newly discovered functions such as being one of the main professional antigen-presenting cells (APC) and phagocytic cells in the body. Macrophages belong to the mononuclear phagocytic system which is a group that is functionally different from other leukocytes. They are resident in many tissues and are involved in maintaining the steady-state homeostasis (Frederic, 2010). With considering all the services to defend the body, macrophages become one of the primary detectors and effectors of danger signals in the host organism.

1.2.1. Development and differentiation of macrophages

The patrolling monocytes that circulate in the bloodstream constitute 5–10% of the peripheral-blood leukocytes in humans. As seen in Figure 2, they develop from myeloid progenitor cells, which are common for other innate immune cells as well, such as dendritic cells, granulocytes and mast cells. The origin of common lymphoid progenitor cells are the pluripotent hematopoietic stem cells found in the bone marrow (Janeway, 2001). The monocytes with bone-marrow origin circulate in the peripheral blood and are in an inert state before migrating into different tissues to mature into cells with specific functions called macrophages (Volkman, 1965) which possess better phagocytic ability and longer half-life (Kumar, 2007). These cells show a considerable phenotypic heterogeneity. For example, the monocytes that migrate to bone tissues become bone-specific macrophages named as osteoclasts; the ones that mature in central nervous system are called microglia, the ones in liver are called Kupffer cells and this continues to all tissues in the body where macrophages are present. The phenotype that the macrophage differentiates depends on the microenvironment that it is found (Gordon & Taylor, 2005).

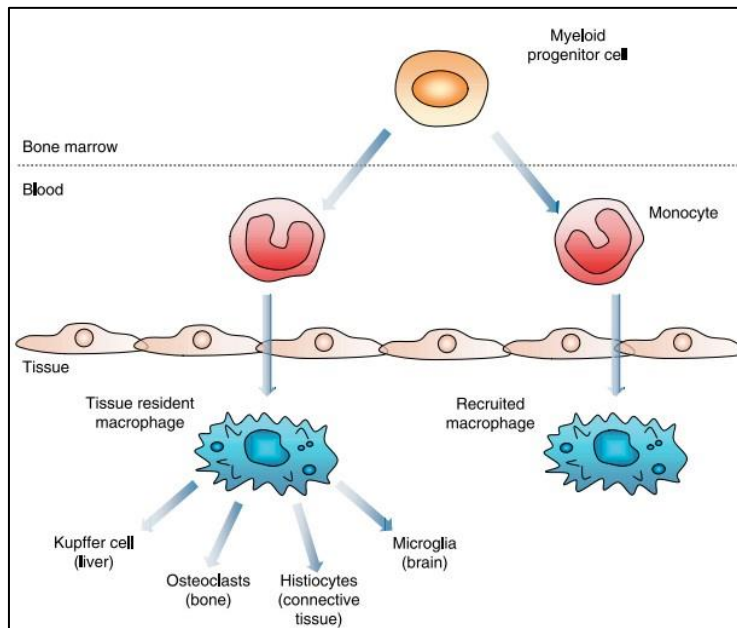


Figure 2: The developmental journey of macrophage cells. The myeloid progenitor cell from bone marrow enters the blood, where it circulates before passing into tissues and become a tissue-specific macrophage cell such as a Kupffer cell (in liver tissue) or an Osteoclast cell (in bone tissue). (Amanda, 2009)

1.2.2. Functions of macrophages

There are two main roles of macrophages in the body: to function as the leading phagocytic cells in the body, and participate as effector cells in immunity system. They always carry out phagocytosis as their first role, and when there is an infection they start the signal transduction processes to function as an innate effector cell. In their phagocytosing function, they clear the body from apoptotic cells, which has a great metabolic contribution to the host. For example, by phagocytosing 2×10^{11} erythrocytes every day, per year they recycle about three

kilograms of iron that is found in the hemoglobins of these erythrocytes. Thus, debris clearance and iron processing is very important and vital for the bodies' correct function. They also remove the cellular debris that is generated from necrotic cells and the remnants made during the re-modelling processes of tissues. (Mosser et al., 2011) Their second function is participating in the innate immunity as an effector cell. Macrophages are the residents of almost every tissue in the body (Siamon, 2003), and this is a property that fits to a cell which forms the first line of defense against infections. At the time the pathogen enters the organism, inflammatory monocytes from the blood leak into the tissue where the pathogen is present, and differentiates to macrophage cells. Recruitment of monocytes happens in 24-72 hours from the starting time of inflammation process (Ross, 2002). This migration and differentiation, marks their last stage in their maturation marathon that started from hematopoietic stem cell in the bone marrow. Crucial for inflammation, is the mounting of adaptive immune response, thus, macrophages play a key role in helping the activation of adaptive immunity as well. With being one member of the antigen-presenting cells, macrophages express almost all antigen-like proteins on their surface by the use of MHC class I and II proteins. Many works now published report that activated macrophages, in many aspects, were virtually as effective in antigen presentation as the best APCs, the dendritic cells (Guidos, 1987). When they encounter an antigen they migrate to the nearest lymphoid organ where they present the antigens on both MHC-I and II. This makes them help the naive T cells to proliferate and differentiate into activated lymphocytes (Pozzi, 2005; Grant, 1993). Infection is not the only stimulus that triggers the response of macrophages. They respond to danger signals from innate or adaptive immunity, damaged/stressed cells, injury or other homeostatic (Mosser, 2008). The detection of danger signals is followed by signal transduction through the adapter molecule, which in most cases is myeloid differentiation primary-response gene 88 (MyD88). With considering all these employments to defend the body, macrophages become one of the primary detectors of danger in the host.

1.3. Toll-like receptors (TLRs)

The innate immune reaction of the host against the invading pathogen starts from the recognition of specific structures located on pathogens by the receptors on/in the innate immune cells. Till late, the presence of such an interaction was known, but the details remained not elucidated. Researchers at the end of 20th century reported the presence of a receptor in *Drosophila Melanogaster*, which they called Toll, in the absence of which *Drosophila* were not able to respond to fungal infections (Takeda & Akira, 2005). The discovery of a homolog of this receptor in mammals, which later they named as TLR4 (Toll-Like Receptor 4), drew the attention of scientists to this family of receptors, since the lack of the TLR4 gene artefact in a mouse strain again made the mouse unable to respond to the infection (Fujihara et al., 2003). With these thorough studies, now it is clear that the innate immunity senses the invading pathogens by the use of Toll-Like Receptors, and that it is this interaction that later aids in the assistance of adaptive immunity to mount an antigen-specific attack. All toll-like receptors are transmembrane proteins present in either cell membrane or endosomal membranes. With their twelve well-known members in mammalian organisms, they are a still-growing family (Tong, 2012). These proteins are receptors for a diverse group of ligands that can be encountered from the threats, including LPS, DNA, and RNA (Fujihara et al., 2003). In the present study, TLR4 and TLR9 are of special interest, which are ligands for LPS and CpG DNA respectively. The signal transduction pathways of certain TLR members are visualized in Figure 4.

1.4. Common activators and suppressors of macrophages

The presence of PAMPs, marks the activation of monocytes to differentiate into macrophages. The PAMPs studied in our research are: CpG (which is a common activator functioning in boosting up the immunity), suppressive ODN (which lowers or stops the CpG induced immune activation), and LPS (which served as a positive control for CpG induced activation). A brief explanation of their origin and their effects on immunity cells is discussed in the subsequent part.

1.4.1. Lipopolysaccharide (LPS)

LPS (Lipopolysaccharide) is one of the main constituents of the cell wall of gram-negative bacteria with occupying approximately 75% of their external surface. This makes it the best indicator of bacterial infection in the body. An intact LPS generally has a molecular mass of 10-20 kDa (Sigma-Aldrich, 2015) and compositionally is made up by a complex glycolipid which is composed of two parts, the hydrophilic polysaccharide part and the hydrophobic lipid part (Qingye, 2011; Munford, 2007). A representative structure of LPS is given in Figure 3.

LPS stimulates the monocytes and macrophages to respond by releasing a wide variety of biological response mediators including platelet-activating factor, enzymes, free-radicals and a mix of pro-inflammatory cytokines, namely tumour necrosis factor- α (TNF- α), interleukin (IL)-1, IL-6, IL-8, and IL-12 (Raetz, 1990) (Cohen, 2002). As a result of these responses, microbial infection is prevented or delayed. The recognition process of LPS is carried out by three proteins, which are TLR4, CD14 and myeloid differentiation protein-2 (MD-2), altogether forming the LPS complex. (Fujihara et al., 2003) While in the serum, LPS binds to LPS binding protein (LBP), which transfers the LPS molecules to membrane-bound CD14 proteins which are positioned on monocytes and macrophages (Schumann et al., 1990).

After having a certain concentration of LPS, CD14 presents the LPS to TLR4-MD-2 complex which after understanding the LPS presence, start to transduce the signal through TLR4's cytoplasmic TIR-domain. The signalling cascade mediated by TLR4 continues by the use of three adapter proteins; namely, MyD88, TIRAP and TRIF, and ends in the nucleus with the expression of new genes (Fujihara et al., 2003). This pathway is visualized in Figure 4. In our study, we used LPS as a positive control for the activation of macrophage cells by CpG ODN's.

1.4.2. CpG motif containing DNA

Bacterial DNA is a well-known PAMP with a distinctive property of having un-methylated CpG-rich motifs in composition (Medzhitov, 1998). Un-methylated CpG motifs are at least twenty times less frequent in the composition of prokaryotic cells than in that of eukaryotic cells. This is partly due to the difference in the methylation process and the consumption of CpG dinucleotides in prokaryotes (Razin, 1981). These un-methylated motifs serve as danger signals for the body's immunity system and have many complex effects, such as: the maturation and proliferation of macrophages, dendritic cells and NK cells, as well as

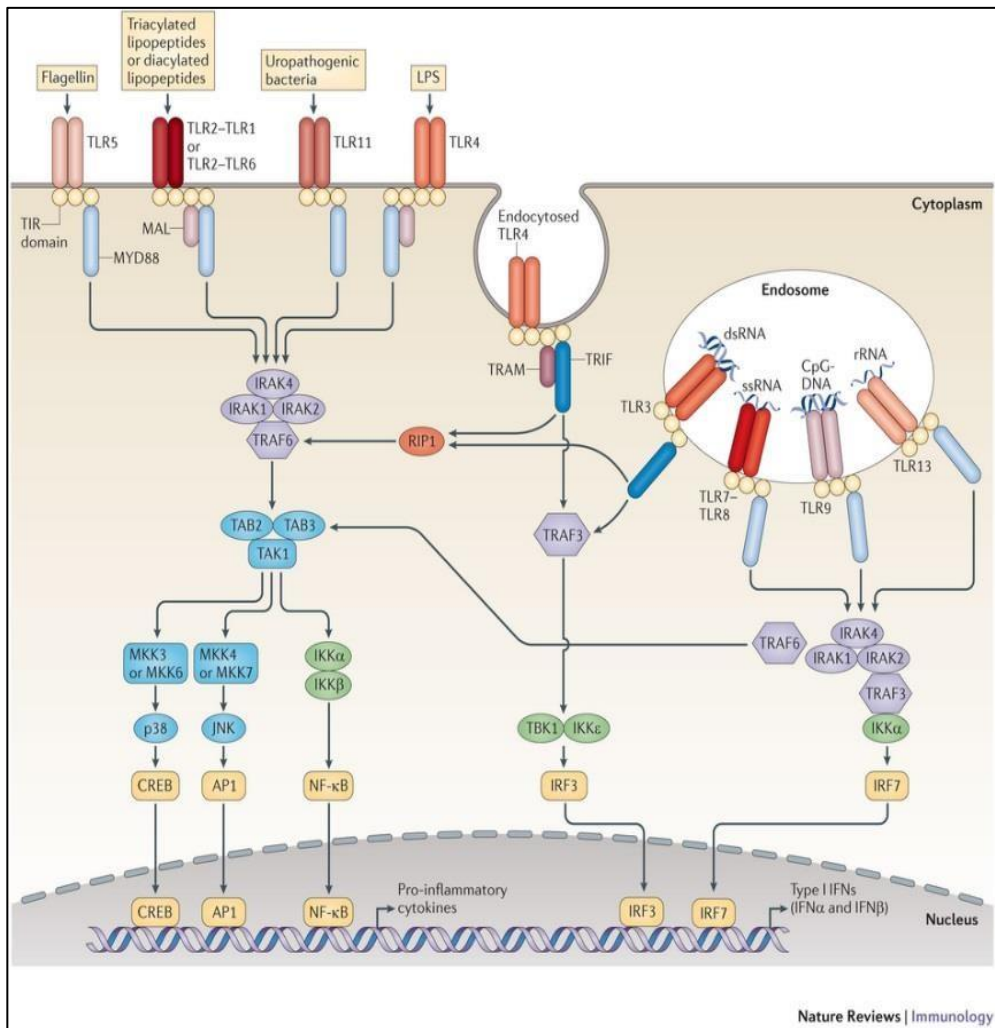


Figure 5: The signal transduction cascade facilitated by the interaction of ligands with TLR's (O'Neill, 2013) and the stimulation of them to secrete cytokines, chemokines and Ig's.

In humans, B cells plasmacytoid dendritic cells (pDC) and alveolar macrophage cells (Esmeralda Juarez, 2010) having the toll-like receptor 9 (TLR9) expressed, are able to recognize the CpG ODNs (Mayda, 2013). The un-methylated CpG motifs are quickly internalized by the innate immunity cells and sensed by TLR9 proteins that are present in endosomal membranes (Hemmi, 2000; Takeshita, 2001). This interaction is a high-affinity interaction which results in the acidification of the endosomal vesicles and the production of reactive oxygen species (ROS) (Yi, 1991). The events that lead to endosomal acidification play a critical role since a potential inhibition in these events can lead to a blockage in immune activation (Hacker, 1998). It is exactly this process that leads the cascade to the induction of a signal transduction process which employs MYD88, IRAK and TRAF6 agents (Hacker, 2000), to activate many transcription factors such as NF-KB and AP1. This pathway is described visually in Figure 5. It is exactly this cascade that serves to up-regulate the pro-inflammatory cytokines/chemokines such as IL-1, IL-6, IL-8, TNF-alpha and IFN-gamma, IL-12 which favor TH1 immunity (Raetz, 1990; Cohen, 2002).

1.4.3. Synthetic CpG oligodeoxynucleotide

The response that immune cells show upon stimulation with bacterial DNA is similar to the one that they show when stimulated with synthetic oligodeoxynucleotides (ODN) containing CpG motifs. As many studies reported, the activity of bacterial DNA is mimicked by the synthetic ones (Mayda G. I., 2006; Yamamoto, 1992); thus, this gives a clue on the probability of using them as potential therapeutic agents. As reviewed in the literature, the CpG ODN that is optimal for stimulation in humans and some other species is TCGTT and/or TCGTA (Klinman, 2004). The most rapid response was accomplished by the hexameric motifs that have two purines flanking at the 5'end, a central un-methylated CpG and two pyrimidines at the 3'end (M. Klinman, 1999). Depending on their activity on human PBMCs, three classes of CpD ODNs are recognized: A (Type D), B (Type K) and C (InvivoGen, 2013). The structure of them is visualized in Figure 6.

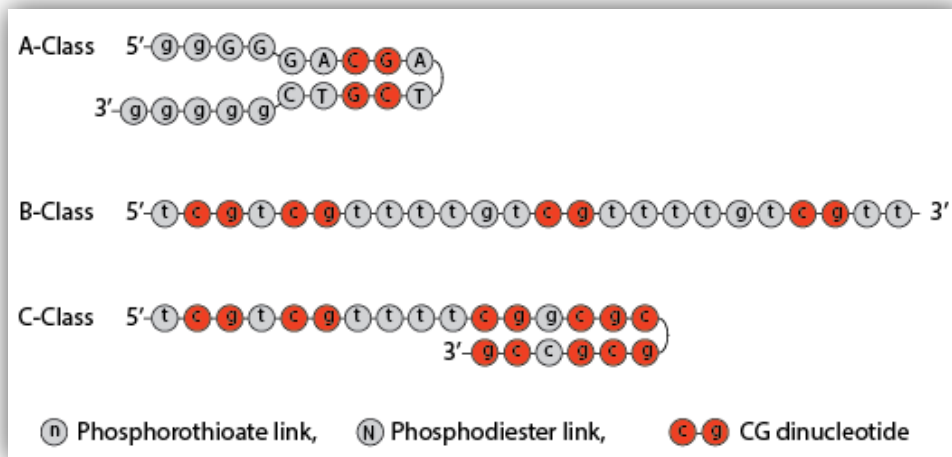


Figure 6: The structure of three main classes of CpG ODN's (InvivoGen, 2013)

One potential application as immunotherapeutic is the use of CpG ODN to protect the host from pathogens by boosting up the innate immunity. The mice that have a pre-administered dose of CpG ODN, were shown to be protected against the great lethal amounts of live vaccine pathogens. The inverted CpG ODNs removed this protection (Elkins, 1999). This immune resistance was found to be persistent for approximately two weeks (Krieg A. M., 1998) and was giving the best protection optimally in 2-3 days (Elkins, 1999). This effect is especially important in patients who have suppressed immunity such as pregnant women and new-born babies, in which CpG ODN administration has proven results in their protection (Ito, 2004). Another potential application of CpG ODN as an immunotherapeutic agent is being a vaccine adjuvant (Elkins, 1999). This is accomplished by assisting the production of TH1, cytokines/chemokines and by inducing the antigen presenting cells to mature and proliferate. In this manner, the administration of CpG ODN prepares the immune milieu for the co-administered antigens. Still another application of CpG ODN can be the prevention of allergy, achieved by stimulating TH1 cell development rather than that of TH2 (Klinman, 2004). Broadly these applications are visualized in Figure 7.

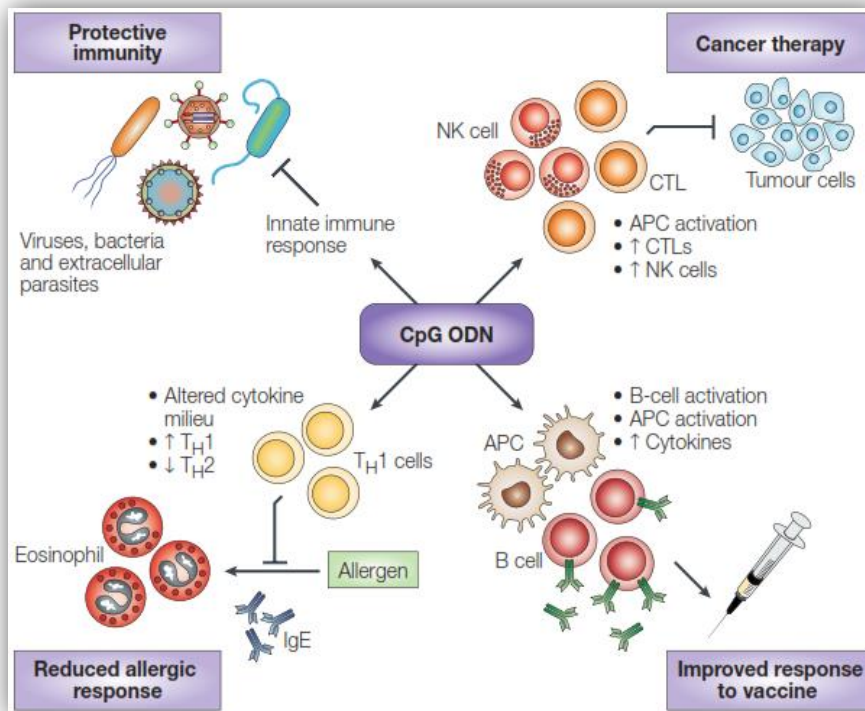


Figure 7: Prospective therapeutic uses of CpG ODNs (Klinman, 2004)

Although there are numerous advantages on the use of CpG ODNs as immune therapies, recent studies report the presence of some safety issues raised with their clinical use (Karbach, 2012). One of these concerns is the trigger of systemic and organ-specific autoimmune diseases by increasing the immunogenicity of self- proteins, and another concern is the induction of toxic shock by increasing the susceptibility of the host to some certain pathogenic agents which can be life-threatening (Bode, 2011). CpG ODN can also tilt the Th1/Th2 cytokine equilibrium and thus produce an altered immune setting (Daniela Verthelyi, 2002). Some studies report that these safety concerns can also have deleterious concerns by the production of cytokines like TNF-alpha in massive amounts, and that overall these issues can extend till the death of the organism (Yamada, 2002)

1.4.4. Suppressive oligodeoxynucleotide

The immune boost that CpG ODN originates on macrophages can be blocked either by the removal of the CpG ODN from the system or by the use of suppressive ODNs which are developed as blocking agents to the activation caused by CpG ODNs (Klinman D., 2003). The first group to report the observation were Krieg et al., who found that certain adenoviral DNA sequences had counteracting effects on the activation by CpG ODNs, by a process that reduced the adjuvant impact of CpG and hampered the cytokine production (Krieg et al., 1998). Many subsequent studies reported the presence of still different motifs that inhibit the actions of CpG ODNs (Peter M., 2008) (Yamada H., 2004). Such findings have shown that methylated CG motifs, telomeric DNA repetitions and poly-G rich sequences had the same effect on suppressing the CpG activation effect (Hidekazu, 2005). However, all these inhibitions were acting in multiple forms and they were non-specific for TLR-9. Recently, Lenert et al. found that GGG sequence headed by pyrimidine triplets inhibits TLR-9 in a specific manner (Lenert, 2005). This work was confirmed by other researchers as well, who analysed the kinetics and mode of action of the inhibition (Yamada, 2002). Both suppressive and stimulatory ODNs bind to and interact with the same cells and same receptors. When administered at the same time, suppressive ODNs tend to be dominant over stimulatory ones. When present at the same strand, the direction of recognition is 5' to 3' (Yamada, 2002).

1.5. Macromolecular changes at various stages following the activation of macrophages

Just as one cannot assign a colour to chameleons, there is an analogous difficulty to assign a certain physiology to macrophages. This is due to the extreme plasticity that they possess. They can successfully respond to the signals coming from their environment and change their phenotype accordingly (Mosser et al., 2011). We can study these responses in two phases: short term and long term. The early, short-term changes that occur just after the infection, include the ones in the cell membrane (specifically, the lipid structure), changes in the protein phosphorylation patterns, in the translocation of proteins (Kopydlowski et al., 1999), and changes in the release of proteins to the extracellular environment (Kathleen et al., 2004). Such changes that occur in the very first seconds or minutes upon activation were studied by Wood et al. in the 800-1800 cm^{-1} spectral region by FTIR spectroscopy. Within 15 minutes of activation, they observed increment in phosphate bands that are distinguishing patterns of nucleic acids and phosphorylated proteins. They also reported increase in the intensity of the bands specific to DNA and RNA ribose C-O vibrations (Wood et al., 2000). In long term, the changes that take place on macrophages upon activation are directed towards the production of different chemicals like chemokines which serve as attractants to more cells, cytokines which serve as signalling molecules and some effector molecules like nitric oxide and defensins that serve as effector molecules upon the invading pathogens. Wood et al. observed new bands attributed to RNA ribose moieties after a one-two hour period of time after stimulation and overall, the long term events include a 6h period after the infection occurs, resulting in the up- regulation of the transcription of RNAs and the translation of new proteins (Timlin et al., 2002). Both short and long term changes that occur upon infection are expected to have huge molecular indications in the infrared spectrum of these cells. Thus, the FTIR comparison study of the resting versus activated/suppressed macrophage cells can enlighten our knowledge on many aspects of activation/suppression that were not known till now.

1.6. Electromagnetic (EM) radiation

Electromagnetic Radiation (Light) has a dual nature. It can behave as a wave and as a corpuscle. When traveling in space, light is a wave that consists of two components: the electric field E and magnetic field B , present at different planes and oscillating at perpendicular angles to each other (Stuart, 1997). The plane polarized light wave is represented in Figure 8, where the oscillating electric field is the red wave and the oscillating magnetic field is the blue wave.

Since light is also a beam of energetic particles called photons, it can show the properties of a corpuscle when striking the matter. The properties that make it become a corpuscle are considered to be the possession of a certain energy E , mass m , momentum I , wavelength λ and wavenumber ν (Ronto, 1999). The relation between these parameters of light can be well expressed by the equations:

$$\Delta E = h \cdot \nu - \text{Bohr's Equation}$$

Where by $\bar{\nu} = \frac{1}{\lambda}$ the formula of energy becomes,

$$E = h\nu = \frac{hc}{\lambda} = hc\bar{\nu}$$

Momentum can be calculated by $I = \frac{h \cdot \nu}{c} = \frac{h}{\lambda}$

And mass by: $m = \frac{h \cdot \nu}{c^2}$

Where h is Planck's constant ($h=6.63 \times 10^{-34} \text{ Js}$) and c is the speed of light in vacuum ($c=3 \times 10^8 \text{ ms}^{-1}$). Wavenumber is the reciprocal of wavelength and is a crucial spectroscopic unit, especially in infrared radiation, with the units given in cm^{-1} . If we plot the energy absorbed by the atomic structure versus λ , ν or $\bar{\nu}$, we obtain a spectrum. A representative spectrum is shown in Figure 21 on page 50.

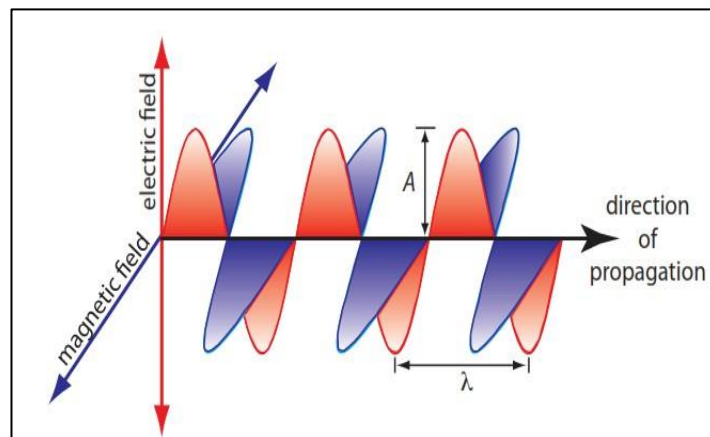


Figure 8: The illustration of the two components of electromagnetic radiation: electric field in red and magnetic field in blue. Amplitude is shown by A and wavelength by λ (Harvey, 2009)

1.6.1. Electromagnetic spectrum

There is a difference of many orders in the magnitude of light in frequency and wavelength throughout the spectrum. This is the reason behind the division of electromagnetic radiation into different regions, making up the so-called electromagnetic spectrum. While the EM spectrum seems to have a continuum, it has some boundaries between its constituting regions which are not rigid, and overlap with each other (Keeler J., 2014). The infrared region of the spectrum has a range from 0.78 μm to 1000 μm (see Figure 9). It is further divided into three components namely, NIR (near infrared) found in the 14000-4000 cm^{-1} wavenumber region, MIR (mid infrared) found in the 4000-400 cm^{-1} region and FIR (far infrared regions) found in the 400-4 cm^{-1} region of the infrared spectrum (Smith, 1999).

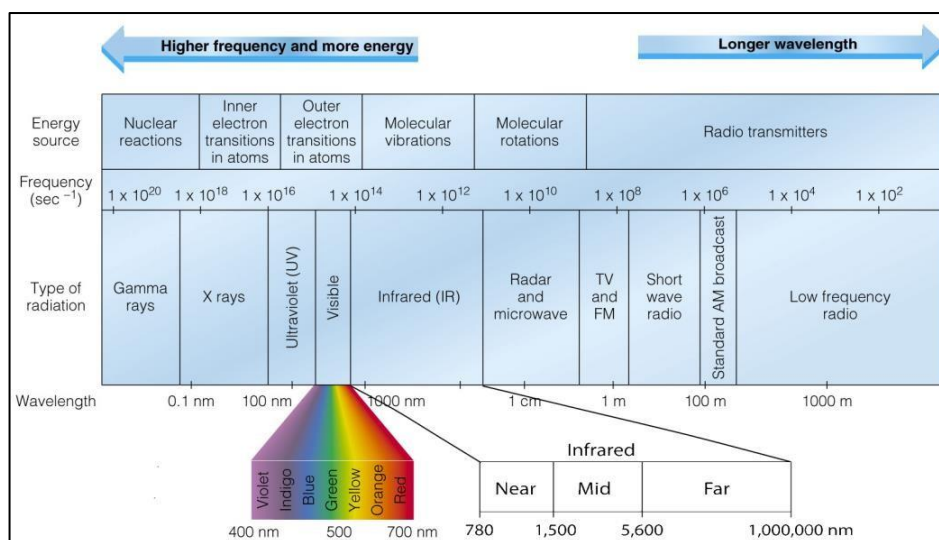


Figure 9: The spectrum of light. The IR window with its components: NIR, MIR and FIR (Halifax Regional School Board, n.d.)

1.7. Spectroscopy

Spectroscopy is the study of the interaction of light with matter. Light can have one of three possible fates following such an interaction:

1. Can be scattered, where the frequency of the scattered wave is same but the direction of propagation changes.
2. Can be emitted, where the energy of the wave is transferred to the atomic system, which is excited from the ground state to the excited state, and during the relaxation process it emits a radiation of different wavelength.
3. Can be absorbed, where the energy of the incident light is transferred to the atomic system (Ronto, 1999)

If absorption takes place, the energy is transferred to the system and the quantum configuration of the atomic systems changes. The simplified energy diagram for the transition of molecules from ground state to an excited state is shown in Figure 10. These transitions occur with defined regulations and are studied by quantum mechanics. According to the principles of quantum mechanics, the electrons of the atomic systems cannot have arbitrary states; they have quantized values (Campbell, 1984). These values correspond to the energy levels that are defined by discrete numbers (Ronto, 1999).

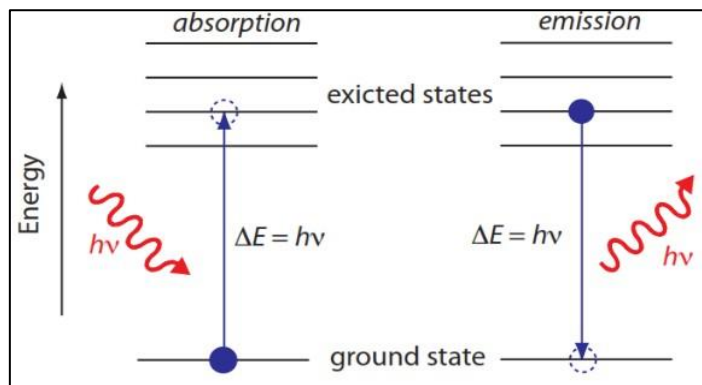


Figure 10: Jablonsky energy diagram. It shows the excitation of molecules from ground to their excited states. Excitation occurs only if the energy of the striking photon is equal to the change in the energy between the ground and excited states. (Harvey, 2009)

The total energy that molecules possess can be summarized in the equation:

$$E_{\text{total}} = E_{\text{transition}} + E_{\text{rotation}} + E_{\text{vibration}} + E_{\text{electronic}} + E_{\text{electron spin orientation}} + E_{\text{nuclear spin orientation}}$$

At the temperatures above absolute zero, all the atoms in molecules are in continuous motion. When a light interacting with the matter transfers extra energy to this system, the molecule is said to be excited and at least one of these energies associated with certain motions of the molecule undergo changes (Campbell et al., 1984). The way of excitation is wavelength-dependent. For example, if the interacting radiation is from the ultraviolet-visible region of the spectrum, the molecule will undergo a change in its electronic energy, since the UV light has an energy that can change electronic energy of the atomic system.

The light from microwave region changes the rotational energy. Etransition, Eelectron spin orientation and Enuclear spin orientation are negligible since the separation between the energy levels that they correspond are very small (Freifelder, 1982).

The types of molecular transitions, the regions of EM spectrum involved in the energy transfer and the spectroscopic techniques used are presented in Table 1.

Table 1: Molecular transitions in different EM regions with their corresponding spectroscopic methods used. [Modified from (Harvey, 2009)].

Energy Transfer	Region	Technique	Molecular transition	
Absorption	γ -ray	Mossbauer spectroscopy	Nuclear	
	X-ray	X-ray absorption spectroscopy	Core-level electrons	
	UV/Vis	UV/Vis spectroscopy	Atomic absorption spectroscopy	Valence electrons
	IR	Infrared spectroscopy	Raman spectroscopy	Molecular Vibrations
	Microwave	Microwave spectroscopy	Molecular rotations electron spins	
	Radio wave	Electron spin resonance spectroscopy	Nuclear magnetic resonance spectroscopy	Nuclear spins

1.7.1. IR spectroscopy

In IR spectroscopy the light that interacts with atomic system is from the infrared region. This interaction is followed by a change in the vibrational and rotational energy of the atomic system, since the energy of the interacting infrared is enough to excite the molecule at its vibrational and rotational levels. The transitions of this nature are generally studied by an energy-level diagram where the ground state and the excited states are shown. Vibrational levels are shown as thin horizontal lines. Possible electronic transitions to the vibrational levels of the excited states or in the ground state itself are specified by arrows (Freifelder, 1982). A typical energy-level diagram of a molecule undergoing electronic and vibrational transitions is shown in Figure 11.

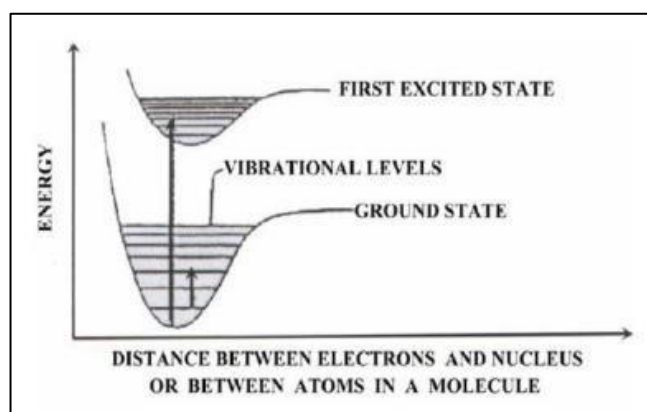


Figure 11: Energy-level diagram showing the vibrational transitions. A credible electronic transition is illustrated with a long arrow from the ground state to the first excited state and the short arrow showing a vibrational excitation in the vibrational levels of the ground state (Freifelder, 1982)

The absorption of IR light by the matter is challenged by the restriction from dipole moment of the covalent bonds of the molecule (see Figure 12). One covalent bond must undergo a change in its dipole moment as a consequence of its rotational or vibrational motion to become IR-active and absorb the energy released by the prominent photon (Siebert et al., 2008).



Figure 12: Dipole moment changes of a molecule. Bonds that are symmetrically stretched are IR-inactive since there is no change in the dipole moment of the molecule. The changing dipole in the antisymmetrically stretched bonds of the molecule makes it IR-active.

There are only few compounds that show pure rotational bands, this is why the IR spectroscopy deals more with the vibrational absorption bands. If we consider the bonds as having two parameters, the bond length and angle, we divide the vibrations into two groups: stretching and bending vibrations, respectively. Stretching can be of symmetric or anti-symmetric nature (Siebert et al., 2008) and bending can be of scissoring, rocking, wagging and twisting nature (Arrondo, 1993) (see Figure 13).

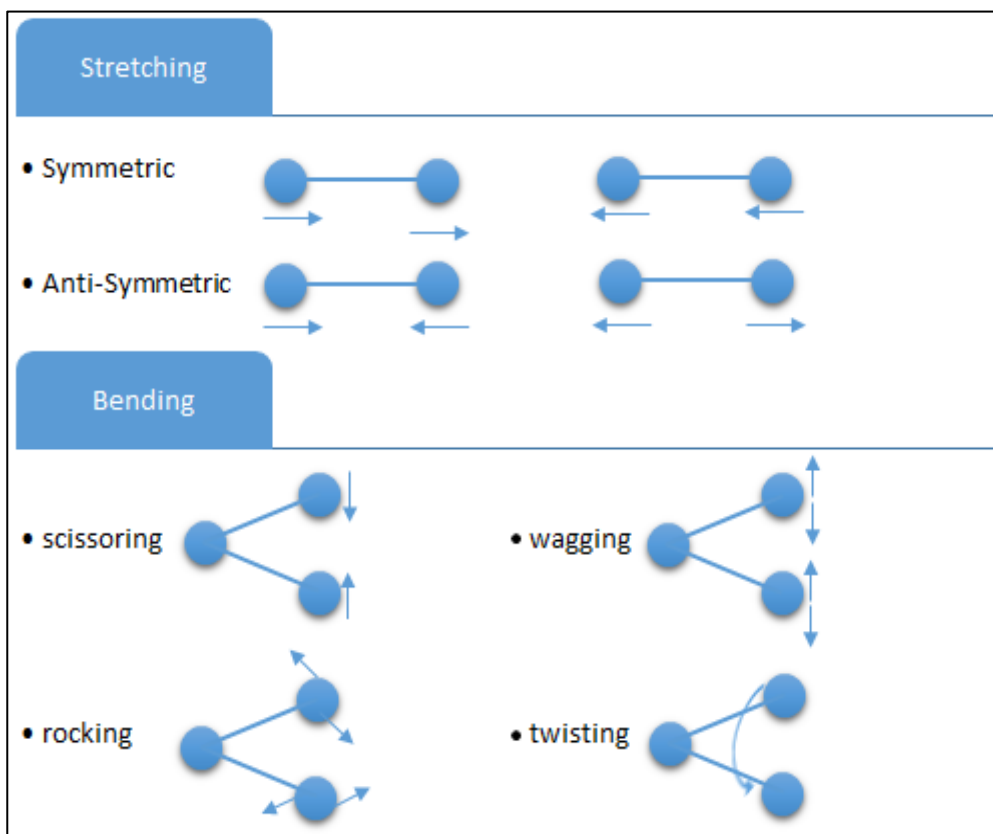


Figure 13: The illustration of common vibrational modes of molecules.

Weak/absent bands in IR spectrum can be found by another spectroscopic technique called Raman spectroscopy. Since the selection rules for Raman and IR complement each other, Raman Spectroscopy is used sometimes as a potential tool to detect vibrations that are absent in the IR spectrum of the compound. The intensity of bands are in inverse relation; prominent vibrations in an IR spectrum [ex. Molecules with polar bonds (e.g. C-H, C-Cl and C=O) and/or strong dipole moments] show low intensity absorption in a Raman spectrum, and vice-versa.

Therefore, in order to find the bonds that show little or no signals in the IR spectrum such as symmetrical vibrations and double or triple C-C stretching vibrations, one can use the Raman spectrum (McClain, 2000). The infrared spectrum contains the information on the total chemical composition of the functional groups that absorb the IR radiation. Since each molecular vibration has a corresponding discrete energy, a unique IR absorption band will be present for each functional group that is present in the matter that is exposed to IR radiation (Aksoy C., 2012). The highly complex IR absorption spectrum, is produced when the vibrations occurring on a portion of time are measured simultaneously and plotted as absorption VS wavenumber (ν) which is expressed in cm^{-1} . The absorption intensity should be high enough to follow the Beer-Lambert Law, in order to be able to use the data in quantitative studies for concentration. Beer-Lambert Law defines the attenuation of light when travelling through chemicals.

Simply, the law is explained by the equation:

$$A = \log_{10} \frac{I_0}{I} = \epsilon * l * c$$

where A is absorbance, I is the final light intensity, I_0 is the incident light intensity, l is the path length which the light passes, E is the absorptivity constant and c is the concentration of the desired chemical.

As clearly seen, the absorbance is directly related to the concentration of the chemical, so the absorbance value can be used to calculate the concentration. Limitations in the use of law however exist. In very high and very low chemical concentrations, the electrostatic forces between the molecules interact to the results, as the linearity changes, and this introduces alterations on absorptivity constant (Pearson, 2015).

There are no compounds that produce exactly the same IR spectrum, since all of them are different in composition. This is why the IR spectrum is considered to be the exact molecular fingerprint of the tissues or cells (Kan-Zhi Liu, 2007).

1.7.2. Basic principles of Fourier Transformation Infra-Red (FTIR) spectroscopy

In IR spectroscopy involving Fourier Transformation, the incoming light containing different frequencies is split into two pathways using a beam splitter. The beams continue their way to detector by being reflected at one of the mirrors: the movable or fixed one, and ultimately are merged at the beam splitter again. This resultant beam is passed to the sample and finally to the detector as a signal that is expressed in units of distance or time and displays the intensity as a function of the moving mirror's position. The final signal is a time-domain spectrum that is also named as an interferogram (AirUCI, 2014). It is processed mathematically in a Fourier transformation procedure and converted to a spectrum. This calculation is done point by point and results in a final spectrum that is a frequency-dependent transmission spectrum of the sample.

Overall, two spectra are obtained. One from the sample through an interferometer (which is generally a Michelson Interferometer) and the other being a background spectrum without the sample (Stuart, 2004).

Since the FTIR instrument has only one optical path, there is a need to compensate for the absorbance of atmospheric CO₂ and H₂O vapour. This is done by keeping the background spectrum in the computer that the instrument is linked, and later using it in the ratio-taking process done between the background and the final Fourier transformed spectra recorded from the sample (Harvey, 2009). See the Figure 14 below for the schematic representation of an FTIR instrument.

1.7.3. Attenuated Total Reflectance (ATR)-FTIR

In Attenuated Total Reflection, the changes that are done on an IR beam, upon the interaction with sample placed on a basement over the totally internally reflected environment, are measured (Thomas, 2009). The main components of an ATR-FTIR instrument are represented in Figure 14.

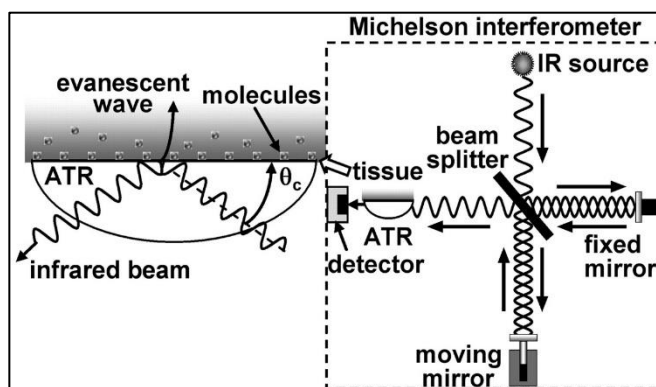


Figure 14: The schematic illustration of an ATR-FTIR instrument (Thomas, 2009)

In order to obtain an internal reflectance, the IR beam hits a crystal that has a high refractive index. This is accomplished at a certain angle so that the IR bubble that is internally reflected extends beyond the crystal surface for few microns, where the sample is in contact with the crystal. The interaction of the evanescent IR ray and the sample induces changes and attenuations on the incident IR ray which is directed to the detector of the FTIR apparatus. The result is the IR spectrum being produced (PerkinElmer, 2005).

One constraint of IR spectroscopy is the absorbance of IR by water molecules which interfere with the results and thus limit the use of IR spectroscopy in probing cells in aqueous solution. Traditionally, to study water-containing materials, transmission studies were carried where the sample would had to be 10-20 micrometres or less in thickness. This challenged the sample preparation steps (Aksoy C., 2012).

However, the development of Attenuated Total Reflectance (ATR) unit, made an alternative for the study of aqueous solutions. By settling onto the crystal, the cells placed on an ATR plate eliminate the majority of the bulk water from the crystal surface. Since the evanescent wave of the ATR unit can penetrate only a few micrometres above the crystal surface, the cells are sampled without much interference from the bulk water. The live bacterial studies of Kardas (Kardas M. A. G., 2014), the characterization of human cervical cells by Wong et al. (Wong, 1995), stem cell studies of Aksoy and Severcan (Aksoy C., 2012), the classification of plant species by Demir (Demir P. S. O., 2012), have shown that ATR-FTIR is a successful method that allows the study of materials in aqueous solution.

1.7.4. Advantages of ATR-FTIR

In this study, the technique used was FT-IR spectroscopy since as in various hematologic studies it has many advantages. Some of these advantages are listed below.

- 1) There are no requirements to chemically pre-treat the sample
- 2) The state of the sample is not important. It can be solid, liquid or gaseous.
- 3) The IR light does not introduce changes to the sample, is non-destructive for functional and structural experiments (Haris and Severcan, 1999; Melin, 2000; Cakmak, 2003). Thus, the sample can be used for subsequent analysis.
- 4) A little amount of sample is enough (i.e. microliters of sample) (Mendelsohn R. a., 1986)
- 5) Measurements are not time consuming. This is called as Fellgett's advantage. All the frequencies are sensed simultaneously by the detector. Thus the time needed to obtain one whole spectrum is almost one second. (Harvey, 2009)
- 6) Measurements are not material limited (almost all biological tissues and many materials can be reused)
- 7) Little training is needed for the user of the equipment.
- 8) Produces a low-noise spectrum. This is termed as Jacquinot's advantage, where by an output of radiation reaching the detector that is 80–200× greater than that for a monochromator, FTIR result in a spectrum with less noise (Harvey, 2009).
- 9) The calibration of the interference information is done by a laser; this ensures high wavenumber accuracy (Babrah, 2009).
- 10) Qualitative and quantitative interpretation of the results is possible
- 11) From a single spectrum all changes in the functional groups can be detected instantaneously (Kneipp, 2000; Bozkurt, 2007; Garip, 2007)

1.7.5. Applications of FTIR spectroscopy

The infrared spectrum contains information on the total chemical composition of the functional groups that absorb the IR radiation, inversely expressed; any functional group or bond in a molecule has a corresponding band in the IR spectrum. Thus, biologically important macromolecules such as proteins, lipids, nucleic acids and carbohydrates altogether can be detected in an IR spectrum (Fabian, 1995; Moore, 1995; Toyran, 2004; Toyran et al., 2005; Akkas, 2007). This constitutes one great advantage of FTIR. Even though molecular vibrations specific to different molecules can be found all-along the IR spectrum (see Figure 15), most of the analytically important IR bands are confined to the ones in the 1800 and 400 cm^{-1} region (Stuart, 1997).

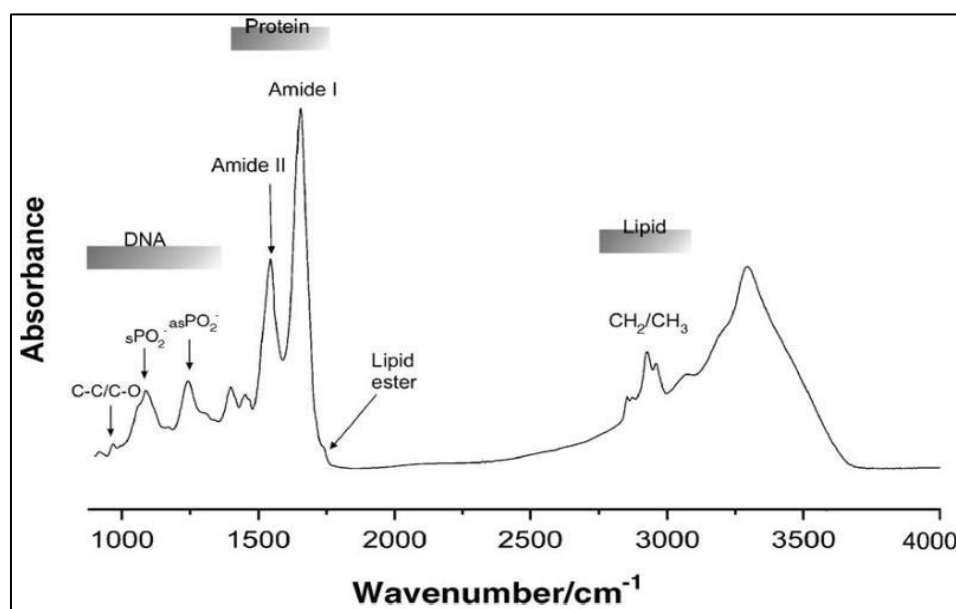


Figure 15: The corresponding bond types resulting from functional group vibrations over the spectrum (Jackson, 1996)

The properties of an IR Spectrum that are studied and analyzed in order to obtain information are: frequency shifts, peak heights, the area under the peaks, half widths and integrated intensities of the vibrational bands (Lamba, 1991). Briefly, bond intensity gives quantitative information, the wavenumber of the peak decides the bond type, and changes in the wavenumber explain changes in the structure and/or the molecular environment that they are in (Liu K., 2005).

Nowadays, these properties of the IR spectrum are used in many applications in many sciences. Broadly, in biomedical sciences FTIR is used in the detection and classification of the changes related with disease states including cancer (Ozek, 2010), obesity and diabetes (Lin, 1997; Severcan, 2000; Severcan, 2003; Severcan, 2010); in the quantification of chemicals and in the identification of microorganisms (Garip, 2007). Moreover, FTIR can be used in apoptosis detection (Gasparri, 2003), cellular destruction indication (Perromat, 2001), membrane lipid studies (such as lipid phase transitions (Mendelsohn & Mantsch, 1986), gauche conformers (Severcan, 1995), fatty acid chain order and mobility calculations (Severcan, 1997), freedom in motion calculation (Boyar & Severcan, 1997) etc.) and in protein structure determination (Severcan & Haris, 2003).

In hematology, FTIR is used to study the order of the phospholipids of RBC membranes (Kucuk, 1992); the protein structure of hemoglobin (Liu, 2003); platelet membrane fluidity (Watala, 1998); to differentiate leukemic cells from normal ones (Schultz C. K., 1996), chemotherapy assessment (Ramesh, 2002) and to predict the drug resistance in leukemia cells (Gaigneaux, 2002).

1.8. Aim of the study

Macrophages have significant flexibility that allows them to powerfully respond to environmental signals. The changes in their structure and physiology can be strikingly altered by both their innate and adaptive immune functions.

With a wide repertoire of PAMPs, macrophages are able to sense many microbial danger signals, and amongst them of bacterial DNA. It is the un-methylated CpG-motif containing DNA that specifically is well-known for the stimulation of macrophages to produce the powerful pro-inflammatory agents such as cytokines, chemokines and Ig's. These actions induced on macrophages by CpG DNA, boost up the innate immunity which in turn is potentially used in many immunotherapeutic therapies. But, although there are numerous advantages on the use of CpG ODNs as immune therapies, recent studies report the presence of some serious safety issues raised with their clinical use. Due to their long-lasting activity, allergy, toxic shock and moreover the death of the organism is reported. The need for a suppressive agent led to the discovery of the suppressive ODNs, which are able to inhibit the stimulation of macrophages directed by CpG DNA. However, the exact mode of inhibition has not been elucidated yet.

The confusing variety of ODN sequences and structures reported to activate and inhibit TLR-9 signalling, makes it challenging to compare the published studies on the effect of them on macrophage immunity.

Certainly, there is a need for the comparison of global changes rather than the specific ones, and this can be done by a method such as Fourier transform infrared spectroscopy. The responses that occur upon activation and suppression of macrophages are expected to have large molecular signals in the infrared spectral region that can be traced with FTIR spectroscopy.

In this study, FTIR Spectroscopy is used to evaluate the global macromolecular changes that occur on macrophages upon their activation by stimulatory CpG ODNs and their suppression with suppressive ODNs.

CHAPTER 2

MATERIALS AND METHODS

2.1. Materials

In our study the following ODNs were used: immunostimulatory K3 CpG ODN (ATCGACTCTCGAGCGTTCTC), suppressive ODNA151 (TTAGGGTTAGGG TTAGGGTTAGGG), and negative control K3 Flip-ODN (ATGCACTCTGC AGGCTTCTC).

2.2. Growth, stimulation and preparation of cells

To perform a relative FTIR study, cell line of homogeneous cell populations was used. This ensures an unlimited supply of cells. Murine macrophage-like cell line (RAW 264.7) was provided by Bilkent University (Ankara, TR). The cells were grown at 37°C with 5% CO₂. The medium was RPMI 1640, containing 10% fetal bovine serum, 2 mM L-glutamine. The incubator used in the study was Benchtop Caron's Oasis™ CO₂/O₂ Incubator. To maintain a logarithmic growth, cells were sub-cultured in 1/10 ratio upon reaching the acceptable confluency that was accomplished generally every 2-3 days.

Cells were harvested, spun at 1000 rpm 208g for 10 min, and re-suspended in 20 ml of culture media and counted by hematocytometer. The cell number was adjusted to $2 \cdot 10^6/\mu\text{L}$.

Five different groups were prepared:

1. Medium treated group
2. K3 CpG ODN stimulated group: (containing 1M of K3 ODN as final concentration.)
3. Lipopolysaccharide (LPS) stimulated positive control group: (Having 0.5g/mL of LPS as final concentration)
4. Suppressive ODN151 containing group: having 1M of suppressive ODN as final concentration.
5. K3Flip ODN applied as negative control group: having 1M of K3Flip ODN as final concentration.

In order to see the effects of treatments in different time points, all groups were returned to the incubator prior to the preparation for the ATR-FTIR analysis. Four different time points were defined: $t_1=10\text{min}$, $t_2=30\text{min}$, $t_3=2\text{h}$ and $t_4=6\text{h}$.

When the corresponding incubation time was reached, the samples were removed from the incubator, were spun again at 1000 rpm and their media was discarded. The cells were washed with 1200–1500 ml of sterile phosphate-buffered saline (PBS) and spun again to ensure the complete removal of media. These steps have importance on the removal of organic compounds, growth medium or biological fluids, which can mask the IR spectrum features (Liu et al, 1997). The wash was discarded and cells were re-suspended in 10ml of sterile PBS. Cell viability was verified on an aliquot of the prepared cells using a trypan blue stain.

2.3. FTIR

All Infrared interferograms were collected using a Perkin-Elmer Spectrum One FTIR spectrometer (Perkin-Elmer Inc., Norwalk, CT, USA), with the ATR accessory attached to it. To overcome the probable atmospheric interference that can be triggered by H₂O and CO₂ molecules present in air, air background was taken and subtracted automatically by using suitable software (Spectrum One software). On the other hand to overcome PBS medium interference, the spectrum of PBS was recorded as sample and subtracted manually using Spectrum One software. The spectra of cell samples were recorded in the 4000-650cm⁻¹ region at a fixed temperature which was set to 25 °C. Graseby Specac was the temperature controller being used. As reported elsewhere, samples were incubated for 5 minutes at 25 °C before data acquisition, to allow cells to settle. Interferograms were collected with high scan number (128 scans) and high spectral resolution (at 2 cm⁻¹ resolution), each taking approximately 7 minutes to collect. ATR sampling was done with a Diamond-ZnSe horizontal ATR plate that was combined with the main FTIR apparatus. The spectra of cells were collected from approximately 2µl of cell suspension (2*10⁶cells/µl), which was placed directly on the ATR surface. During the FTIR analysis of the samples, the ATR surface was cleaned using water–ethanol–water sequence and then dried. Each sample was scanned under the same conditions in triplicates, all of which resulted in similar spectra. The average spectra of these three replicates were used in detailed data analysis and statistical analysis. Post-processing of the spectral data was performed using Spectrum One software (Perkin-Elmer).

2.3.1. Optimization studies

Choice of co-added scans

The optimum number of co-added scans was determined by collecting the spectra with different scan numbers. Due to better signal-to-noise ratio, 128 scan number was determined to serve the project's needs (see Figure 16).

Choice of spectral resolution

Resolution is defined as the ability to discriminate two adjacent objects as different. In spectroscopy this is related to the specific wavenumbers in the spectrum. The optimum spectral resolution was determined by collecting the spectra having different resolutions. Since it is important to identify the precise position of the fine absorbance bands, a high resolution of 2cm^{-1} was determined to be used throughout the project, as shown in the representative spectra in Figure 16.

Choice of subtraction method

Water has a high interference in the spectrum. The use of ATR plate helps to improve the results, but a further subtraction of the PBS buffer is needed to be done to the spectra obtained. One way to do it, is to record the PBS spectrum as background and to allow the subsequent recorded spectra to subtract it automatically (blue spectrum in Figure 17) and the other way is to record the spectra with air as background and PBS as sample, at the end subtract the PBS as sample spectrum from the recorded spectra manually (red spectrum in Figure 17). As shown in the representative spectra in the figure, the bands were better resolved with manual subtraction and the water band at around 2100cm^{-1} was flattened, so we have chosen manual subtraction. The software used for subtraction was Spectrum One software. A summary of the subtraction steps is given in Figure 18.

Choice of cell concentration

To have a comparative study, same number of cells is needed to be used in every record of replicates. So the next step was to determine the optimum cell concentration, which was determined by collecting the spectra of different cell concentrations. Two million cells per one μL PBS was the concentration that gave the best resolved spectrum as seen in Figure 19.

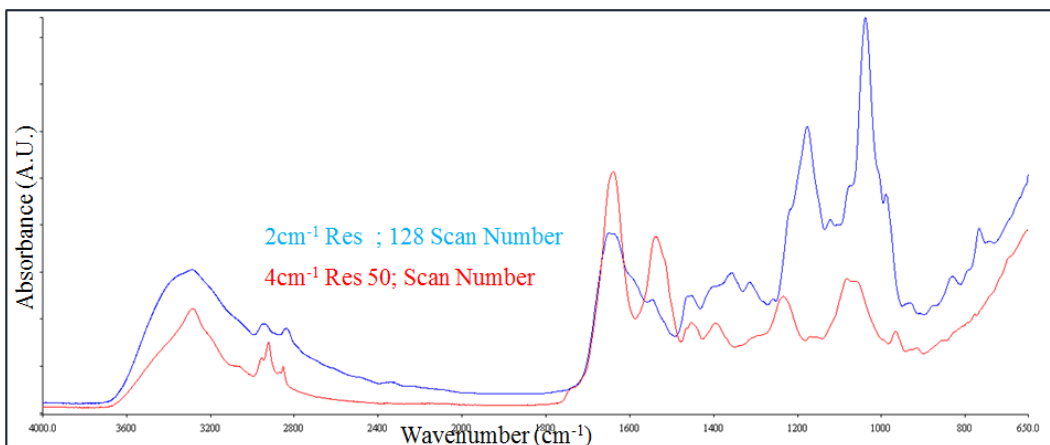


Figure 16: The effect of spectral resolution on the signal-to-noise ratio of ATR-FTIR spectra.

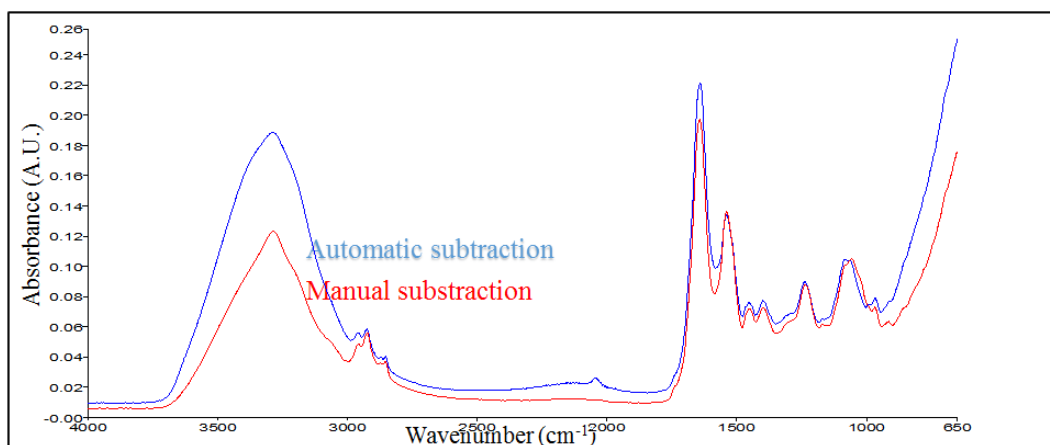


Figure 17: The effect of subtraction method on the signal-to-noise ratio of ATR-FTIR spectra.

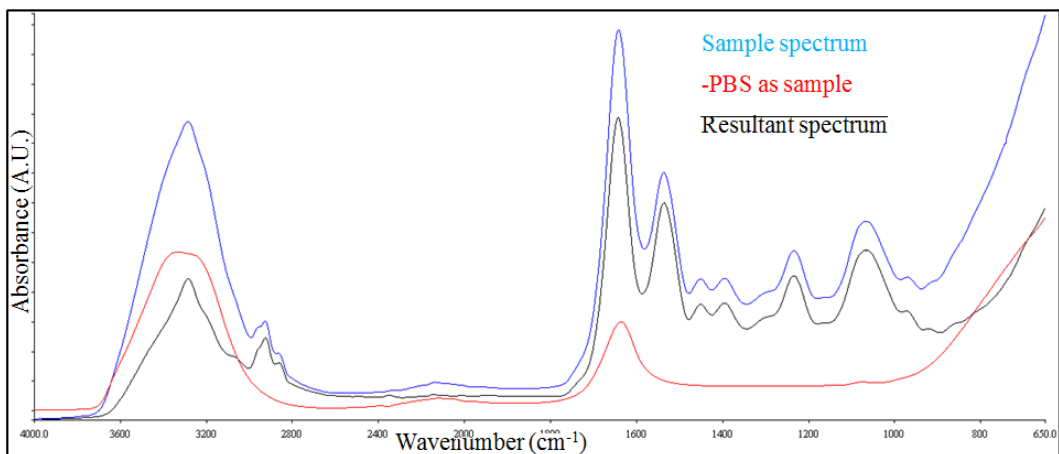


Figure 18: Subtraction procedure. PBS recorded as a sample is subtracted from the sample spectra manually.

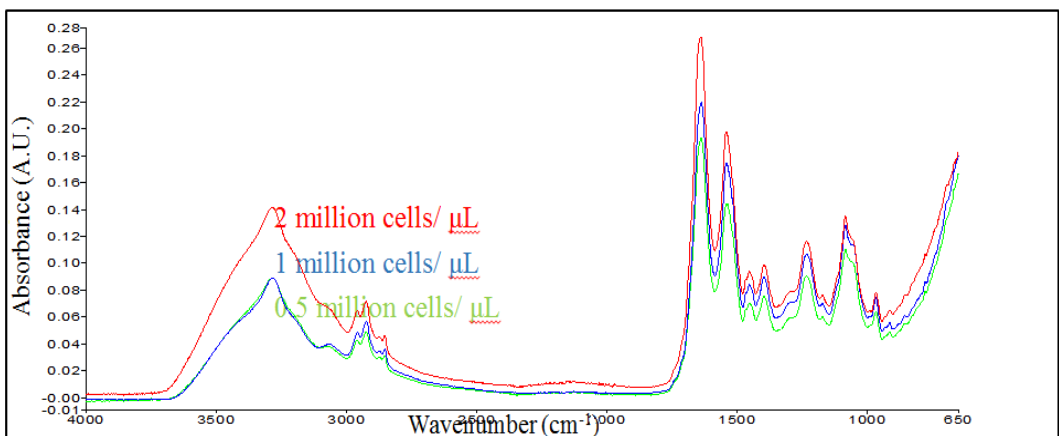


Figure 19: The effect of cell concentration on the signal-to-noise ratio of ATR-FTIR spectra.

2.3.2. Data analysis procedures

The overview of the steps followed in data analysis is shown schematically below.

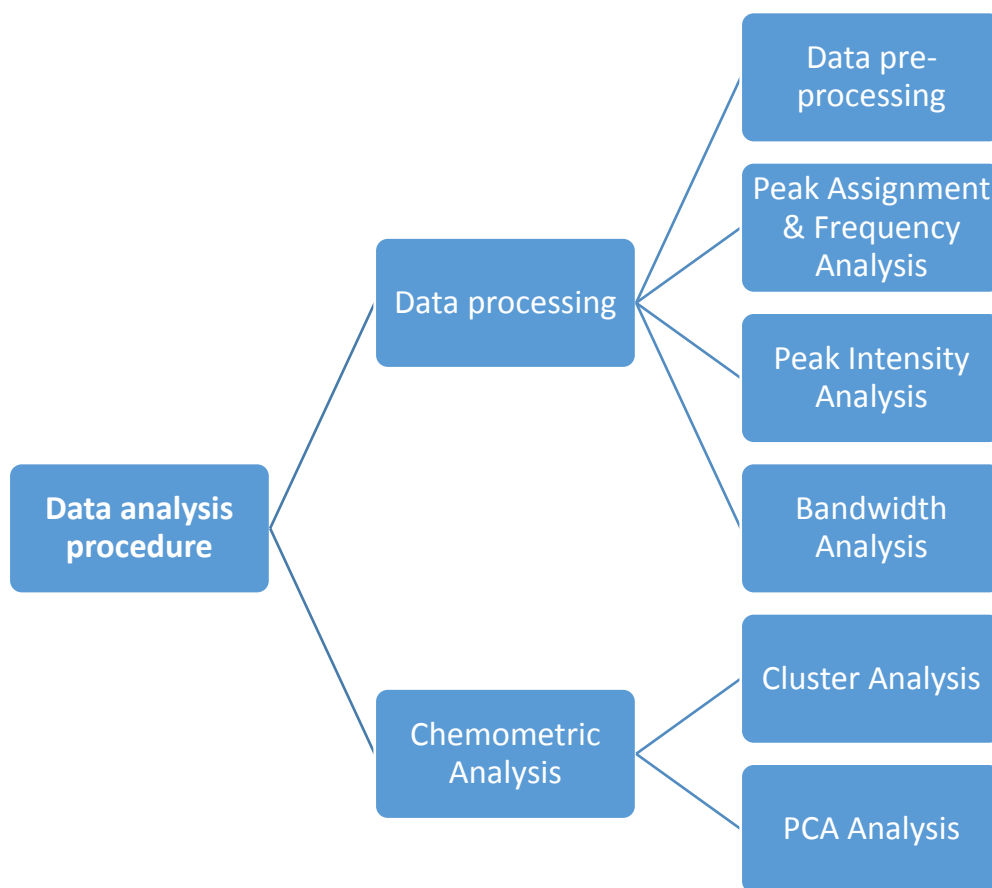


Figure 20: The overview of data analysis procedures

2.3.2.1. Data processing

Pre-processing steps

The spectra recorded underwent smoothing, baseline correction and normalization steps. These steps aid in the preparation of spectra for a comparative study of them in a relative manner.

Smoothing

The presence of noise due to recurrent oscillations in frequency makes some spectral features to become hidden, which is an artefact. The Savitzky-Golay was the smoothing filters used (Savitzky&Golay, 1964) to eliminate the unwanted noise. A 13-point Savitzky-Golay smoothing was used throughout the study, to ensure the removal of noise without changing the band shapes.

Baseline Correction

Due to occasional very small deviations of ATR crystal, many times the baseline of spectra does not start from the same absorbance level. To remove this deviation, certain baseline points are defined, and baseline correction is performed. In our study, baseline points were defined to be 3800 and 2750 for C-H region and 1800-900 for fingerprinting region.

Normalization

Due to the sensitivity of FTIR, the minor differences in conditions during the spectra collection process, sometimes cause variations in the signal intensity of bands. To remove this variation normalization step is performed, which aids in the presentation of differences between the spectra as well.

Peak assignment

The frequency defined by the centre of weight of every peak in the FTIR spectrum, corresponds to a certain band. Every band is a representative of a certain functional group of molecules which corresponds to a certain wavelength. By using this parameter, the band assignment is done and the molecules present in the sample are determined. Some bands absorb the IR in wavelength near to each other, and this produces shoulders. In order to define the exact position of such bands, the second derivative of the spectrum is taken and thus, the accuracy is increased since second derivative spectrum is more specific and bands are resolved more (see Figure 21). The shifts in this parameter indicate changes in the conformation of the molecules. So, one can study these conformational changes, lipid order and hydrogen bonding, by studying the shifts in the frequency of equivalent bands.

Peak intensity analysis

The integral of the curve of a certain band, gives the area of the band that corresponds to a certain functional group. The area of the bands is directly proportional to the concentration of that functional group in the sample, in a fairly accurate manner. We use the ratio of the areas of different bands in order to make the study of concentration changes relative. For the bands that are in fingerprint region, that correspond to functional groups that are not shared among other molecules, individual areas are used. The area of sub-bands of Amide I, which corresponds to proteins, is used to define the concentration of different secondary structures of proteins.

Bandwidth analysis

The bandwidth can be calculated in two ways; by measuring the width of the bands in their 75% height, or by subtracting the maxima and minima of their first derivative spectra. Indications on membrane fluidity and protein conformation are obtained using this parameter.

2.3.2.2. Chemometric analysis

Cluster analysis

The variations in the spectra in a certain region can be used to build clusters between the similar spectra and differences in clustering can be used to classify between the control and treated groups. Cluster Analysis was accomplished by The Unscrambler X spectra analysis software.

Pca analysis

One of the most common ways to look at the variations in the IR spectra is achieved by Principal-Component-Analysis (PCA). The aim of PCA is to simplify the spectral variations and by drawing the attention to only the significant ones, helps to graphically represent the spread of data.

The geometrical transformation of variables happens in a vectorial way in space. This transformation is carried out on the coordinate axis, not on data, thus, the new coordinates now are named as principal components (PCs). Each PC represents certain variability, where PC1 has greater variability than PC2, PC2 more than PC3 and so on.

2.4. Statistical analysis

We used the Kolmogorov–Smirnov test with D-W-L, to determine for the bell shaped normal distribution of our datasets with GraphPad Prism 6.0. One way-ANOVA with Dunnet’s test for multiple comparisons and Kruskal–Wallis with Dunn's test for multiple comparisons was used for the analysis of normally and non-normally distributed data, respectively. The significant data of these analysis were specified by degrees of less than or equal to $p < 0.05^*$, $p < 0.01^{**}$, and $p < 0.001^{***}$. The results are stated as mean \pm SEM.

CHAPTER 3

RESULTS

3.1. General FTIR spectra and band assignment of medium treated control macrophage group

Figure 21 shows a representative IR spectrum of medium treated RAW 264.7 cell line together with its second derivative, in 4000-650 cm^{-1} IR spectral region. Bands are assigned to functional groups by measuring the wavelength of the peaks at their centre of weight and then were compared with literature. Special attention was given on the certain bands of important macromolecules:

- 1- For lipids: olefinic=CH stretching, symmetric and antisymmetric CH_2 stretching, C=O stretching of cholesterol esters and triglycerides, the COO-symmetric stretching of fatty acids and antisymmetric CO-O-C stretching of cholesteryl esters.
- 2- For proteins: C=O stretching corresponding to amide I and the N-H bending and C-N stretching of amide II
- 3- For polysaccharides: C-O stretching from glycogen
- 4- For nucleic acids: symmetric and antisymmetric PO-2 stretching, Ribose skeleton vibration, RNA and DNA backbone CC stretching, DNA-Z form and C^+ -N-C stretching from RNA.

In a broader way, the main bands are labelled with numbers in Figure 21 and specific assignments of these spectral bands are listed in Table 2.

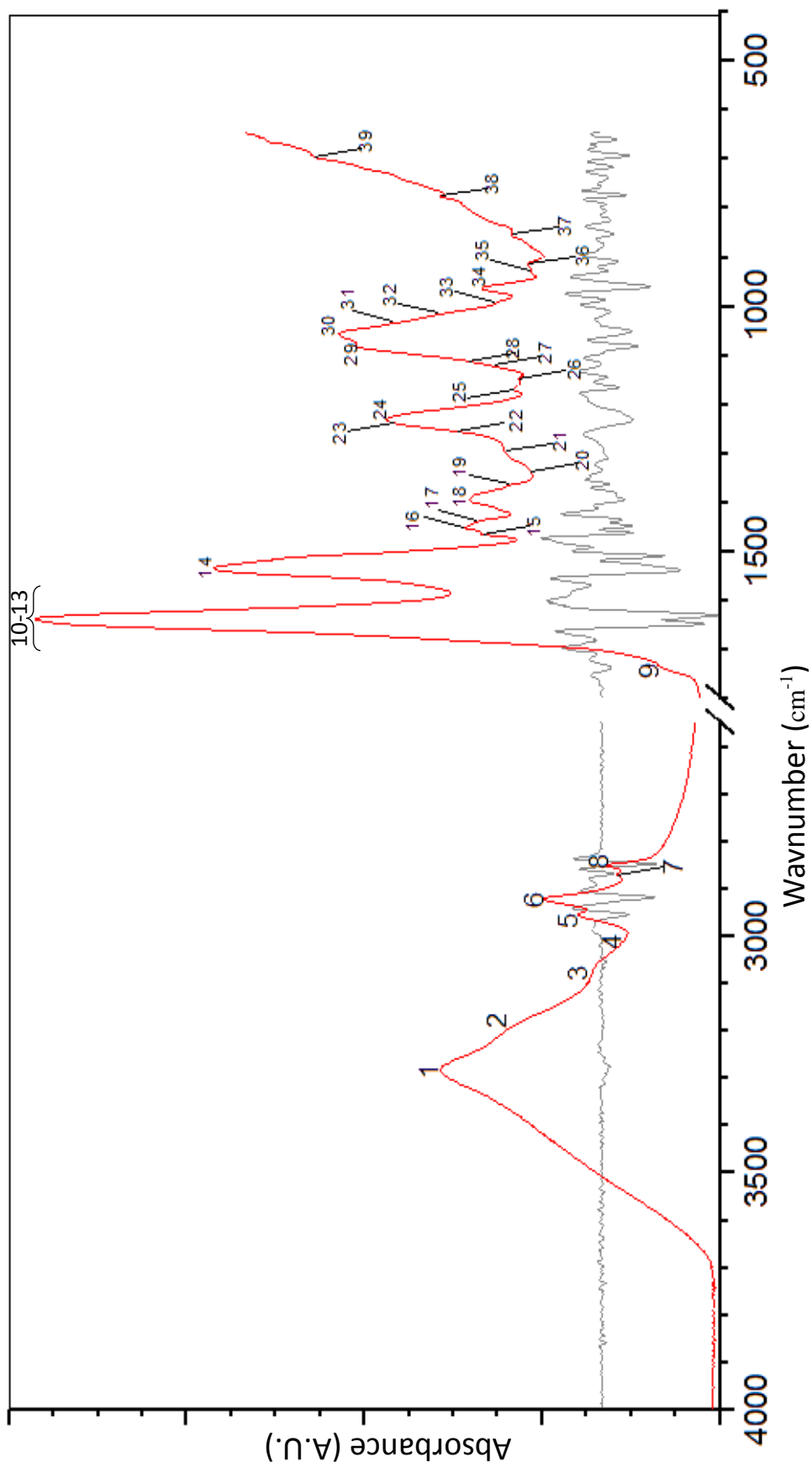


Figure 21: A representative FTIR spectrum of murine macrophage cells with band assignments in 4000-400cm⁻¹

Table 2: Band assignment of main absorption peaks in the ATR-FTIR spectra of murine macrophage RAW 264.7 cells.

Peak	Wavenumber (cm ⁻¹)	Band Explanation
1	3285	Amide A : N-H and O-H stretching of proteins and glycogen
2	3202	Symmetric N-H stretching
3	3014	Olefinic=CH stretching vibration: unsaturated lipids and cholesterol esters
4	3064	Amide B : N-H vibrations of proteins
5	2960	CH₃ antisymmetric stretching : lipids, protein side chains, DNA
6	2923	CH₂ antisymmetric stretching : mainly lipids , with little contribution from proteins, carbohydrates, and nucleic acids
7	2874	CH₃ symmetric stretching : mainly proteins , with little contribution from lipids, carbohydrates, and nucleic acids
8	2852	CH₂ symmetric stretching : mainly lipids , with little contribution from proteins, carbohydrates, and nucleic acids
9	1741	Ester C=O stretch : triglycerides and cholesterol esters
10	1683	Proteins : antiparallel β -sheet
11	1640	Amide I: C=O stretching vibrations of proteins
12	1656	Amide I: C=O (80%) and C-N (10%) stretching, N-H (10%) bending vibrations: proteins α-helix
13	1649	Amide I: C=O (80%) and C-N (10%) stretching, N-H (10%) bending vibrations: proteins random coil
14	1636	Amide I: C=O (80%) and C-N (10%) stretching, N-H (10%) bending vibrations: proteins β-structure
15	1543	Amide II (protein , N-H bend, C-N stretch)
16	1467	Cholesterol-methyl band
17	1453	Asymmetric methyl deformation of cellular proteins
18	1441	δ (CH ₂) of fatty acids, δ (CH) of polysaccharides

Table 2: Continued

19	1400	COO ⁻ symmetric stretching: fatty acid side chains
20	1368	δ (CH ₂), ν (CC), polysaccharides
21	1339	CH ₂ side chains of collagen
22	1313	Peptide side chain vibrations
23	1261	asPO ₂ ⁻ -stretching, non-hydrogen bonded: mainly nucleic acids with the little contribution from phospholipids
24	1242	Amide III and phosphate vibration of nucleic acids
25	1236	asPO ₂ ⁻ -stretching, fully hydrogen bonded: mainly nucleic acids with little contribution from phospholipids
26	1170	asCO-O-C stretching: ester bonds in cholesterol esters and phospholipids
27	1150	Glycogen , ν (C-O-C)
28	1123	Cellular nucleic acids, proteins, including collagen I
29	1110	sC-C of ribose
30	1086	sPO ₂ ⁻ -stretching: mainly nucleic acids and phospholipids
31	1040	C-O stretching: polysaccharides (glycogen)
32	1055	C-O of nucleic acids
33	1020	Mainly from glycogen
34	993	RNA : Ribose skeleton
35	967	RNA and DNA backbone CC stretching of nucleic acids
36	925	Sugar vibrations in backbone of DNA-Z form
37	915	Ribose vibration, one of the distinct RNA modes
38	857	N-type sugar vibrations of nucleic acids' backbone
39	780	Out-of-plane bending

3.2. General differences between resting, activated and suppressed macrophages

The spectra were recorded in $4000\text{-}650\text{cm}^{-1}$ region of the IR spectrum. The spectrum of samples in the same group did not show any significant difference, so, for a general comparison, their average representative spectra are taken. The overall comparison is done in two regions: in the so-called C-H region covering $3600\text{-}2800\text{cm}^{-1}$ (see Figure 22), and in the “fingerprinting” region which spans the spectrum in $1800\text{-}650\text{cm}^{-1}$ (see Figure 23). As it can be seen clearly, there are many variances in peak intensities, positions and widths that treatments introduced to the medium treated control group.

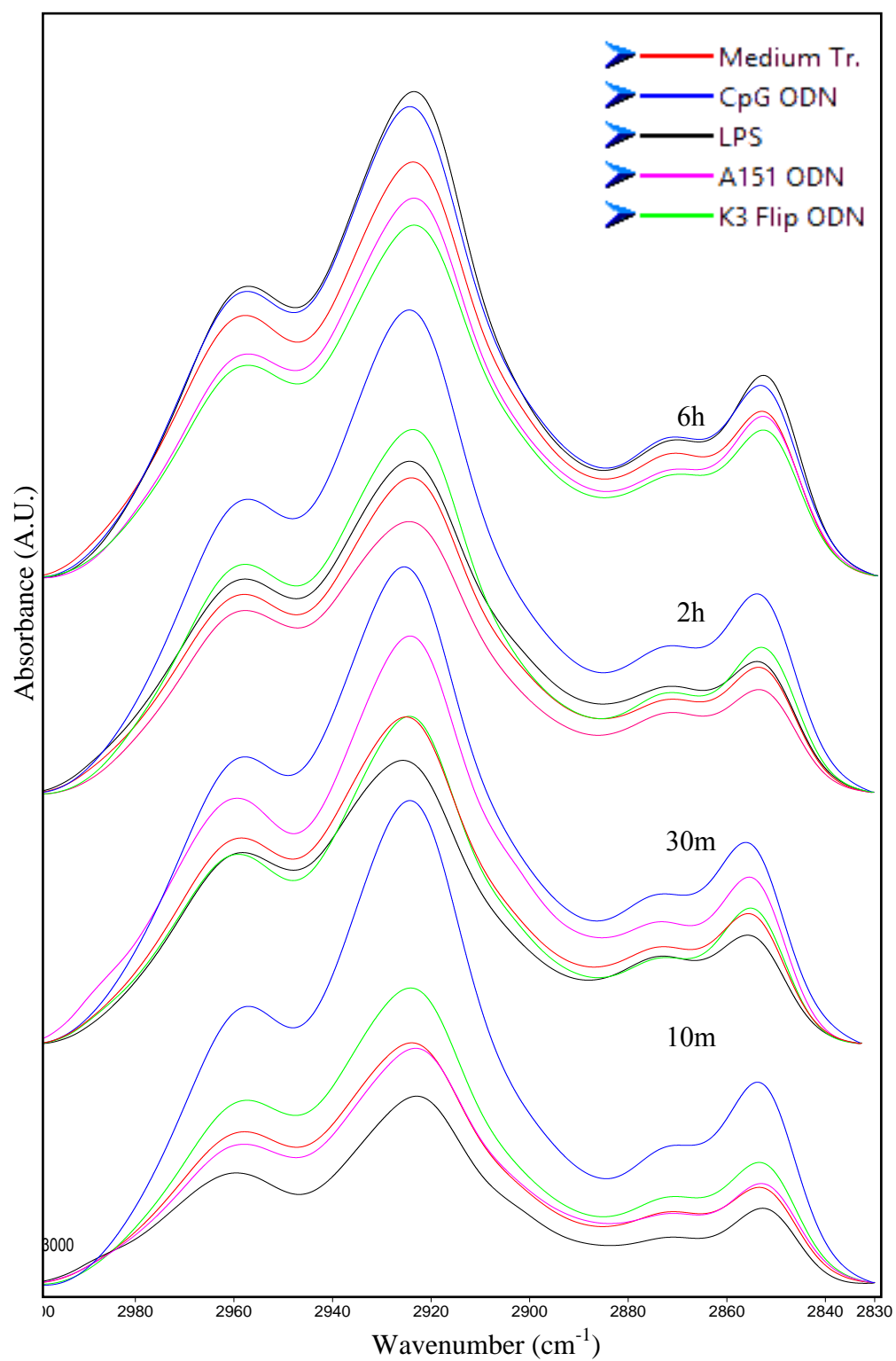


Figure 22: The representative infrared spectra of control and treated (CpG, LPS, A151 and K3F) groups of murine macrophage RAW 264.7 cells in the 3000-2830 cm⁻¹ region.

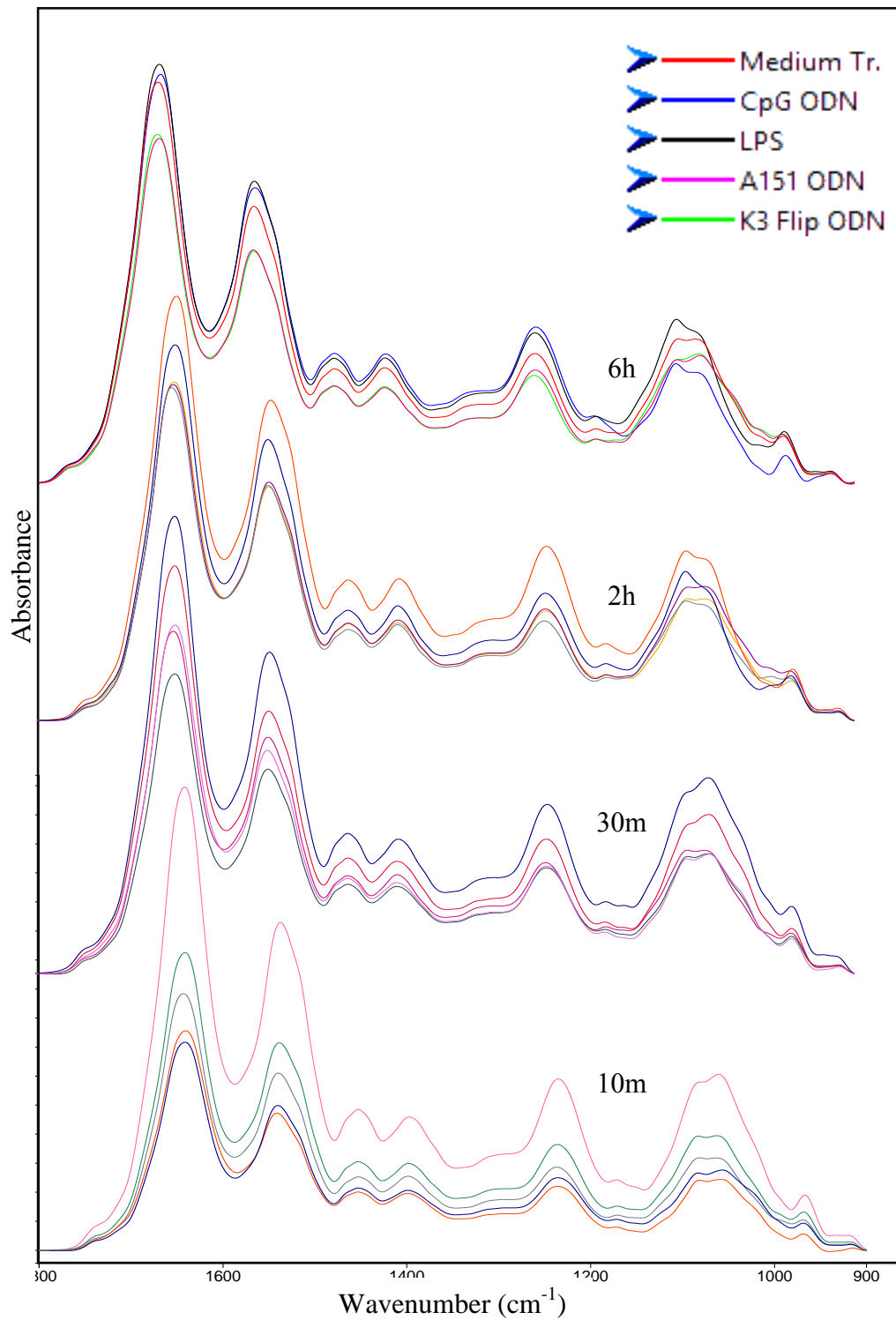


Figure 23: The representative infrared spectra of control and treated (CpG, LPS, A151 and K3F) groups of murine macrophage RAW 264.7 cells in the 1800- 900 cm⁻¹ regions.

Difference spectrum

To have a general view of the differences in the structure of macromolecular components of murine macrophage cells upon treatment with CpG ODN, LPS, A151 suppressive ODN and K3Flip ODN, their average spectra was subtracted from the medium treated one to obtain a difference spectrum. Thus, the bands that extend positively upside seem to be lower than the medium treated control. As seen from these figures at the first glance, the spectra substantially differ in band positions, band heights and band widths. For CpG ODN (blue) stimulation, the positive-going bands are distinguished at around 3014 and 2960 cm^{-1} and negative-going bands are distinguished at 1400, 1236, 1080, 925, 915 cm^{-1} . For A151 ODN (purple) suppression, the positive-going bands are distinguished at around: 2960, 1640 and a negative-going band is distinguished at 1400 cm^{-1} . The details of these differences between medium treated control murine macrophage cells and their treated states were discussed in Chapter 4 more specifically.

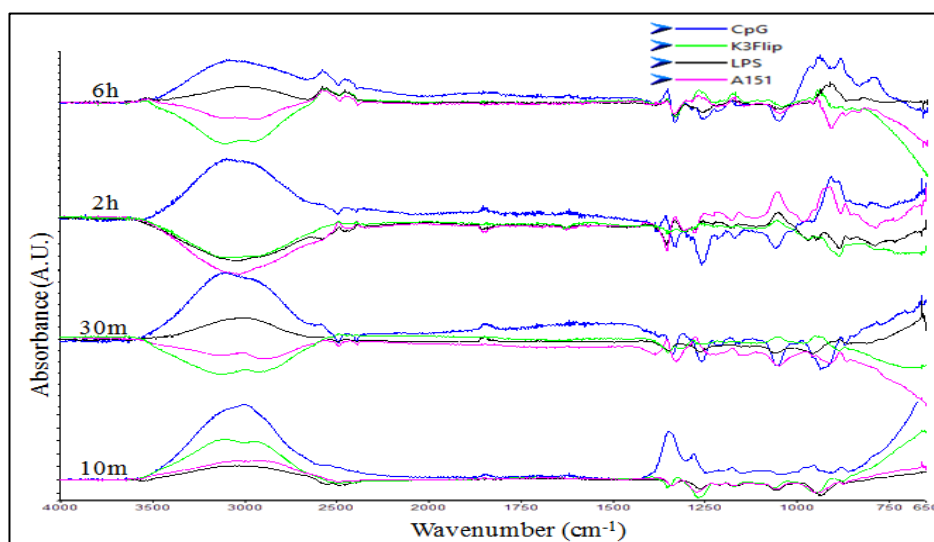


Figure 24: ATR-FTIR difference spectra (treated-control). General view of the changes introduced on murine macrophage cells in 4000-650 cm^{-1} region.

3.3. Lipid profile of murine macrophage cells

The so-called C-H region, lying between 3000 and 2800 cm^{-1} , bears in it bands that help to screen the lipid content of the sample. The most intense bands in this region are from: CH₃ antisymmetric (2960 cm^{-1}) and symmetric (2874 cm^{-1}) stretching vibrations and from CH₂ antisymmetric (2923 cm^{-1}) and symmetric (2852 cm^{-1}) stretching vibrations. Also in fingerprinting region, we have the ester C-O stretching band lying at about 1741 cm^{-1} and the carboxyl's C=O moiety at around 1400 cm^{-1} , among the important bands to evaluate the lipids inside the sample.

It should be noted that these bands are mainly from lipids, but depending on the band, there can be contributions from proteins, carbohydrates, and nucleic acids present as well. For this reason, to promote accuracy, the ratios of these bands with others bands are used during quantitative analysis.

3.3.1. Saturated lipids

The CH₂ antisymmetric stretching band at 2923 cm^{-1} and the symmetric CH₂ stretching band located at around 2852 cm^{-1} , arise mainly from lipids. The antisymmetric CH₂ to total lipid (asCH₂ + sCH₂) ratio can be used to evaluate the saturated lipid content of the samples (Demir P., 2015). As can be seen in Figure 25, the saturated lipid content of the system was decreased significantly in LPS, A151 ODN and K3 Flip ODN at 2h and 6h periods of time. On the other hand CpG ODN did not show a significant change, moreover shows a tendency to increase the saturated lipid content of macrophage cells in a period of time for 6h.

Table 3: Numerical analysis of saturated lipid content by the use of differences in 1500cm^{-1} IR band area of Medium, CpG ODN, A151 ODN, LPS and K3f ODN treated macrophage cell spectra, in different time points (10min, 30min, 2h and 6h). The statistically significant data are specified with $p < 0.05^*$, $p < 0.01^{**}$, and $p < 0.001^{***}$ in comparison to medium treated group. The results are specified as mean \pm SEM.

Treatment\Time	10 min	30 m	2 h	6 h
Medium Treated	0.744 ± 0.002	0.745 ± 0.001	0.744 ± 0.002	0.743 ± 0.001
CpG ODN	0.743 ± 0.001	0.74 ± 0.00	0.737 ± 0.000	0.746 ± 0.000
A151 ODN	0.737 ± 0.002	0.746 ± 0.003	$0.729 \pm 0.003^{***} \downarrow$	$0.727 \pm 0.002^{****} \downarrow$
LPS	0.75 ± 0.004	0.745 ± 0.003	$0.731 \pm 0.004^{***} \downarrow$	$0.730 \pm 0.001^{***} \downarrow$
K3Flip ODN	0.737 ± 0.001	0.744 ± 0.003	$0.725 \pm 0.002^{****} \downarrow$	$0.730 \pm 0.002^{***} \downarrow$

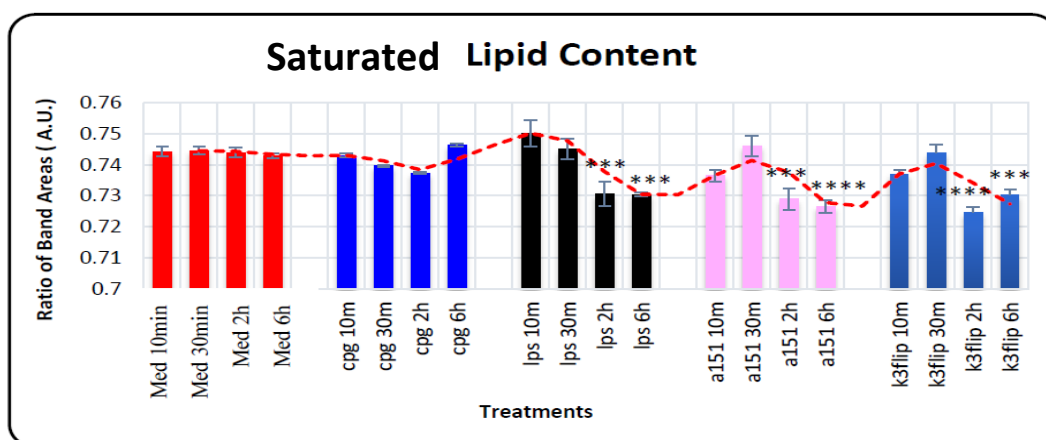


Figure 25: Histogram illustration of the saturated lipid content analysis by the use of differences in 1500cm^{-1} IR band area ratio of Medium, CpG ODN, A151 ODN, LPS and K3f ODN treated macrophage cells, in different time points (10min, 30min, 2h and 6h). The error bars specify the SEM and stars the statistical significance as: $p < 0.05^*$, $p < 0.01^{**}$, and $p < 0.001^{***}$ in comparison to medium treated group.

3.3.2. Unsaturated lipids

The Olefinic=CH band, used to evaluate the degree of unsaturation of phospholipid acyl chains, shows itself in murine macrophage cells at 3014cm^{-1} , and is assigned to vibrations of the H-C=C-H functional groups (Severcan F., 2005; Ozek N., 2004). For precision, the ratio of Olefinic=CH band to total lipid (asCH₂ + sCH₂) is used in our calculations. As clearly seen in Figure 26, stimulation with CpG ODN is significantly decreasing the unsaturation degree in 30m ($p<0.0001$ ****), 2h ($p<0.0001$ ****) and 6h ($p<0.1$ *), and suppression with A151 ODN is increasing it significantly in 2h ($p<0.1$ *) and 6h ($p<0.1$ *). LPS seems to have a similar trend with CpG ODN, but the results are not significant. Unexpectedly, K3Flip significantly has increased unsaturated lipids till 6h with ($p<0.001$ ***).

Table 4: Numerical analysis of Olefinic=CH band as a measurement of the unsaturation level of phospholipid acyl chains, by the use of differences in 3014cm^{-1} IR band area of Medium, CpG ODN, A151 ODN, LPS and K3f ODN treated macrophage cell spectra, in different time points (10min, 30min, 2h and 6h). The statistically significant data are specified with $p<0.05$ *, $p<0.01$ **, and $p<0.001$ *** in comparison to medium treated group. The results are specified as mean \pm SEM.

Treatment/Time	10 min	30 m	2 h	6 h
Medium Treated	0.265 \pm 0.008	0.245 \pm 0.01	0.237 \pm 0.009	0.244 \pm 0.008
CpG ODN	0.226 \pm 0.012	0.185 \pm 0.008* \downarrow	0.159 \pm 0.004**** \downarrow	0.231 \pm 0.013**** \downarrow
A151 ODN	0.257 \pm 0.026	0.276 \pm 0.03* \uparrow	0.258 \pm 0.005* \uparrow	0.284 \pm 0.008* \uparrow

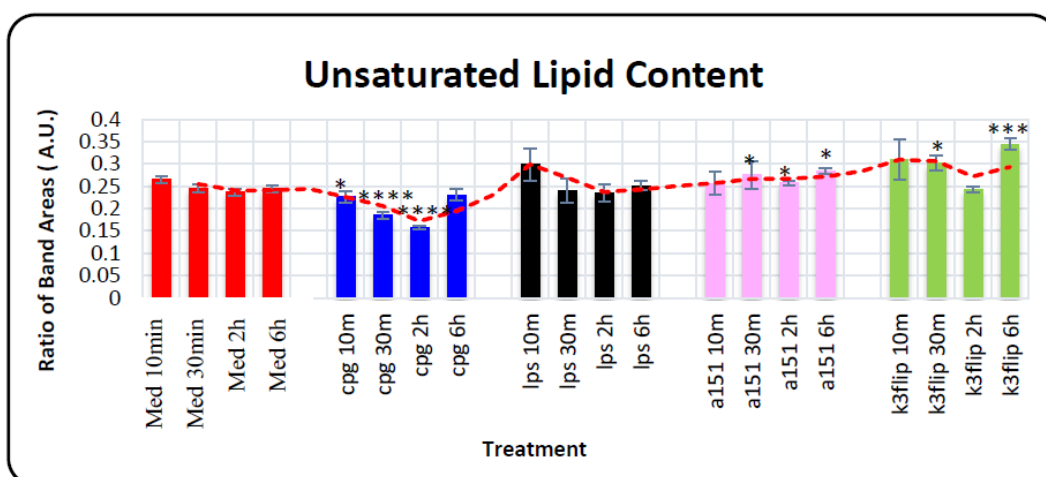


Figure 26: Histogram illustration of the unsaturated lipid content analysis by the use of differences in 3014cm⁻¹ IR band area ratio of Medium, CpG ODN, A151 ODN, LPS and K3f ODN treated macrophage cells, in different time points (10min, 30min, 2h and 6h). The error bars specify the SEM and stars the statistical significance as: p<0.05*, p<0.01**, and p<0.001*** in comparison to medium treated group.

3.3.3. Cholesterol ester and triglycerides

The ester C-O stretching band, used to evaluate the concentration of cholesterol ester and triglycerides, appears in macrophage cells at about 1741cm⁻¹, and is allocated to stretching vibration of C=O ester functional groups (Severcan F., 2003; Cakmak G., 2003; Kardas M., 2014). Also the band at 1170cm⁻¹ is allocated to the antisymmetric stretching of CO-O-C functional group of cholesterol esters and phospholipids. For precise conclusions, the ratio of these two related bands is taken into consideration in our calculations. As clearly seen in Table 5, stimulation with CpG ODN is significantly increasing the concentration of cholesterol ester and

triglycerides in early stimulation of 10m with and decreases significantly at late stimulation of 2h and 6h; while on the other side suppression with A151 ODN has increased in early suppression of 30m with and no significant result was seen in late phases. K3Flip follows a similar trend with A151 ODN and LPS, significantly increases the concentration at as early as 30min phase and keeps decreasing till 6h phase.

Table 5: Numerical analysis of cholesteryl ester and triglyceride content, by the use of differences in 1741cm^{-1} and 1170cm^{-1} IR band area of Medium, CpG ODN, A151 ODN, LPS and K3f ODN treated macrophage cell spectra, in different time points (10min, 30min, 2h and 6h). The statistically significant data are specified with $p < 0.05^*$, $p < 0.01^{**}$, and $p < 0.001^{***}$ in comparison to medium treated group. The results are specified as mean \pm SEM.

Treatment/Time	10 min	30 m	2 h	6 h
Medium Treated	1.119 \pm 0.084	1.149 \pm 0.035	1.034 \pm 0.061	1.056 \pm 0.016
CpG ODN	1.343 \pm 0.048* \uparrow	1.212 \pm 0.025* \uparrow	0.875 \pm 0.011**** \downarrow	0.976 \pm 0.033**** \downarrow
A151 ODN	1.172 \pm 0.016	1.493 \pm 0.098**** \uparrow	1.061 \pm 0.051	1.191 \pm 0.06

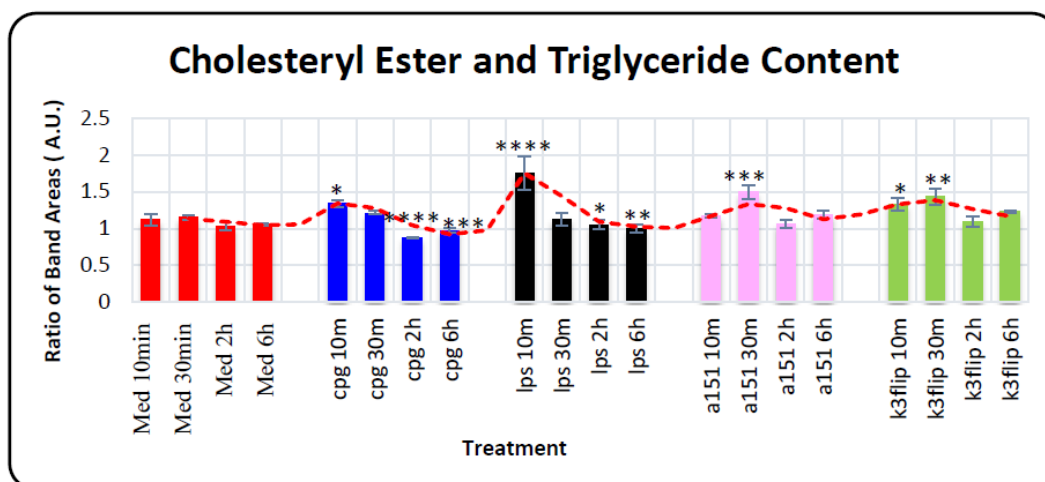


Figure 27: Histogram illustration of the cholesteryl ester and triglyceride content analysis by the use of differences in 1741cm^{-1} and 1170cm^{-1} IR band area ratio of Medium, CpG ODN, A151 ODN, LPS and K3f ODN treated macrophage cells, in different time points (10min, 30min, 2h and 6h). The error bars specify the SEM and stars the statistical significance as: $p < 0.05^*$, $p < 0.01^{**}$, and $p < 0.001^{***}$ in comparison to medium treated group.

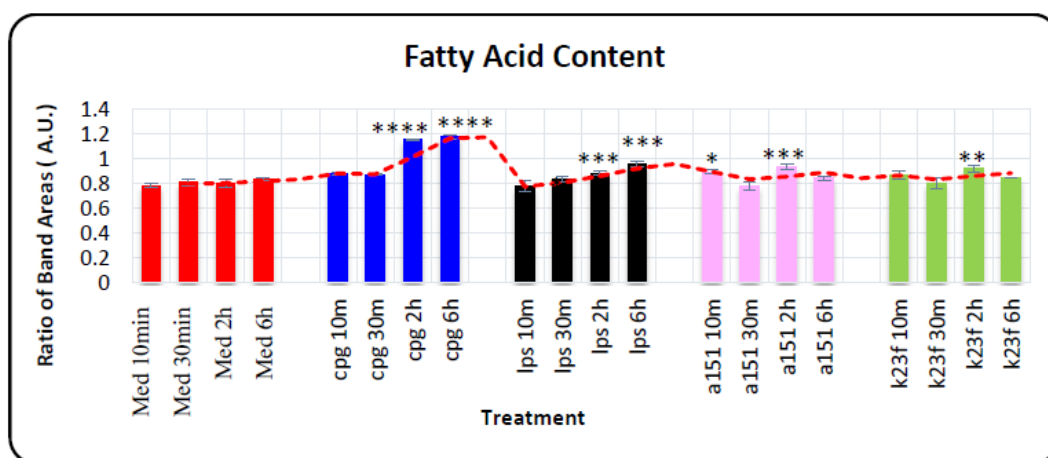
3.3.4. Fatty acids

The carboxyl functional group of fatty acids and amino acid side chains has an IR-active moiety in its $\text{C}=\text{O}$ part which shows a stretching vibration (Cakmak G., 2006; Melchiori, 2010). In our sample of macrophages, this band is observed around 1400cm^{-1} . A change in the ratio of this band to total lipid content ($\text{asCH}_2 + \text{sCH}_2$), is used to evaluate the concentration of fatty acids in our samples. As clearly seen in Figure 28 and Table 6, the fatty acid content of the CpG and LPS stimulated samples was increased significantly after 2h of stimulation and was consistent in 6h as well. The A151 suppressed and K3F samples had a significant increase in only 2h of application.

Table 6: Numerical analysis of fatty acid content, by the use of differences in 1400cm^{-1} IR band area of Medium, CpG ODN, A151 ODN, LPS and K3f ODN treated macrophage cell spectra, in different time points (10min, 30min, 2h and 6h). The statistically significant data are specified with $p < 0.05^*$, $p < 0.01^{**}$, and $p < 0.001^{***}$ in comparison to medium treated group. The results are specified as mean \pm SEM.

Treatment/Time	10 min	30 m	2 h	6 h
Medium Treated	0.784 ± 0.014	0.807 ± 0.029	0.801 ± 0.033	0.836 ± 0.007
CPG ODN	0.88 ± 0.008	0.871 ± 0.005	$1.156 \pm 0.005^{***\uparrow}$	$1.173 \pm 0.013^{***\uparrow}$
A151 ODN	$0.894 \pm 0.02^*\uparrow$	0.777 ± 0.03	$0.934 \pm 0.02^{***\uparrow}$	0.843 ± 0.015
LPS	0.777 ± 0.045	0.835 ± 0.022	$0.884 \pm 0.02^{***\uparrow}$	$0.957 \pm 0.023^{***\uparrow}$
K3Flip ODN	0.866 ± 0.034	0.8 ± 0.041	$0.922 \pm 0.028^{\uparrow}$	0.843 ± 0.003

Figure 28: Histogram illustration of the fatty acid content analysis by the use of differences in 1440cm^{-1} IR band area ratio of Medium, CpG ODN, A151 ODN, LPS and K3f ODN treated macrophage cells, in different time points (10min, 30min, 2h and 6h). The error bars specify the SEM and stars the statistical significance as: $p < 0.05^*$, $p < 0.01^{**}$, and $p < 0.001^{***}$ in comparison to medium treated group.



3.4. Protein profile

The Amide I and Amide II bands, used for protein content of the sample, shows themselves in murine macrophage cells at about 1640 cm^{-1} and 1543 cm^{-1} . The functional groups that are assigned to Amide I band are: stretching vibrations of the C=O together with C-N (60%) and a 40% contribution from the bending of N-H functional group of polypeptides and protein (Haris and Severcan, 1999). On the other hand, Amide II is assigned to the N-H bending (60%) and the C-N stretching (40%) of proteins (Melin et al., 2000; Haris and Severcan, 1999; Cakmak et al., 2003). For accuracy, the ratio of Amide I band to total protein (Amide I + Amide II) is used in our calculations of the total protein content. As clearly seen in Table 8 and Figure 29, there was a significant reduction of protein content in CpG ODN throughout the stimulation from 30m-6h. LPS stimulation was also decreasing the protein content of macrophage cells with a slight slope starting at 30m of stimulation, till 6h. Suppression with A151 ODN, initially decreased the protein content at 10m, but a steady state was observed during the other periods of time. Similar behaviour is observed with K3F ODN as well.

Since Amide I band is very sensitive to conformational changes of proteins, the bandwidth of it, can be used to infer about the conformational changes on proteins. As seen in figure, although the bandwidth of Amide I band doesn't seem to change significantly, there is an observed trend of firstly decrease and then increase in K3 Flip ODN and similarly in LPS. In stimulated groups, the decrease that is seen in 30m goes on with an increasing slope till 6h. This may be due to change in the conformation of proteins while stimulation takes place. The frequency changes of Amide I band are indications of conformational changes of proteins as well. As seen in figure, in our samples, the frequencies shifts of amide bands were significant in CpG ODN, where a decrease is observed starting from 2 to 6 hours of application. LPS has a slight increase which is persistent from 30 minutes of application. A151 ODN and K3Flip again show a similar pattern. A151 ODN has a high increase in 2h of application, and K3Flip increases the frequency of Amide I band from 30 minutes.

Table 7: Numerical analysis of protein content, by the use of differences in 1640 cm^{-1} and 1543 cm^{-1} IR band area of Medium, CpG ODN, A151 ODN, LPS and K3f ODN treated macrophage cell spectra, in different time points (10m, 30m, 2h and 6h). The statistically significant data are specified with $p < 0.05^*$, $p < 0.01^{**}$, and $p < 0.001^{***}$ in comparison to medium treated group.

Treatment/Time	10 min	30 m	2 h	6 h
Medium Treated	1.449 \pm 0.041	1.42 \pm 0.045	1.391 \pm 0.049	1.408 \pm 0.037
CpG ODN	1.356 \pm 0.013 ^{****} ↓	1.354 \pm 0.008 ^{****} ↓	1.224 \pm 0.004 ^{****} ↓	1.251 \pm 0.009 ^{****} ↓
A151 ODN	1.351 \pm 0.01	1.459 \pm 0.032	1.333 \pm 0.009 ^{****} ↓	1.382 \pm 0.012
LPS	1.467 \pm 0.05	1.398 \pm 0.026 ^{**} ↓	1.336 \pm 0.015 ^{****} ↓	1.301 \pm 0.0 ^{****} ↓
K3Flip ODN	1.396 \pm 0.03	1.442 \pm 0.037	1.333 \pm 0.025	1.412 \pm 0.014

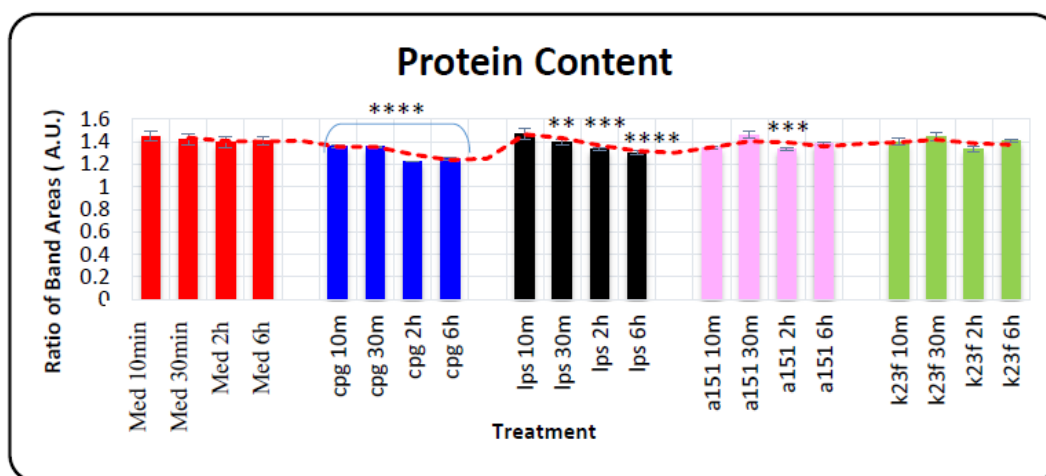


Figure 29: Histogram illustration of the protein content analysis by the use of differences in 1640 cm^{-1} and 1543 cm^{-1} IR band area ratio of Medium, CpG ODN, A151 ODN, LPS and K3f ODN treated macrophage cells, in different time points (10min, 30min, 2h and 6h). The error bars specify the SEM and stars the statistical significance as: $p < 0.05^*$, $p < 0.01^{**}$, and $p < 0.001^{***}$ in comparison to medium treated group.

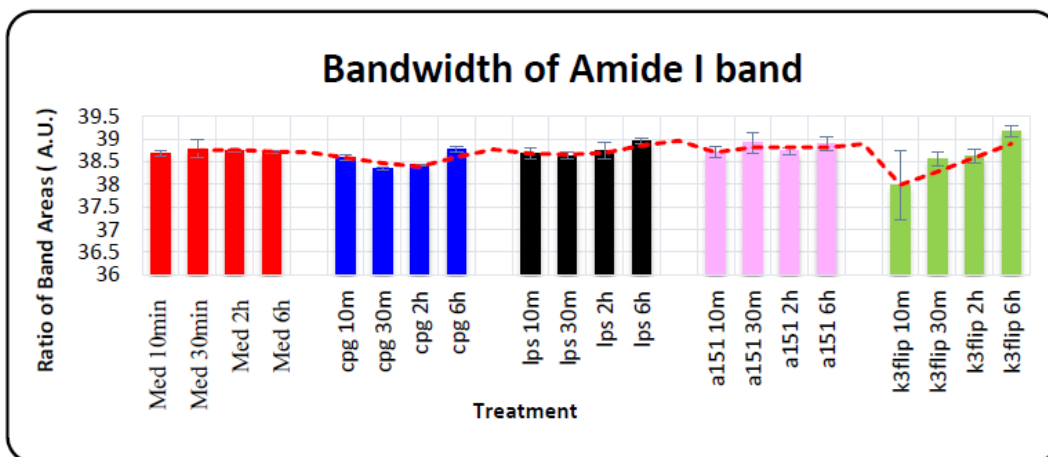


Figure 30: Histogram illustration of Amide I bandwidth analysis for conformational change on proteins.

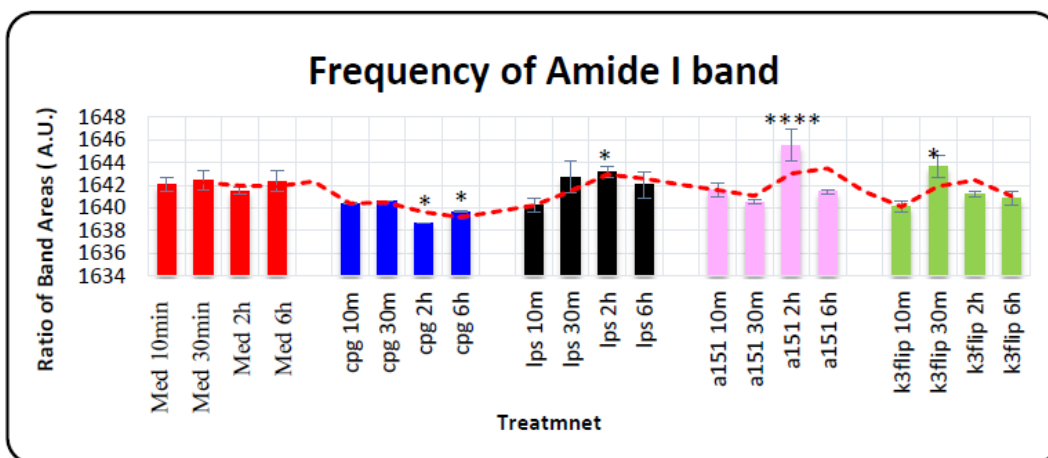


Figure 31: Histogram illustration of Amide I frequency analysis as indicator of conformational changes of proteins

3.5. Nucleic acids

The IR active important bands that one can draw conclusions about cellular nucleic acids are the bands at around:

1. 1236cm^{-1} and 1261cm^{-1} assigned to antisymmetric PO^{2-} stretching,
2. 1080cm^{-1} assigned to symmetric PO^{2-} stretching,
3. 967cm^{-1} assigned to RNA and DNA backbone CC stretching,
4. 1055cm^{-1} assigned to C–O stretch of deoxyribose and ribose,
5. 925cm^{-1} assigned to sugar vibrations in backbone of DNA-Z form,
6. 857cm^{-1} assigned to N-type sugars of nucleic acid backbone
7. 993cm^{-1} assigned to ribose skeleton,
8. 1100cm^{-1} assigned to stretching C-C moiety of ribose,
9. 915cm^{-1} assigned to ribose vibration (distinct RNA mode) RNA specific bands

3.5.1. DNA

The bands at 1236 and 1261 cm^{-1} are related to stretching PO^{2-} vibrations of non-hydrogen bonded and hydrogen bonded nucleic acids, respectively, together with slight influence from phospholipids. Two more relatively weak peaks are seen at 925 cm^{-1} and 857 cm^{-1} , which in the literature are assigned for sugar vibrations, in DNA-Z form backbones and N-type sugars of nucleic acids, respectively (Banyay, 2003). To obtain relative results, which are more accurate, the PO^{2-} symmetric and antisymmetric band intensities are divided to the CC backbone stretching of nucleic acids at 967 cm^{-1} . Evidently, CpG ODN stimulation induces changes on nucleic acid content of the macrophage cells, starting within 10m of stimulation and going on till 6h. While the other treatments do not confer such a result. To confirm these results, the DNA-Z form band at 925 cm^{-1} is used, where CpG ODN stimulation shows the same trend of increase as in nucleic acid content, in direct relation with time of stimulation. At 2h and 6h of stimulation has a significant increase. Unexpected results are seen from K3Flip at 6h, with a significant increase.

Table 8: Numerical analysis of DNA content, by the use of differences in 1236 cm^{-1} , 1261 cm^{-1} , 1080 cm^{-1} and 1100 cm^{-1} IR band areas of Medium, CpG ODN, A151 ODN, LPS and K3f ODN treated macrophage cell spectra, in different time points (10min, 30min, 2h and 6h). The statistically significant data are specified with $p < 0.05^*$, $p < 0.01^{**}$, and $p < 0.001^{***}$ in comparison to medium treated group. The results are specified as mean \pm SEM.

Treatment/Time	10 min	30 m	2 h	6 h
Medium Treated	20.438 \pm 0.7455	21.302 \pm 0.66	21.878 \pm 0.374	18.897 \pm 0.292
CPG ODN	23.916 \pm 0.7322	23.29 \pm 0.1511	23.078 \pm 0.1034	27.291 \pm 0.2974* \uparrow
A151 ODN	18.796 \pm 1.5786	22.416 \pm 0.4509	19.581 \pm 0.7037	20.721 \pm 0.3179
LPS	21.217 \pm 0.7627	21.08 \pm 0.739	19.745 \pm 0.4467	19.873 \pm 0.8648
K3Flip ODN	19.157 \pm 2.5571	20.53 \pm 0.543	20.645 \pm	20.045 \pm 0.1257

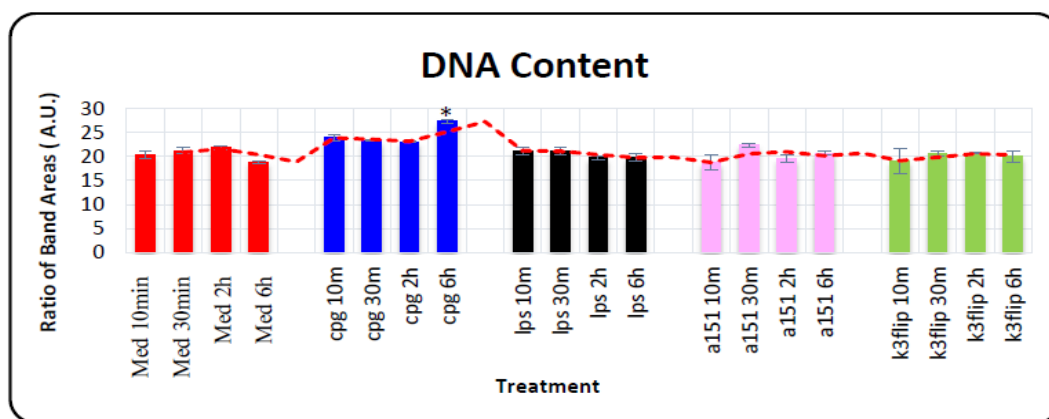


Figure 32: Histogram illustration of the DNA content analysis by the use of differences in 1236cm^{-1} , 1261cm^{-1} , 1080cm^{-1} and 1100cm^{-1} IR band area ratio of Medium, CpG ODN, A151 ODN, LPS and K3f ODN treated macrophage cells, in different time points (10min, 30min, 2h and 6h). The error bars specify the SEM and stars the statistical significance as: $p < 0.05^*$, $p < 0.01^{**}$, and $p < 0.001^{***}$ in comparison to medium treated group.

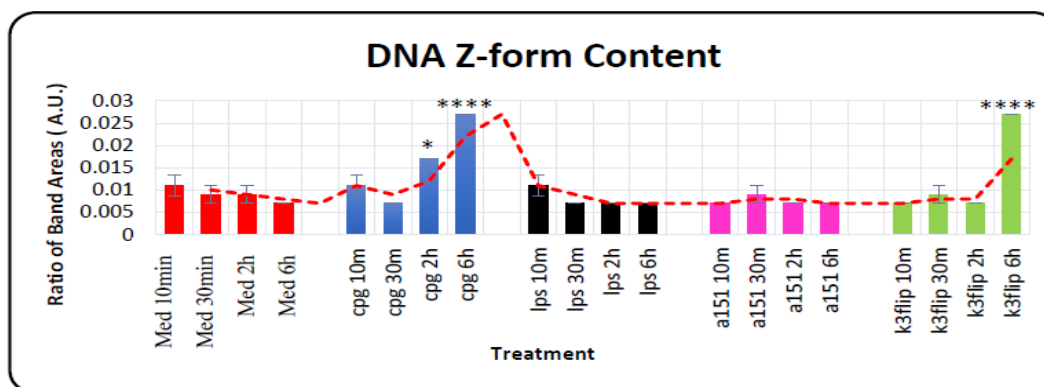


Figure 33: Histogram illustration of the DNA-Z form content analysis by the use of differences in 925cm^{-1} IR band area ratio of Medium, CpG ODN, A151 ODN, LPS and K3f ODN treated macrophage cells, in different time points (10min, 30min, 2h and 6h). The error bars specify the SEM and stars the statistical significance as: $p < 0.05^*$, $p < 0.01^{**}$, and $p < 0.001^{***}$ in comparison to medium treated group.

3.5.2. RNA

The ribose vibration band at 915cm^{-1} and the ribose-phosphate main chain vibration band at 993cm^{-1} are amongst RNA distinct modes used to discuss the RNA content of cells (Wood B., 2000). As seen in Figure 34 and Table 9, CpG ODN has a significant increase in RNA specific band from the very first minutes. This increase is maintained till 2h after stimulation. A151 suppression on the other hand, has no meaningful changes in RNA content. LPS and K3 Flip ODN, have a slope of increase till 2h after stimulation, and then it ceases. An accurate indicator of protein synthesis is the RNA/protein ratio, which is obtained by dividing the 915cm^{-1} band to Amide I and Amide II. As seen in Figure 35, CpG ODN in this analysis has significant increase in 10m and in 30m and then goes with a decreasing slope as stimulation goes on at 6th hour. LPS has very low ratio in 10m after stimulation and then an increase occurs from 30 min to 2h, and a plateau is achieved. K3Flip has a steady increase in this ratio, from the very first moments of application. This increase achieves a significance in 2 hours.

Table 9: Numerical analysis of RNA content, by the use of differences in 915cm^{-1} IR band areas of Medium, CpG ODN, A151 ODN, LPS and K3f ODN treated macrophage cell spectra, in different time points (10min, 30min, 2h and 6h). The statistically significant data are specified with $p < 0.05^*$, $p < 0.01^{**}$, and $p < 0.001^{***}$ in comparison to medium treated group. The results are specified as mean \pm SEM.

Treatment/Time	10 min	30 m	2 h	6 h
Medium Treated	0.056 ± 0.0181	0.176 ± 0.0403	0.184 ± 0.0341	0.114 ± 0.006
CPG ODN	$0.352 \pm 0.0086^{***\uparrow}$	$0.312 \pm 0.0097^{***\uparrow}$	$0.208 \pm 0.0037^{*\uparrow}$	0.12 ± 0.0089
A151 ODN	0.156 ± 0.0413	0.162 ± 0.0402	0.12 ± 0.0249	0.144 ± 0.0098
LPS	0.095 ± 0.0724	0.2 ± 0.046	0.172 ± 0.0489	0.164 ± 0.0093
K3Flip ODN	0.124 ± 0.0366	0.176 ± 0.049	$0.206 \pm 0.0271^{*\uparrow}$	0.102 ± 0.0156

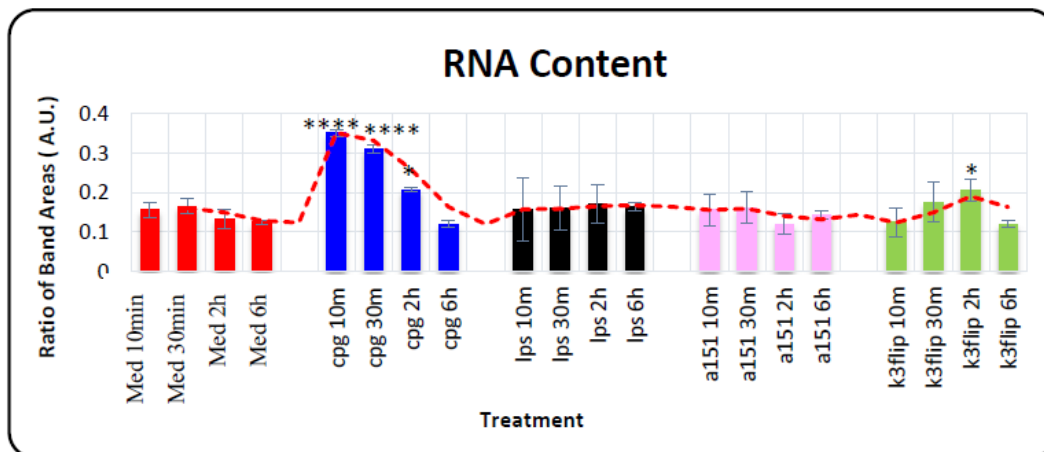


Figure 34: Histogram illustration of the RNA form content analysis by the use of differences in 915cm^{-1} IR band area of Medium, CpG ODN, A151 ODN, LPS and K3f ODN treated macrophage cells, in different time points (10m, 30m, 2h and 6h).

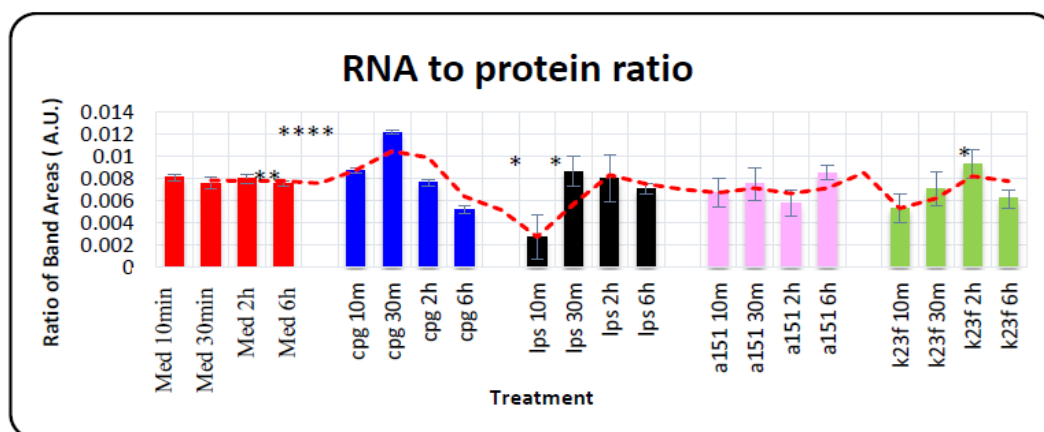


Figure 35: Histogram illustration of the RNA to protein ratio form content analysis by the use of differences in 915cm^{-1} IR band area to total protein ratio of Medium, CpG ODN, A151 ODN, LPS and K3f ODN treated macrophage cells, in different time points (10min, 30min, 2h and 6h). The error bars specify the SEM and stars the statistical significance as: $p < 0.05$ *, $p < 0.01$ **, and $p < 0.001$ ***.

3.6. Examination of specific issues

3.6.1. Membrane fluidity

Changes in the membrane dynamics can be traced by the frequency shifts and bandwidth difference of CH₂ antisymmetric and symmetric bands that in our samples were at around 2923cm⁻¹ and 2850cm⁻¹, respectively. The frequency did not change by the treatments and by time. On the other hand, as seen in Figure 36, the bandwidth has shown a significant increase in CpG ODN treatment after 6 hours of stimulation. LPS shows a similar trend of increase, but this increase had no statistical significance, as was for K3 Flip as well. Bandwidth increase of this band, suggests an increase in the membrane fluidity of the system (Severcan F, 2003; Severcan F., 2005). Generally, a rise of membrane fluidity means an increase in lipid order, if domain formation has not occurred (Ozek N., 2004).

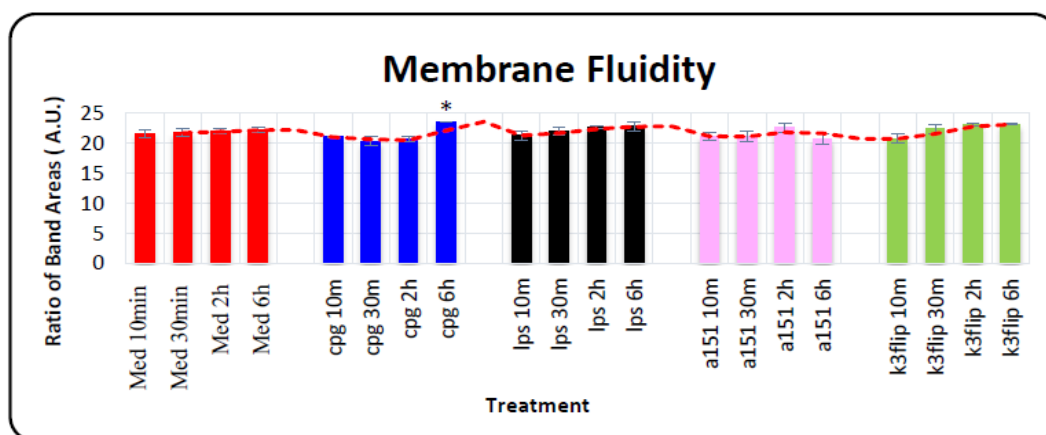


Figure 36: Histogram illustration of the membrane fluidity analysis by the use of differences in 2923cm⁻¹ and 2850cm⁻¹ IR bandwidth of Medium, CpG ODN, A151 ODN, LPS and K3f ODN treated macrophage cells, in different time points (10min, 30min, 2h and 6h). The error bars specify the SEM and stars the statistical significance as: p<0.05*, p<0.01**, and p<0.001***.

3.6.2. Lipid / protein

The lipid to protein ratio, found by the division of the total lipid (asCH₂ + sCH₂) to the total protein (Amide I + Amide II). It can give information on the lipid to protein asymmetry in the cell, and thus, has direct effect on the membrane fluidity and structure (Turker S., 2014). As seen in the figure below, a similar shape is present in both stimulants, CpG ODN and LPS. CpG ODN decreases the ratio significantly at two through six hours after stimulation together with LPS which with a lower slope decreases till 6h steadily. The suppressive A151 ODN and K3 Flip ODN do not have a significant change.

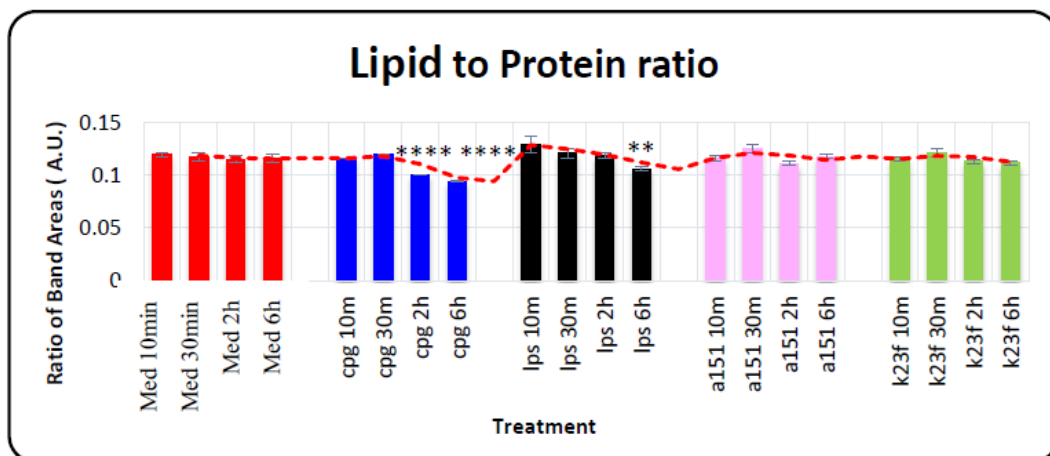


Figure 37: Histogram illustration of the lipid to protein ratio form content analysis by the use of differences in total lipid bands' area to total protein bands' area ratio of Medium, CpG ODN, A151 ODN, LPS and K3f ODN treated macrophage cells, in different time points (10min, 30min, 2h and 6h). The error bars specify the SEM and stars the statistical significance as: $p < 0.05^*$, $p < 0.01^{**}$, and $p < 0.001^{***}$ in comparison to medium treated group.

3.7. Cluster analysis

The variations in macromolecular level in our samples were further supported by the overall classification of their IR spectra using cluster analysis. Cluster Analysis was done to see the overall spectral differences between the medium treated samples and other treatments on different time points. When performed on 99 samples altogether in 20 groups, the accuracy of separation was 100% in all groups except K3 ODN 10min group (3/5), Medium treated 10min (3/5) together with 2h group (4/5) and A151 ODN 10min group (4/5). In the divided stimulation and suppression clusters, 100% accuracy was achieved. Related to their treatment and the time point that they were stimulated, all groups were successfully differentiated by Cluster Analysis, which confirm the results of PCA analysis (see Figure 38 and 39).

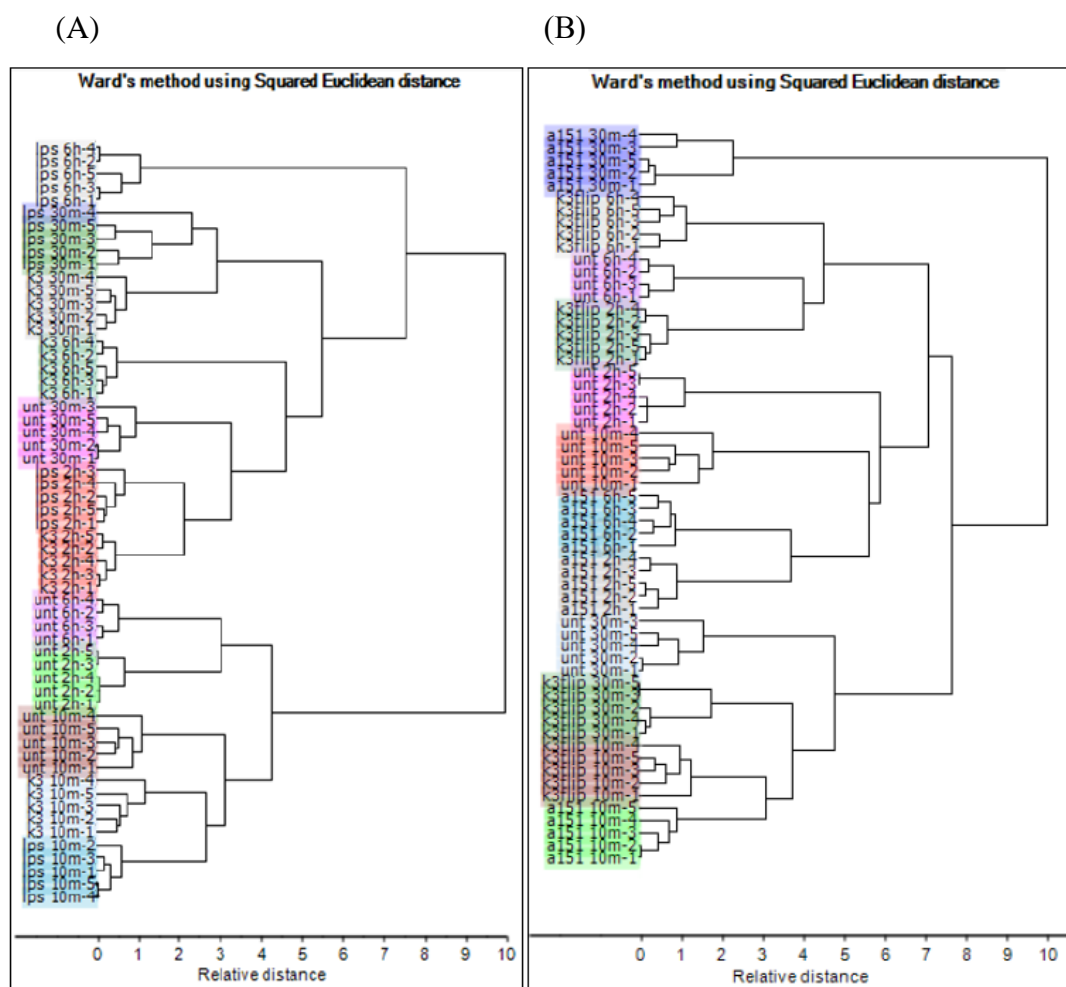


Figure 38: Separation of murine macrophage samples by using Cluster Analysis, implemented on ATR-FTIR spectra smoothed in $4000-650\text{cm}^{-1}$ region with nine-point Savitsky-Golay. (A) Stimulated samples: Medium treated, K3 ODN and LPS. (B) Suppressed samples: Medium treated, K3f ODN and A151 ODN. All samples are separated successfully in different time points (10min, 30min, 2h and 6h). *Medium treated group is denoted as Unt.

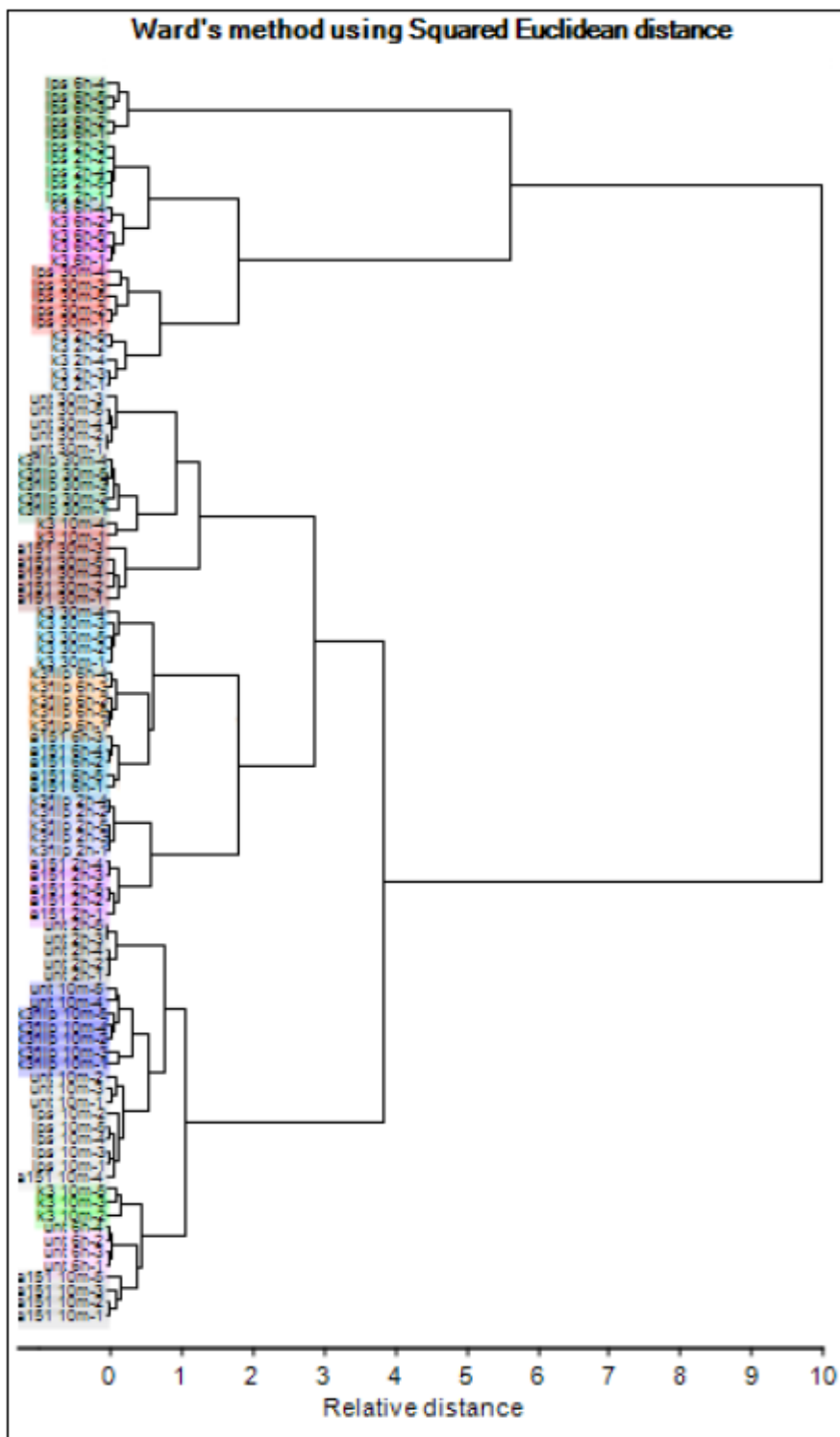


Figure 39: Separation of murine macrophage samples by using Cluster Analysis, accomplished on all treatments' ATR-FTIR spectra smoothed in $4000\text{-}650\text{cm}^{-1}$ region with nine-point Savitsky-Golay. *Medium treated group is denoted as "Unt".

3.8. PRINCIPAL COMPONENT ANALYSIS (PCA)

The extensive differences in the spectra of medium treated macrophage cells and the treated ones, was clearly seen in the difference FTIR spectra in figure. As seen in Figure 40 and 41, PCA differentiated all 20 groups successfully depending on their treatment and time of application.

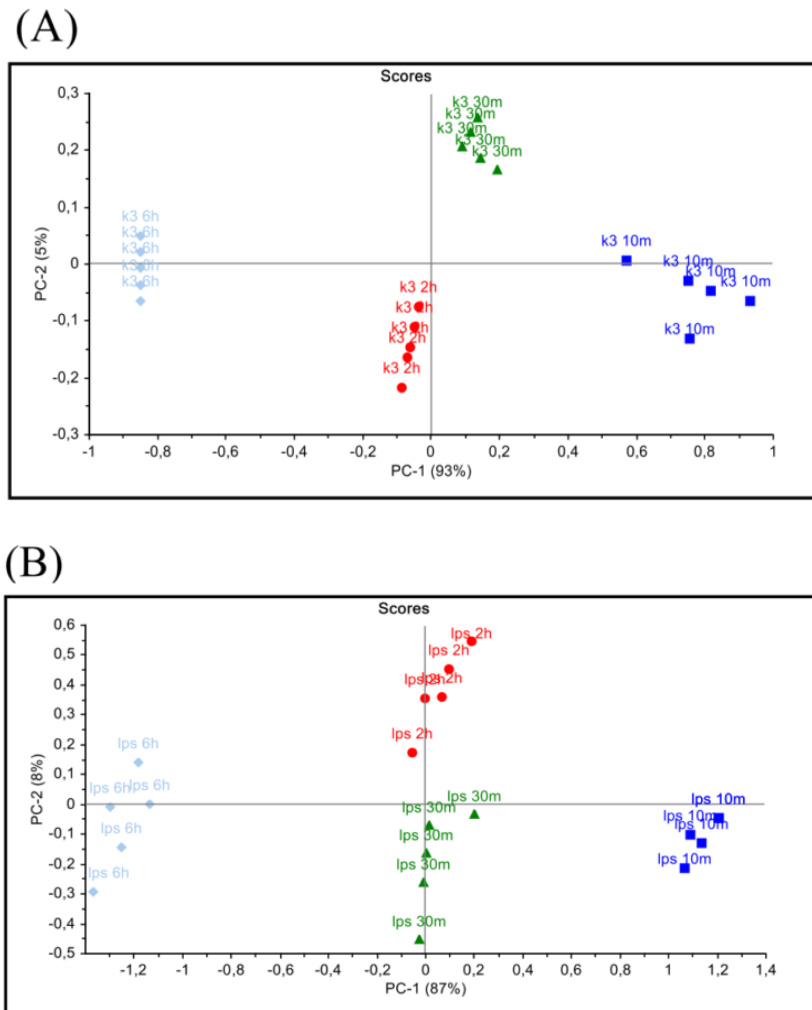
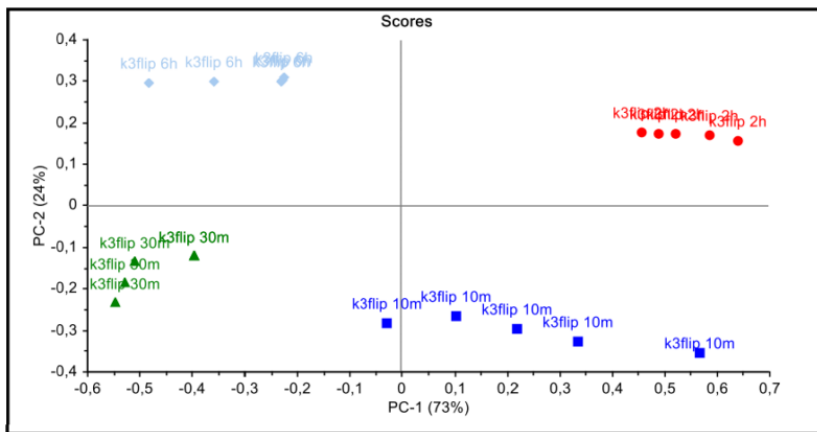


Figure 40: Treatment based separation of RAW 264.7 macrophage samples by using PCA analysis on ATR-FTIR spectra in 4000-650cm region with nine-point Savitsky-Golay smoothing. Five treatments: (A) K3 CpG ODN, (B) LPS, (C) K3f ODN, and (D) A151 ODN; are separated successfully in different time points (10min, 30min, 2h and 6h).

(C)



(D)

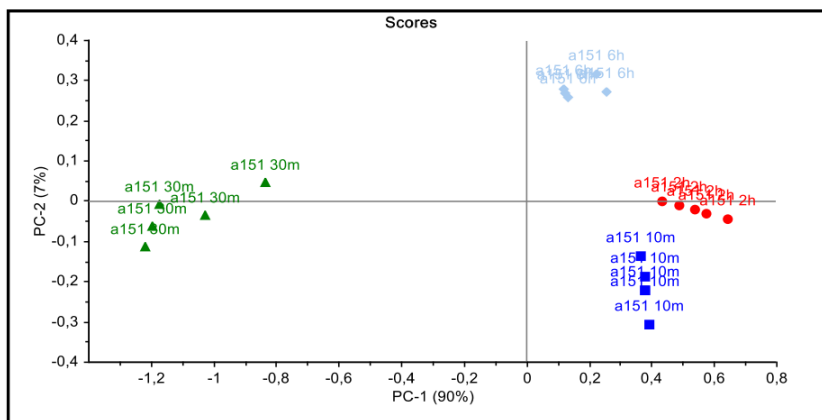


Figure 40: Continued

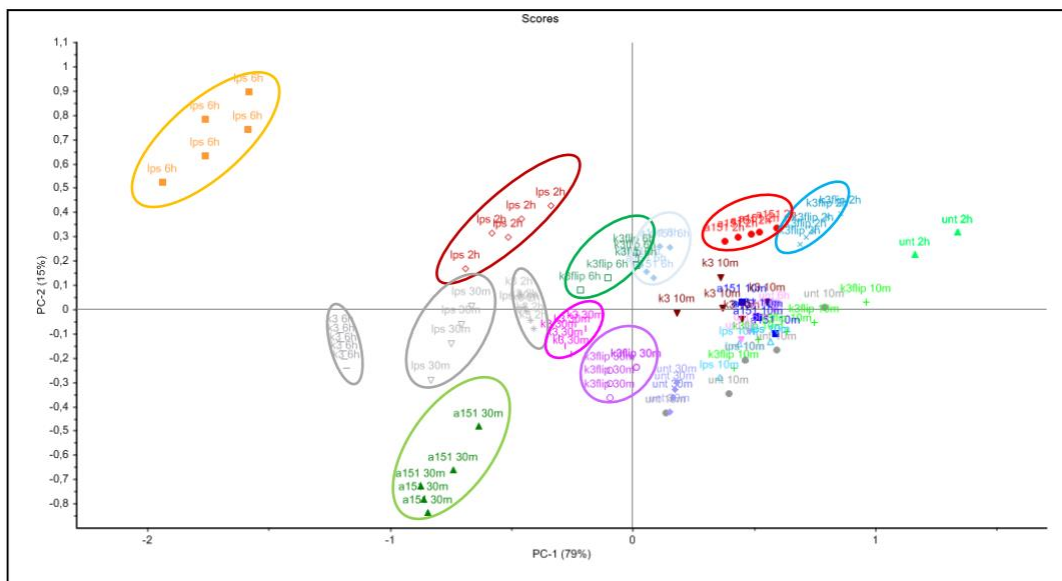


Figure 41: Separation of macrophage cell samples by using PCA analysis on the second derivative, vector normalized ATR-FTIR spectra in 4000-650cm region with nine-point Savitsky-Golay smoothing. Five treatments: K3 CpG ODN, LPS, K3f ODN, and A151 ODN; are divided effectively on different time points (10min, 30min, 2h and 6h). *Medium treated group is denoted as “Unt”.

CHAPTER 4

DISCUSSION

Macrophage cells play a key role in innate immunity for phagocytosis and important role in adaptive immunity as an antigen presenting cell. With being resident of almost all tissues in the body, they perform many specific functions, such as helping the antimicrobial combats, helping the bone resorption and wound healing processes. To perform all these functions, macrophages possess a high flexibility, a property that helps them to successfully respond to environmental signals. In this context, they can impressively alter their physiology in relation to their function. In our study, CpG ODN is used as a well-known stimulant of macrophages to produce the powerful pro-inflammatory agents such as cytokines, chemokines and highly specific Ig's. The boost of innate immunity caused by CpG ODN, which in turn is potentially used in many immunotherapeutic therapies, is found to cause allergy, toxic shock and death. This increased the need for a suppressive agent that innovatively was suppressive ODN. In our study, A151 suppressive ODN was used, whose exact mode of inhibition has not been explained yet. Another agent used for stimulation in our study was LPS, which shares a high degree of homology with CpG-DNA. The signalling cascade that is used by LPS through TLR-4 and by CpG through TLR-9, includes the employment of a mutual adapter protein, MyD88. The result of this signal transduction is the activation of NF-KB and AP-1. In a study involving 11,000 genes of mouse, gene regulation as a result of LPS and CpG-DNA application was clarified. It was found that actually there were significant differences between these two forms of macrophage activation (Gao J., 2002). In the present study, the comparison of global secondary changes induced on macrophages by different agents is achieved by

Fourier Transform Infrared Spectroscopy. In FTIR spectroscopy, each molecular vibration caused by IR light, has a corresponding discrete energy, thus, a distinct IR band will be present for each functional group in the sample (Aksoy C., 2012). Nearly all biologically significant macromolecules such as proteins, lipids, nucleic acids and carbohydrates can be detected in the spectrum (Fabian, 1995; Moore, 1995; Toyran, 2004; Toyran et al., 2005; Akkas, 2007). In an IR spectrum: frequency is used to assign the bond, the area under that bond is used to quantify its amount, and the bandwidth and frequency shifts are used to explain the structural changes (Liu K., 2005). Before going into the discussion of specific bands using these spectral parameters, difference spectra would be worth discussed since it serve to give us a general view of the differences in the structure of macromolecular components of murine macrophage cells upon treatment. It is clearly seen that the bands at C-H region are fairly elevated. These bands are related to mainly lipid content and slightly protein content of the samples. On the other hand, the Amide I and II region of proteins seem not to be disturbed too much. The fingerprinting region, bearing the pure bands, seems to have important differences, especially in the phosphate stretching bonds, which are indicators of nucleic acids and phospholipids. Upon stimulation, some bands seem to become more intense, such as RNA band, and some new bands appear as time goes on, such as DNA-Z form. Obviously, there are many changes pronounced with the application of CpG ODN, LPS, A151 ODN and K3Flip. The quantitative analysis of these features follows up our discussion. Obviously, one may firstly expect changes on nucleic acid content, due to the fact that these stimulants introduce an altered gene regulation, as discussed earlier. To check this, the band area of antisymmetric and symmetric phosphate functional groups were evaluated, which show vibrations at around 1236, 1261 and 1080 cm^{-1} . Only CpG ODN stimulation induced significant changes on nucleic acid content of macrophage cells, starting from 10 minutes of stimulation and going on till 6 hours ($p < 0.1^*$). Other treatments had no significant changes. Since to this band there is contribution from phospholipids as well, DNA-Z form specific band at 925cm^{-1} is used to validate the data regarding the reason of increase. In this band as well, CpG ODN stimulation shows the same trend of increase as in the phosphate band, in direct relation with the time of stimulation. At 2h of stimulation, has a significant increase with $p < 0.1^*$

and continues till 6h with $p < 0.0001$ ****. This cross-validation makes clear that the increase is from nucleic acid content of CpG ODN stimulated cells. It is well-known that DNA synthesis occurs after a longer period of time, starting from 6 hours of stimulation (Timlin J., 2009). So the increase in nucleic acid content at early stages should be due to RNA content. This is verified using the RNA specific band at around 915cm^{-1} . It has been found that 1% change in the total RNA content of the sample can have significant changes in the IR spectrum (Benedetti E, 1997). As seen in Figure 32, CpG ODN has a significantly increased in this band from the very first minutes ($p < 0.0001$ ****). This increase is maintained till 2h after stimulation ($p < 0.1$ *). All put together, the time period till 2h of stimulation seems to be the period of extensive RNA synthesis, and as it ceases, DNA synthesis starts from 6h of stimulation with CpG ODN. LPS on the other hand, in RNA specific band had a slope of increase till 2h after stimulation ($p < 0.1$ *), and then it ceases at 6h. It is reported elsewhere that LPS induces as much as 193 genes during the stimulation process and that it is a strong pro-inflammatory and anti-proliferative agent (Gao J., 2002). This explains the reason of no significant changes occurring on nucleic acid content after 6h of stimulation and of significant changes on RNA synthesis till 2 hours after stimulation. Unexpected results are seen with K3Flip applied sample, which was not expected to have impact on cells. The nucleic acid bands at the 6th hour of application had a significant increase of $p < 0.0001$ ****. Also in RNA specific band, it had a positive slope till 2h after application ($p < 0.1$ *). This profile for RNA and DNA synthesis resembles the one observed with stimulation. A151 suppression has no changes in nucleic acid, DNA-Z form and RNA content. In another study of murine macrophage activation using LPS, it was achieved to define the activation state of the cells at as early as 41 minutes after stimulation, by using LDA classification (Timlin J., 2009). The results of our study deduce that by using the RNA-specific band, one can define the activation state of macrophages at the very early stages of activation as well. There was a significant reduction of protein content in CpG ODN throughout the stimulation from 30m to 6h with $p < 0.0001$ ****. LPS stimulation was also decreasing the protein content of macrophage cells with a slight slope starting with $p < 0.01$ ** at 30m of stimulation, till $p < 0.0001$ **** at 6h. Generally, decreases of protein content are explained as either increase in protein degradation, or decrease in protein synthesis (Ozek N.,

2010). It is reported that stimulation of macrophage cells with PMA leads to the production of numerous oxidants, causing high oxidative stress (Gieche J., 2001). In other studies, it was noted that in intention to protect the cell, proteasomes in the cell start the degradation of oxidized proteins (Grune T., 1995; Sitte N., 1998). This may explain the decreased protein content upon stimulation with CpG ODN and LPS as well. The decrease of protein content was less in suppression with A151 ODN, where an initial decrease of the protein content at 10m was observed, but a steady state was maintained during the other periods of time. Similar behaviour is observed with K3F ODN too. Stimulation with CpG ODN is significantly decreasing the unsaturation degree in 30 m ($p < 0.0001^{****}$), 2h ($p < 0.0001^{****}$) and 6h ($p < 0.1^*$), and suppression with A151 ODN is increasing this value significantly in 2h ($p < 0.1^*$) and 6h ($p < 0.1^*$). LPS seems to have a similar trend with CpG ODN, but the results are not significant. Unexpectedly, K3Flip significantly has increased unsaturated lipids till 6h with ($p < 0.001^{***}$). As elsewhere explained, the decrease in olefinic=CH/saturated lipid ratio, arises from the increased lipid peroxidation (Turker S., 2014). Lipid peroxidation process is driven by free-radicals that cause oxidative stress on the membranous systems of the cell. These findings are supported by studies showing the occurrence of oxidative stress as a result of nitric oxide production in LPS activated macrophage cells (Liu KL., 2006). In another study, this reaction was apparent with LPS and PMA stimulation in as early as 30minutes (Jones E., 2007), in correlation to our results, where in 30minutes CpG ODN and LPS had a decrease of olefinic=CH band are. Like LPS, CpG ODN may have the same effect of producing free radicals that can induce oxidative stress in the cell. Moreover, nitric oxide can interact with cytochrome c oxidase of mitochondria and can cause defected oxidative phosphorylation. This can cause mitochondrial damage as well (Turker S., 2014). From our ratio of ester C-O stretching band 1741cm^{-1} , used to evaluate the concentration of cholesterol ester and triglycerides, and the antisymmetric stretching of CO-O-C functional group band at 1170cm^{-1} , we see that stimulation with CpG ODN is significantly increasing the concentration of cholesterol ester and triglycerides in early stimulation of 10m with $p < 0.1^*$ and decreases significantly at late stimulation of 2h ($p < 0.0001^{****}$) and 6h ($p < 0.001^{***}$); while on the other side suppression with A151 ODN has increased in early suppression of

30m with $p < 0.001^{***}$ and no significant result was seen in late phases. K3Flip follows a similar trend with A151 ODN and LPS, significantly increases the concentration at as early as 30min ($p < 0.01^{**}$) phase and keeps to decrease till 6h phase. The decrease of cholesterol esters and triglycerides by CpG ODN induces an increase in membrane fluidity, since cholesterol content is in direct proportion to the fluidity of membranes in liquid crystalline phase.

For sure cholesterol levels are not clear indicators of membrane fluidity. The main spectral parameter to trace for the changes on membrane dynamics are of CH_2 antisymmetric band (2923cm^{-1}) frequency shift, which is an indicator of lipid order (rigidity) and bandwidth alteration, which is an indicator of membrane fluidity. The frequency analysis did not give significant results of any change caused by the treatments and by time on this band. Important information on membrane fluidity is deduced by the bandwidth at 2923cm^{-1} , which has shown a significant increase in CpG ODN treatment after 6 hours of stimulation ($p < 0.1^*$). LPS and K3Flip show a similar trend line, but this increase had no statistical significance. An increase in the bandwidth value suggests an increase in the membrane fluidity of the system (Severcan F, 2003; Severcan F., 2005). Generally, a rise of membrane fluidity means an increase in lipid order as well, if domain formation has not occurred (Ozek N., 2004). All put together, CpG ODN has increased the membrane fluidity, as also supported by the data from cholesterol content and confirmed by the unsaturated/saturated lipid content. The increased lipid peroxidation in CpG ODN treatment is an indication of decreased membrane fluidity. This happens due to membrane width and curvature alterations which have an impact on membrane dynamics and the kinetics of ion channels (Awayda M., 2004). Basically, the main properties of membranes such as lipid order of fatty acids, phase behaviour, ion permeability and fusions are regulated by the lipid configuration of the cell. Consequently, many vital cellular processes such as cell signaling and catalytic reactions dependent on membrane-linked enzymes, are critically influenced by the membrane dynamics (Schoeniger A., 2011).

Cluster and PCA Analysis were performed to all ATR-FTIR spectra in $4000\text{-}650\text{cm}^{-1}$, and a successful segregation was achieved, where all groups were grouped together. In Cluster Analysis, 10 minute treated groups as expected had

few mismatches. This is due to the very little changes on the cells in the very first minutes of stimulation. In PCA, all groups seem to have small variation between each other till 10 minutes of stimulation,. However in 30 minutes of stimulation and on, all treated groups show an evident segregation from the medium treated one, whose all-time points are grouped in one general area, showing that no significant changes occur till 6 hours on the medium treated culture cells. Also PCA plot shows evidently that LPS and K3 groups on different time points are grouped near to each other. This is the same for A151 and K3F ODN as well. These observations support the previous quantitative studies of the ATR-FTIR spectra.

CHAPTER 5

CONCLUSIONS

This study demonstrates the use of FTIR spectroscopy as an independent modality to monitor the activation dynamics of murine macrophage cells upon treatment with CpG and LPS and upon suppression with A151 ODN. The results clearly indicate that CpG-induced macrophages show prominent features in their IR spectra for their activation. The time period till 2h of stimulation seems to be the period of extensive RNA synthesis, and as it ceases, DNA synthesis starts from 6h of stimulation with both CpG ODN and LPS, except LPS not having significant change at 6 hours of stimulation, due to being anti-proliferative agent. It is also found that stimulation of macrophage cells with CpG ODN and LPS decreased protein content. This is explained by the production of numerous oxidants, causing oxidative stress and in intention of protecting the cell; proteasomes start the degradation of oxidized proteins.

One more outcome of the results was on the dynamics of cell membrane where increased membrane fluidity during activation with CpG ODN and LPS was observed. This is supported by the decreased unsaturated lipid content, increased lipid peroxidation and decreased cholesterol content. It was also noted that these changes may have altered the signal transduction processes, ion permeability and many other primary functions of cell membranes could be altered.

The present study was a unique piece of work on the effects of different agents on murine macrophage cells on different time points. For the first time, not just a resting- activated state changes, but a a broad biophysical and macromolecular

profile on the changes upon the application of CpG ODN and a suppressive agent-A151 ODN, is monitored on the course of time. Experiments including more time-points will certainly reveal many more details on the mechanisms that underlie LPS, CpG ODN, A151 ODN and K3Flip application.

REFERENCES

- AirUCI. (2014, June 17). *Fourier Transform Infrared Spectroscopy*. Retrieved from UCI Aerosol Photochemistry Group: http://aerosol.chem.uci.edu/AirUCI_summer/PDFs/labs/2014_FTIR_Lab.pdf
- Akkas, S. S. (2007). Effects of lipoic acid supplementation on rat brain tissue: An FTIR spectroscopic and neural network study. *Food Chemistry*, *105*(3), 1281-1288.
- Aksoy C., S. F. (2012). Role of Vibrational Spectroscopy in Stem Cell Research. *Spectroscopy: An International Journal*, 167–184.
- Alberts B, J. A. (2002). *Molecular Biology of the Cell. 4th edition*. New York: Garland Science.
- Amanda, J. a. (2009). Corticosteroid receptors, macrophages and cardiovascular disease. *Journal of Molecular Endocrinology* *42*, 449–459 .
- Argov, S. S. (2004). Inflammatory bowel diseases as an intermediate stage between normal and cancer: A FTIR-microspectroscopy approach. *Biopolymers* *75*, 384–392.
- Arrondo, J. M. (1993). Quantative Studies of the Structure of Proteins in Solution by Fourier Transform Infrared Spectroscopy. *Progress. Biophys. Acta*, 63-72.
- Babrah, J. (2009, June). A Study of FT-IR spectroscopy for the identification and classification of haematological malignancies. CRANFIELD UNIVERSITY.
- Banyay, M. a. (2003). A library of IR bands of nucleic acids in solution. *Biophys. Chem.*, 477-488.
- Benedetti E, B. E. (1997). Determination of the relative amount of nucleic acids and proteins in leukemic and normal lymphocytes by means of Fourier transform infrared microspectroscopy. *Appl Spectrosc*, 51:792.
- Bode, C. . (2011). CpG DNA as a vaccine adjuvant. *Expert Rev Vaccines*. *10*(4), 499–511.
- Boyar, H., & Severcan, F. (1997). Oestrogen-phospholipid membrane interactions: An FTIR study. *J. Mol. Structure*, 408-409, 269-272.
- Bozkurt, O. B. (2007). The effect of diabetes mellitus on rat skeletal extensor digitorum longus muscle tissue: An FTIR study. *Spectroscopy*, *21*(3), 151-160.
- Cakmak, G. T. (2003). FT-IR spectroscopic analysis of rainbow trout liver exposed to nonylphenol. *Applied spectroscopy* *57*, 835-841.
- Cakmak, G. T. (2006). Beta-estradiol induced compositional, structural and functional changes in rainbow trout liver, revealed by FT-IR spectroscopy: a comparative study with nonylphenol. *Aquatic toxicology* *77*(1), 53-63.
- Campbell et al., J. D. (1984). *Biological Spectroscopy, chp3-4*. The Benjamin/Cummings Publishing Company, Inc.
- Campbell, I. D. (1984). *Biological Spectroscopy*. The Benjamin/Cummings Publishing Company, Inc.

- Chan, J. W. (2006). Micro-Raman spectroscopy detects individual neoplastic and normal hematopoietic cells. *Biophys. J.* 90, 648–656.
- Chiriboga, L. X. (1998). Infrared spectroscopy of human tissue. I. Differentiation and maturation of epithelial cells in the human cervix. *Biospectroscopy* 4, 47–53.
- Cohen, J. (2002). The immunopathogenesis of sepsis. *Nature*, 885–891.
- Daniela Verthelyi, D. M. (2002). CpG-ODN—Safety Considerations. *Microbial DNA and Host Immunity*, 385-396.
- Demir P., A. S. (2015). Ionizing Radiation Induces Structural and Functional Damages on the Molecules of Rat Brain Homogenate Membranes: A Fourier Transform Infrared (FT-IR) Spectroscopic Study. *APPLIED SPECTROSCOPY*, 1-11.
- Demir P., S. O. (2012). Phylogenetic differentiation of *Aegilops* and *Triticum* species by using ATR-FTIR spectroscopy. *Journal of Biotechnology*, 32.
- Dovbeshko, G. I. (2000). FTIR spectroscopy studies of nucleic acid damage. *Talanta* 53, 233–246.
- Dranoff, G. (2004). Cytokines in cancer pathogenesis and cancer therapy. *Nature Reviews Cancer*, 11-12.
- Elkins, K. L.-J. (1999). Bacterial DNA containing CpG motifs stimulates lymphocyte-dependent protection of mice against lethal infection with intracellular bacteria. *J. Immunol.* 162, 2991–2998.
- Esmeralda Juarez, C. N. (2010). Differential expression of Toll-like receptors on human alveolar macrophages and autologous peripheral monocytes. *Respiratory Research*, 2.
- Fabian, H. J. (1995). A comparative infrared spectroscopic study of human breast tumors and breast tumor cell xenografts. *Biospectroscopy*, 1(1), 37-45.
- Frederic, G. M. (2010). Development of Monocytes, Macrophages, and Dendritic Cells. *SCIENCE* 327, 656-661.
- Freifelder, D. (1982). *Physical Chemistry. Applications to biochemistry and molecular biology*. New York: Freeman, W. H. (Ed).
- Fujihara et al., M. (2003). Molecular mechanisms of macrophage activation and deactivation by lipopolysaccharide: roles of the receptor complex. *Pharmacology & Therapeutics*, 171–194.
- Fukuyama, Y. Y. (1999). A study on the differences between oral squamous cell carcinomas and normal oral mucosae measured by Fourier transform infrared spectroscopy. *Biospectroscopy* 5, 117–126.
- Fumihiko Takeshita, I. G. (2004). Signal transduction pathways mediated by the interaction of CpG DNA with Toll-like receptor 9. *Seminars in Immunology* 16, 17–22.
- Fung, M. F. (1996). Pressure-tuning Fourier transform infrared spectroscopic study of carcinogenesis in human endometrium. *Biospectroscopy* 2, 155–165.
- Fung, M. F. (1996). Pressure-tuning Fourier transform infrared spectroscopic study of carcinogenesis in human endometrium. *Biospectroscopy* 2, 155–165.
- Gaigneaux, A. J. (2002). Infrared spectroscopy as a tool for discrimination between sensitive and multiresistant K562 cells. *Eur. J. Biochem.* 269, 1968–1973.
- Gao J., V. D. (2002). Regulation of gene expression in mouse macrophages stimulated with bacterial CpG-DNA and lipopolysaccharide. *Journal of Leukocyte Biology*, 1234-1245.

- Garip, S. B. (2007). Differentiation of mesophilic and thermophilic bacteria with fourier transform infrared spectroscopy. *Applied spectroscopy*, 61(2), 186-192.
- Gasparri, F. a. (2003). Monitoring of apoptosis of HL60 cells by Fourier-transform infrared spectroscopy. *Biochemical Journal*, 369, 239-248.
- Gieche J., M. J. (2001). Protein oxidation and proteolysis in RAW264.7 macrophages: effects of PMA activation. *Biochim Biophys Acta.*, 321-8.
- Gordon, S., & Taylor, P. R. (2005). Monocyte And Macrophage Heterogenity. *NATURE REVIEWS | IMMUNOLOGY*. volume5, 953-964.
- Grant, E. P. (1993). MHC class I-restricted presentation of exogenous antigen by thymic antigen-presenting cells in vitro and in vivo. *J. Immunol.* 148, 13-18.
- Guidos, A. A. (1987). Functional differences and complementation between dendritic cells and macrophages in T-cell activation. *Immunology*, 269–276.
- Hacker, H. e. (1998). CpG-DNA-specific activation of antigen presenting cells requires stress kinase activity and is preceded by non-specific endocytosis and endosomal maturation. *EMBO J.* 17, 6230–6540.
- Hacker, H. e. (2000). Immune cell activation by bacterial CpG-DNA through myeroid differentiation marker 88 and tumor necrosis factor receptor-associated factor (TRAF)6. *J. Exp. Med.* 192, 595–600.
- Halifax Regional School Board. (n.d.). Retrieved from <http://hrsbstaff.ednet.ns.ca/http://hrsbstaff.ednet.ns.ca/hicksca/Bonding/electron%20config.htm>
- Haris and Severcan, P. I. (1999). FTIR spectroscopic characterization of protein structure in aqueous and non-aqueous media. *Journal of Molecular Catalysis B: Enzymatic*, 7, 207-221.
- Harvey, D. (2009). *Analytical Chemistry 2.0*. McGraw-Hill Companies.
- Hemmi, H. e. (2000). A Toll-like receptor recognizes bacterial DNA. *Nature* 408, 740–745.
- Hidekazu, S. I. (2005). Suppressive Oligodeoxynucleotides Protect Mice from Lethal Endotoxic Shock. *The Journal of Immunology*, 4579-4583.
- Hiroshi Yamada, I. G. (2002). Effect of Suppressive DNA on CpG-Induced Immune Activation. *The Journal of Immunology*, 5590 –5594.
- Huleihel, M. S. (2001). Novel optical method for study of viral carcinogenesis in vitro. *J. Biochem. Biophys. Methods* 50, 111–121.
- InvivoGen. (2013). *InvivoGen*. Retrieved from InvivoGen: <http://www.invivogen.com/tlr9-agonist>
- Ito, S.-i. . (2004). CpG Oligodeoxynucleotides Improve the Survival of Pregnant and Fetal Mice following *Listeria monocytogenes* Infection. *Infect Immun.* 72(6), 3543–3548.
- Jackson, M. H. (1996). Biomedical infrared spectroscopy. In D. C. H.H. Mantsch, *Infrared Spectroscopy of Biomolecules*, , (p. p. 311). Wiley-Liss, Inc.
- Janeway, C. J. (2001). Principles of innate and adaptive immunity. In *Immunobiology: The Immune System in Health and Disease*. 5th edition. New York: Garland Science.
- Jones E., I. M. (2007). Modulation of LPS stimulated NF-kappaB mediated Nitric Oxide production by PKCε and JAK2 in RAW macrophages. *Journal of Inflammation* , 4:23.
- Julia Karbach, A. N. (2012). Therapeutic administration of a synthetic CpG oligodeoxynucleotide triggers formation of anti-CpG antibodies . *Cancer*

Research.

- Kan-Zhi Liu, M. X. (2007). Biomolecular characterisation of leucocytes by infrared spectroscopy. *British Journal of Haematology*, 136, 713–722.
- Kardas M., A. G. (2014). FTIR spectroscopy offers hints towards widespread molecular changes in cobalt-acclimated freshwater bacteria. *Aquatic Toxicology*, 15–23.
- Kardas M., G. A. (2014). FTIR spectroscopy offers hints towards widespread molecular changes in cobalt-acclimated freshwater bacteria. *Aquatic Toxicology*, 15–23.
- Kathleen et al., A. M. (2004). Spectroscopic evaluation of living murine macrophage cells before and after activation using attenuated total reflectance infrared spectroscopy. *Vibrational Spectroscopy*, 3-11.
- Keeler J., P. W. (2014). *Chemical Structure and Reactivity: An Integrated Approach*. Glasgow: Oxford University Press.
- Klinman D., Z. R. (2003). Regulation of CpG induced immune activation by suppressive oligodeoxynucleotides. *Ann.N.Y.Acad.Sci*, 112-123.
- Klinman, D. M. (2004). Immunotherapeutic uses of CpG Oligodeoxynucleotide. *NATURE REVIEWS | IMMUNOLOGY*, 1-10.
- Kneipp, J. L. (2000). Detection of pathological molecular alterations in scrapie-infected hamster brain by fourier transform infrared (FT-IR) spectroscopy. *Biochimica et Biophysica Acta (BBA) Molecular Basis of Disease*, 1501(2-3), 189-199.
- Kopydlowski et al., K. M. (1999). Regulation of macrophage chemokine expression by lipopolysaccharide in vitro and in vivo. *J Immunol*, 1537-1544.
- Krafft, C. N. (2005). Near-infrared Raman spectra of human brain lipids. *Spectrochimia Acta* 61, 1529–1535.
- Krieg A., T. W.-H.-K. (1998). Sequence motifs in adenoviral DNA block immune activation by stimulatory CpG motifs. *Proc Natl Acad Sci*, 12631–12636.
- Krieg, A. M. (1998). CpG DNA induces sustained IL-12 expression in vivo and resistance to *Listeria monocytogenes* challenge. *J. Immunol.* 161, 2428–2434.
- Krieg, A. M. (1998). Sequence motifs in adenoviral DNA block immune activation by stimulatory CpG motifs. *Proc. Natl. Acad. Sci. USA* 95, 12631.
- Kucuk, O. . (1992). The effects of cholesterol oxidation products in sickle and normal red blood cell membranes. *Biochim. Biophys. Acta* 1103, 296–302.
- Kumar, V. A. (2007). *Robbins Basic Pathology*, 8th ed. Philadelphia: Saunders Elsevier.
- Lamba, O. P. (1991). Spectroscopic detection of lipid peroxidation products and structural changes in a sphingomyelin model system. *BBA*, 1081, 181-187.
- Lasch, P. H. (2004). Imaging of colorectal adenocarcinoma using FT-IR microspectroscopy and cluster analysis. *Biochimica et Biophysica Acta (BBA) - Molecular Basis of Disease*, 1688(2), 176-186.
- Lenert, P. (2005). Inhibitory oligodeoxynucleotides – therapeutic promise for systemic autoimmune diseases? *Clin Exp Immunol*; 140, 1-10.
- Lin, S. Y. (1997). Fourier transform infrared spectral evidences for protein conformational changes in immature cataractous human lens capsules accelerated by myopia and/or systemic hypertension. *Spectrochimica acta. Part A, Molecular and biomolecular spectroscopy* 53A(9), 1507-1513.

- Liu KL., C. H. (2006). DATS reduces LPS-induced iNOS expression, NO production, oxidative stress, and NF-kappaB activation in RAW 264.7 macrophages. *J Agric Food Chem.*, 3472-8.
- Liu, K. K. (2003). Infrared spectroscopic identification of patients with beta-thalassemia. *Clin.Chem.* 49, 1125– 1132.
- Liu, K.-Z. M.-H. (2005). Molecular and chemical characterization of blood cells by infrared spectroscopy: A new optical tool in hematology. *Blood Cells, Molecules, and Diseases* 35, 404 – 412.
- Lynch, M. B. (1993). A study of differentiation of living bacteria by ATR/FTIR spectroscopy. *Can J Appl Spectrosc*, 38, pp. 18-21.
- M. Klinman, D. ,. (1999). Repeated Administration of Synthetic Oligodeoxynucleotides Expressing CpG Motifs Provides Long-Term Protection against Bacterial Infection. *Infect. Immun.* vol. 67 no. 11 , 5658-5663.
- M.S. Awayda, W. S. (2004). NaC–membrane interactions: regulation of channel activity by membrane order. *J. Gen. Physiol.* , 709–727.
- Mayda, G. D. (2013). Plasmacytoid Dendritic Cell Response to CpG ODN Correlates with CXCL16 Expression and Is Inhibited by ox-LDL. *Mediators of Inflammation*, 1-7.
- Mayda, G. I. (2006). CXCL16 Influences the Nature and Specificity of CpG-Induced Immune Activation. *J Immunol* 177, 1575-1580.
- McClain, B. C.-A. (2000). Educational applications of IR and Raman Spectroscopy: A comparison of experiment and theory . *Journal of Chemical Education*, 654-660.
- Medadmin. (2011, April 29). Retrieved from http://php.med.unsw.edu.au/medwiki/index.php?title=The_role_of_macrophages_in_inflammation&oldid=14600
- Medzhitov, R. &. (1998). Innate immunity, the virtues of a nonclonal system of recognition. *Cell* 91, 295–298.
- Melchiori, L. G. (2010). β -Thalassemia: HiJAKing ineffective erythropoiesis and iron overload. *Adv. Hemat.*, Article ID 938640.
- Melin, A. M. (2000). Pharmacologic application of fourier transform IR spectroscopy: in vivo toxicity of carbon tetrachloride on rat liver. *Biopolymers*, 57, 160-168.
- Mendelsohn, R. a. (1986). Fourier transform infrared studies of lipid-protein interaction. In *Progress in Protein-Lipid Interactions Volume 2*. Netherlands: Elsevier Science Publishers.
- Mendelsohn, R., & Mantsch, H. H. (1986). Fourier transform infrared studies of lipid-protein interaction. In *Progress in Protein-Lipid Interactions, Volume 2* (pp. 103-147). Netherlands: Elsevier Science Publishers.
- Moore, D. J. (1995). Peroxidation of erythrocytes: FTIR spectroscopy studies of extracted lipids, isolated membranes, and intact cells. *Biospectroscopy*, 1(2), 133-140.
- Mosser at al., D. (2011). Exploring the full spectrum of macrophage activation. *Nat Rev Immunol.*, 1-26.
- Mosser, X. Z. (2008). Macrophage activation by endogenous danger signals. *J Pathol. Jan* , 161–178.
- Munford, R. S. (2007). Sensing Gram-Negative Bacterial Lipopolysaccharides: a Human Disease Determinant? *Infect. Immun.* 2008, 76(2), 454–465.

- O'Neill, L. A. (2013). The history of Toll-like receptors — redefining innate immunity. *Nature Reviews Immunology* 13, 453–460.
- Ozek N., B. B. (2004). Structural and functional characterization of simvastatin-induced myotoxicity in different skeletal muscles. *Biochimica et Biophysica Acta* , 406–415.
- OZEK N., Y. S. (2010). Low dose simvastatin induces compositional, structural and dynamic changes in rat skeletal extensor digitorum longus muscle tissue. *Bioscience Reports*, 41–50.
- Ozek, N. S.-B. (2010). Characterization of microRNA-125b expression in MCF7 breast cancer cells by ATR-FTIR spectroscopy. *The Analyst*, 135(12), 3094-3102.
- Paluszkiewicz, C. a. (2001). Analysis of human cancer prostate tissues using FTIR microscopy and SXIXE techniques. *J. Mol. Structures* 565–566, 329–334.
- Paluszkiewicz, C. a. (2001). Analysis of human cancer prostate tissues using FTIR microscopy and SXIXE techniques. . *J. Mol. Structures* 565–566, 329–334.
- PerkinElmer, L. a. (2005). FT-IR Spectroscopy. Attenuated Total Reflectance (ATR). Shelton, CT, USA.
- Perromat, A. ., (2001). *Appl. Spectrosc.* 55, 1166–1172.
- Peter M., K. B. (2008). Characterization of suppressive oligodeoxynucleotides that inhibit Toll-like receptor-9-mediated activation of innate immunity. *Immunology*, 118–128.
- Pozzi, L.-A. M. (2005). Both Dendritic Cells and Macrophages Can Stimulate Naive CD8 T Cells In Vivo to Proliferate, Develop Effector Function, and Differentiate into Memory Cells. *The Journal of Immunology* vol. 175 no. 4 , 2071-2081.
- Qingye, L. e. (2011). Understanding the molecular interactions of lipopolysaccharides during E. coli initial adhesion with a surface forces apparatus. *Soft Matter*, 1-15.
- Raetz, C. R. (1990). Biochemistry of endotoxins. *Annu Rev Biochem* , 129– 170.
- Ramesh, J. ., (2002). Novel methodology for the follow-up of acute lymphoblastic leukemia using FTIR microspectroscopy. *J. Biochem. Biophys. Methods* 51, 251–261.
- Razin, A. &. (1981). DNA methylation and its possible biological roles. *Prog. Nucl. Acid Res.* 25,, 33–52.
- Ronto, G. a. (1999). *An introduction to biophysics with medical orientation*. Budapest: Akademiai Kiado.
- Ross, J. &. (2002). The biology of the macrophage. In *The macrophage* (pp. 1-72). New York: Oxford University Press.
- Savitzky, A., & Golay, M. (1964). Smoothing and differentiation of data by simplified least squares procedures. *Anal. Chem.*, 36:1627.
- Schoeniger A., S. A. (2011). The Impact of Membrane Lipid Composition on Macrophage Activation in the Immune Defense against *Rhodococcus equi* and *Pseudomonas aeruginosa*. *Int. J. Mol. Sci.*, 7510-7528.
- Schultz, C. K. (1996). Differentiation of leukemic from normal human lymphocytes by FT-IR spectroscopy and cluster analysis. *Leukemia Res.* 20, 649–655.
- Schultz, H. a. (2007). Identification and qualification of valuable plant substances by IR and Raman spectroscopy. *Vibrational Spectroscopy* 43, 13-25.
- Schumann et al., R. R. (1990). Structure and function of lipopolysaccharide

- binding protein. *Science*, 1429–1431.
- Severcan F., G. G. (2005). Rapid monitoring of diabetes-induced lipid peroxidation by Fourier transform infrared spectroscopy: Evidence from rat liver microsomal membranes. *Analytical Biochemistry*, 36–40.
- Severcan, F. (1997). Vitamin E decreases the order of the phospholipid model membranes in the gel phase: An FTIR study. *Bioscience Reports*, 17, 231-235.
- Severcan, F. B. (2010). FT-IR spectroscopy in diagnosis of diabetes in rat animal model. *Journal of biophotonics*, 3(8-9), 621-631.
- Severcan, F. K. (1995). IR and turbidity studies of vitamin E-cholesterol-phospholipid membrane interactions. *Bioscience Reports*, 15 (4) , 221-229.
- Severcan, F. K. (2003). Fourier transform infrared spectroscopic studies of diabetic rat heart crude membranes. *Spectroscopy* 17(2), 569-577.
- Severcan, F. T. (2000). Fourier transform infrared study of the effect of diabetes on rat liver and heart tissues in the CH region. *Talanta*, 53(1), 55-59.
- Severcan, F., & Haris, P. I. (2003). Fourier transform infrared spectroscopy suggests unfolding of loop structures precedes complete unfolding of pig citrate synthase. *Biopolymers*, 69(4), 440-447.
- Siamon, G. (2003). Alternative activation of macrophages. *Nature Reviews Immunology* 3, 23-35.
- Siebert et al., F. a. (2008). *Vibrational Spectroscopy in Life Science: Tutorials in Biophysics*. Weinheim: WILEY-VCH.
- Sigma-Aldrich. (2015). *Sigma-Aldrich*. Retrieved from Glycobiology Analysis Manual, 2nd Edition: <http://www.sigmaaldrich.com/technical-documents/articles/biology/glycobiology/lipopolysaccharides.html#products>
- Sitte N., K. M. (1998). Proteasome-dependent degradation of oxidized proteins in MRC-5 fibroblasts. *FEBS Lett.*, 399–402.
- Smith, G. a. (1999). The DNA dependant protein kinase. *Genes Dev.* 13, 916-934.
- Stuart, B. (1997). *Biological Applications of Infrared Spectroscopy*. England: John Wiley and Sons.
- Stuart, B. (2004). *Infrared Spectroscopy Fundamentals and Applications of Analytical Techniques in the Sciences*. England: John & Sons, Ltd.
- Sukuta, S. a. (1999). Factor analysis of cancer Fourier transform infrared evanescent wave fiberoptical (FTIR-FEW) spectra. *Lasers Surg. Med.*, 24, 382–388.
- T. Grune, T. R. (1995). Protein degradation in cultured liver epithelial cells during oxidative stress. *J. Biol. Chem.*, 2344–2351.
- Takeda, K., & Akira, S. (2005). Toll-like receptors in innate immunity. *International Immunology*, Vol. 17, No. 1, , pp. 1–14 .
- Takeshita, F. e. (2001). Cutting Edge, role of toll-like receptor 9 in CpG DNA-induced activation of human cells. *J. Immunol.* 167, 3555–3558.
- Thomas, D. W. (2009). Detection of endogenous biomolecules in Barrett's esophagus by Fourier transform infrared spectroscopy. *PNAS vol. 104 no. 40*, 15864–15869.
- Timlin et al., J. A. (2002). Infrared ATR: A Probe for Cellular Activation. *Proceedings of SPIE*, 40-48.
- Timlin J., L. E. (2009). Dynamics of cellular activation as revealed by attenuated total reflectance infrared spectroscopy. *Vibrational Spectroscopy*, 78–85.

- Tong, L. Y.-J.-R. (2012). Emerging role of toll-like receptors in the control of pain and itch. *Neurosci Bull.* 28(2), 131–144.
- Toyran et al., N. Z. (2005). Effect of stereotactic radiosurgery on lipids and proteins of normal and hypoperfused rat brain homogenates: a fourier transform infrared spectroscopy study. *International journal of radiation biology* 81(12), 911-918.
- Toyran, N. Z. (2004). Chronic hypoperfusion alters the content and structure of proteins and lipids of rat brain homogenates: a fourier transform infrared spectroscopy study. *European biophysics journal : EBJ*, 33(6), 549-554.
- Turker S., I. G. (2014). Investigation of Compositional, Structural, and Dynamical Changes of Pentylene-tetrazol-Induced Seizures on a Rat Brain by FT-IR Spectroscopy. *Anal. Chem.*, 1395–1403.
- Volkman, A. G. (1965). The origin of macrophages from bone marrow in the rat. *British Journal of Experimental Pathology* 46, 62–70.
- Wang, H. P. (1997). Microscopic FTIR studies of lung cancer cells in pleural fluid. *The Sci. Total Envir.* 204, 283–287.
- Watala, C. . (1998). Platelet membrane lipid fluidity and intraplatelet calcium mobilization in type 2 diabetes mellitus. *Eur. J. Haematol.* 61, 319– 326.
- Wong, P. T. (1995). Characterization of exfoliated cells and tissues from human endocervix and ectocervix by FTIR and ATR/FTIR spectroscopy. *Biospectroscopy*, 1, pp. 357-364.
- WOOD B., B. T. (2000). Fourier Transform Infrared Spectroscopy as a Method for Monitoring the Molecular Dynamics of Lymphocyte Activation. *APPLIED SPECTROSCOPY*, 353-359.
- Wood et al., B. R. (2000). Fourier transform infrared spectroscopy as a method for monitoring the molecular dynamics of lymphocyte activation. *Appl Spectrosc*, 353-359.
- Wood, B. R. (1996). An investigation into FT-IR spectroscopy as a bio-diagnostic tool for cervical cancer. *Biospectroscopy* 2, , 143–153.
- Wood, B. R. (1998). FTIR microspectroscopic study of cell types and potential confounding variables in screening for cervical malignancies. *Biospectroscopy* 4, , 75–91.
- Yamada H., I. K. (2004). Suppressive oligodeoxynucleotides inhibit CpG-induced inflammation of the mouse lung. *Crit Care Med.* , 2045-9.
- Yamada, H. . (2002). Effect of Suppressive DNA on CpG-Induced Immune Activation. *The Journal of Immunology*, 5590-5594 .
- Yamamoto, S. e. (1992). Unique palindromic sequences in synthetic oligonucleotides are required to induce IFN and augment IFN-mediated natural killer activity. *J. Immunol.* 148, 4072–4076.
- Yang, Y. S.-S. (2005). Study of tumor cell invasion by Fourier transform infrared microspectroscopy. . *Biopolymers*, 78, 311–317.
- Yi, A. K. (1991). CpG motifs in bacterial DNA activate leukocytes through the pH-dependent generation of reactive oxygen species. *J. Immunol.* 160, 4755–4761.